UV-VISIBLE LIGHT ABSORPTION PROPERTIES OF ORGANIC CARBON AEROSOL IN ATMOSPHERE

By

MIN ZHONG

A DISSERTATION PRESENTED TO THE GRADUATE SCHOOL
OF THE UNIVERSITY OF FLORIDA IN PARTIAL FULFILLMENT
OF THE REQUIREMENTS FOR THE DEGREE OF
DOCTOR OF PHILOSOPHY

UNIVERSITY OF FLORIDA

2013

To my beloved parents and family

ACKNOWLEDGMENTS

This work was supported by a grant from the National Science Foundation (ATM-0852747) and by a UF Alumni Scholarship.

I would like to first give thanks to my advisor, Dr. Myoseon Jang, for offering me the opportunity to study the exciting research topic, providing me countless support of my research, and writing of this dissertation. Besides, I would like to thank Dr. Nicolo Omenetto, Dr. Jennifer S. Curtis, Dr. Ben Koopman, and Dr. Barron H. Henderson for being my committee members and giving me insightful comments and hard questions.

Next, I would like to give thanks to all my current and past lab mates. Together with these bright guys, I had many unforgettable moments in Florida such as nighttime camping, beach fishing, and river tubing.

I want to thank my husband who always stands by me and cheers me up when I have difficulties, and my daughter who gives me endless happiness.

Last but not the least; I would also like to thank my dad, who is in China, for his love and spiritual supports over the past years, and also my mother, who gave me life and provided me the financial supports to cover the cost of education. I would also like to thank my parents-in-law, who came to the United States to help me taking care of my daughter when I had to work.

TABLE OF CONTENTS

page

LIST OF TABLES

LIST OF FIGURES

LIST OF ABBREVIATIONS

AP	alpha-Pinene (AP) is a major biogenic volatile organic compound, mainly emitted from pine trees, with molecular formula of $C_{10}H_{16}$
BC	Black Carbon (BC) is a type of carbonaceous material formed in flames during combustion of carbon-based fuels.
DL	D-Limonene (DL) is a common biogenic volatile organic compound, emitted from citrus trees, with molecular formula of $C_{10}H_{16.}$
MAC	Mass absorption cross section (MAC m^2g^{-1}) is a measurement for light absorption property of aerosol.
MCM	The master chemical mechanism (MCM) is a near-explicit chemical mechanism which describes the gas phase chemical oxidation of volatile organic compounds.
OC	Organic Carbon (OC) aerosol is a type of organic aerosol contains only carbon and hydrogen, usually oxygen.
POA	Primary Organic Aerosol (POA) is the aerosol which directly emitted from combustion sources.
SOA	Secondary Organic Aerosol (SOA) is a type of organic aerosol that formed through condensation of semivolatile organic compounds in gas phase.
SVOC	Semi volatile organic compounds (VOC) is any organic compound having a boiling point between 250℃ and 400℃ measured at a standard atmospheric pressure of 101.3 kPa
TOL	Toluene (TOL) is a major anthropogenic volatile organic compound, with molecular formula of C_7H_8
UV	Ultraviolet (UV) light is electromagnetic radiation with a wavelength shorter than that of visible light, but longer than X-rays. UV light reaches to troposphere has wavelength ranging from 280nm to 400nm.
VOC	Volatile organic compounds (VOC) is any organic compound having a boiling point less than or equal to 250℃ measured at a standard atmospheric pressure of 101.3 kPa

Abstract of Dissertation Presented to the Graduate School
of the University of Florida in Partial Fulfillment of the
Requirements for the Degree of Doctor of Philosophy

UV-VISIBLE LIGHT ABSORPTION PROPERTIES OF ORGANIC CARBON AEROSOL IN ATMOSPHERE

By

Min Zhong

August 2013

Chair: Myoseon Jang
Major: Environmental Engineering Sciences

Atmospheric aerosols play an import role in climate change through direct interaction with sunlight. Organic carbon (OC) aerosol, which absorbs ultraviolet and short visible wavelength sunlight, is one of the least understood factors in climate change. To quantify the climate effect of organic aerosol, the first step is to obtain its fundamental optical parameters. This study explored a solvent-free method to measure the mass absorption cross-section (*MAC*) of OC, and applied this method to both secondary organic aerosol (SOA) and primary organic aerosol (POA). SOA was produced through photooxidation of different precursor hydrocarbons such as toluene, *d*-limonene, and *α*-pinene using a 2 m^3 indoor Teflon film chamber. Of these three precursor hydrocarbons, the *MAC* value of toluene SOA was the highest compared with *MAC* of *d*-limonene and *α*-pinene SOA. To understand how the composition of SOA affects its *MAC*, a new model to predict the UV-visible absorption spectrum of SOA was developed. The model predicted that, with higher level of NO_x(~100ppb), absorption of toluene SOA would be higher due to the formation of more nitrocatechols. This method was also used to measure *MAC* of POA. Wood burning OC produced under smoldering conditions were photochemically aged using a 104 m^3 dual outdoor chamber under

natural sunlight. Overall, the mass absorption cross-section of OC increased by 11-54% in the morning and then gradually decreased by 19-68% in the afternoon. A similar trend in the change of light absorption was observed in ambient smoke aerosol originating from the 2012 County Line Wildfire in Florida. To quantify the climate forcing of OC, a simple forcing efficiency was used to provide a first estimate of the climate impact of SOA and POA. Our results confirm that SOA can be treated as cooling aerosol, with negative climate forcing similar to inorganic sulfates. POA has the potential to release heat to atmosphere with net positive forcing.

CHAPTER 1
INTRODUCTION

Atmospheric Aerosols and Climate Impact

Atmospheric aerosols are generally defined as those liquid, semi-solid or solid particles suspended in air, having diameters in the range of 1 nm to 10 μm (Seinfeld and Pandis, 1998). Based on their formation mechanisms, atmospheric aerosols can be divided into two categories: secondary aerosols and primary aerosols. Secondary particles are formed through gas-to-particle conversion. For example, ammonium sulfate, $(NH_4)_2SO_4$, is formed through the ammonia titration with sulfuric acid. Primary particles are directly emitted from sources such as biomass burning, sea salt, volcano eruption, and soil. Elemental carbon and most inorganic species are usually the components of primary particles. Figure 1 summarizes typical atmospheric aerosol compositions based on current ambient studies.

Concerns on anthropogenic climate change have drawn attention to the role of atmospheric aerosol in the earth's climate system. Atmospheric aerosols have a significant impact on climate through their direct and indirect influences on climate (Pöschl, 2005;Rosenfeld et al., 2008). Aerosols have a direct climate forcing effect because they scatter and absorb sunlight. They also change the formation and precipitation efficiency of cloud, thus causing an indirect radiative forcing. To measure the influence of aerosol on climate, radiative forcing has been typically used. Radiative forcing (W/m^2) is the rate of energy change per unit area of the globe as measured at the top of the atmosphere. The positive and negative sign of radiative forcing indicate warming and cooling influence of aerosols, respectively.

Unlike greenhouse gases, which are well mixed in the atmosphere and have a long life time in atmosphere, aerosol has much shorter life time, typically on the order of 6 days. The mass concentration, size distribution, and physiochemical properties of aerosols are highly variable in space and time. According to Intergovernmental Panel on Climate Change (IPCC) Assessment (2007), atmospheric aerosols are the largest source of uncertainty in climate forcing estimation.

Among various atmospheric aerosols, inorganic salts such as sea salt and sulfate can cool down the atmosphere by scattering solar radiation (Randles et al., 2004;Tegen et al., 1996). Only a few types of aerosols, such as carbonaceous aerosol and some mineral dusts, have the potential to cause climate warming by directly absorbing solar radiation (Menon et al., 2002). Carbonaceous aerosol includes both organic carbon (OC) and black carbon (BC) aerosol. Light absorption of OC has been poorly understood mainly due to its complex chemical composition as well as evolution of chemical, physical, and optical properties.

Organic Carbon Aerosol

Organic carbon (OC) aerosol is defined as the aerosol which is composed of primarily carbon-containing compounds that include hydrogen and, usually, oxygen. On a global scale, OC is a significant fraction of ambient aerosol, accounting for 20-50% to the total fine aerosol mass at continent (Putaud et al., 2004) and as much as about 90% in tropical forest areas (Andreae and Crutzen, 1997). Compared with other atmospheric aerosols, OC has some unique physical and chemical properties:

1. It absorbs sun light in certain wavelength region, particularly in the UV and short visible range.
2. It has very complex chemical composition, with thousands of chemical compounds present simultaneously in the particle phase.

3. It can undergo a wide range of chemical transformation (oxidation, photolysis, polymerization, etc.) under atmospheric conditions.

OC has been categorized as primary organic aerosol (POA) and secondary organic aerosol (SOA) depending on the source and formation mechanism. POA is directly emitted from sources such as biomass burning and fuel combustion. In the global emission budget, the total POA emission is about 35 TgC per year (Hallquist et al., 2009), which accounts for 23% of total OC flux. SOA is formed from the photochemical oxidation of volatile (VOCs) or semivolatile organic compounds (SVOCs). Biogenic terpenes from vegetation and aromatics from anthropogenic sources can react with oxidants such as OH radical and O_3, to produce less volatile compounds, which can condense on preexisting particles or self-nucleate to form SOA. The total flux of biogenic SOA is 115 TgC per year, contributing to 77% of total OC. Among SOA, 76% is from biogenic VOCs, such as isoprene, α-pinene, and d-limonene.

Optical Properties of Organic Aerosol

Radiative transfer models require the input of optical properties of aerosol, including asymmetry factor, single-scattering albedo, and extinction coefficients (m^2m^{-3} or m^{-1}). The estimation of these parameters is needed in all wavelengths, particularly in the UV-visible wavelength range between 280nm to 700nm. For longer wavelength in the infrared range, scattering and absorption of particles are less important than gas molecules. With given particle size distribution and complex refractive index, it is possible to calculate the optical parameters of aerosol using Mie scattering theory.

The complex refractive index (m) is expressed as: $m = n + k\mathrm{i}$. For organic aerosol, the real part, n, has a value between 1.3-1.7 in the wavelength range of 280-800nm (Nakayama et al., 2013). The real refractive index decreased slightly with

increasing wavelength. The imaginary part, *k*, is directly related to the light absorption capacity of aerosol. Light absorption of OC is wavelength dependent (Kirchstetter et al., 2004;Schnaiter et al., 2005), dramatically increasing towards shorter wavelengths. Since *n* does not change too much and *k* is the optical property most relevant to the positive forcing, this study is focused on light absorption of organic aerosol.

This study uses mass absorption cross section (*MAC*, m^2g^{-1}) to quantitatively describe the light absorption properties of organic aerosol. *MAC* of OC can be calculated from the light absorption coefficient of OC divided by OC mass concentration. *MAC* is related to *k* through the following equation.

$$k = \frac{MAC\ \rho\ \lambda}{4\pi}\ , \qquad (1\text{-}1)$$

where ρ is the density (g/m^3) of OC, λ is the wavelength.

POA from combustion organic carbon has been suggested to a main source of brown carbon, an important light absorbing particulate matter (Andreae and Gelencser, 2006). There is growing evidence (Nozière and Esteve, 2005;Shapiro et al., 2009;Sareen et al., 2010;Laskin et al., 2010b;Bones et al., 2010a;Nakayama et al., 2010a;Zhong and Jang, 2011) to show that SOA potentially would contribute to brown carbon. The recent study by Noziere and Esteve (2005) has demonstrated the formation of light absorbing organic matter due to aldehydes and ketones absorbed by sulfuric acid aqueous solution. Shapiro et al. (2009) and Sareen et al. (2010) also reported the production of chromophores when ammonium ions were added to glyoxal and methylglyoxal. The formation of colored SOA has been observed in either the ozonolysis of biogenic terpenes (Laskin et al., 2010b;Bones et al., 2010a) or the photooxidation of toluene(Nakayama et al., 2010a;Zhong and Jang, 2011).

Direct Climate Impact of Organic Carbon

A relatively limited number of studies have investigated the direct radiative forcing of organic carbon. The estimated value of radiative forcing of organic carbon was -0.3 ~ -0.09 w/m^2 (IPCC, 2007;Maria et al., 2004;Chung and Seinfeld, 2002;Myhre et al., 2009;Hoyle et al., 2009). Both Maria et al.(2004) and Myher et al. (2009) reported the radiative forcing of SOA was -0.1w/m^2. For POA, the average value was -0.14 w/m^2 (Schulz et al., 2006). The results of current model simulation show that both SOA and POA have a direct cooling effect on climate.

However, one big uncertainty in the above models is the optical properties of organic carbon. Models which predict the radiative forcing of SOA took the optical properties of POA for SOA. But the optical properties of POA were treated as the same as those of inorganic aerosols. For example, in the work of Chuang and Seinfeld (2002), the optical properties of OC were similar to sulfate and nitrates. Myher et al (2009) treated POA equivalent to sulfate. These inorganic aerosols are known to be cooling aerosols with negligible absorption in the UV-visible range. However, organic carbon might absorb both UV and visible light. Considering the large source of OC in the atmosphere, quantification of the light absorption properties of organic aerosol is necessary to reduce the uncertainty in climate models.

Motivation and Objectives

Although OC is a major component in atmospheric aerosol, their impact on climate is not well evaluated due to the lack of optical properties of OC. Thus detailed measurement and evaluation of the optical properties of both SOA and POA are necessary to accurately model the climate impact of organic aerosols in atmosphere. The objectives of this work are therefore to:

1. Develop a new methodology to quantify the light absorption properties of organic aerosol;
2. Measure the mass absorption cross section (MAC) of SOA;
3. Investigate the contribution of chemicals to SOA light absorption;
4. Quantify MAC of POA;
5. Evaluate the forcing efficiency of SOA and POA

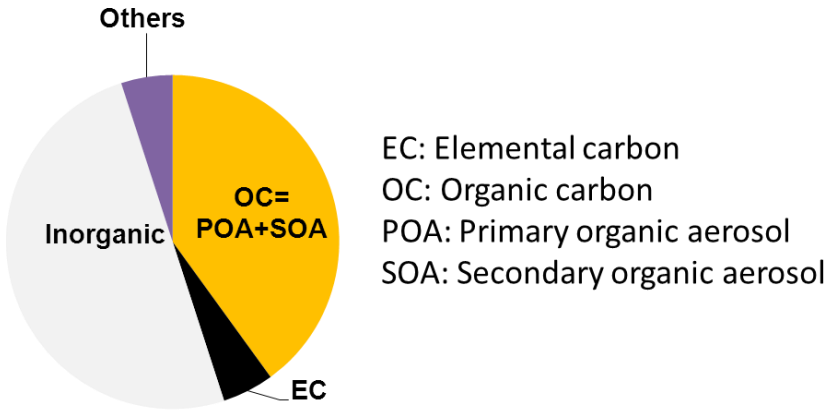

Figure 1-1. Composition of ambient particular matter

CHAPTER 2
MASS ABSORPTION CROSS SECTION MEASUREMENT OF SOA USING A UV-VISBILE SPECTROMETER CONNECTED WITH AN INTEGRATING SPHERE

Background

A substantial fraction (~70%) (Hallquist et al., 2009) of atmospheric organic carbon (20 - 50% of the total fine aerosol mass) (EPA, 2004) is in the form of secondary organic aerosol (SOA), which is produced from atmospheric photochemical reactions of volatile organic compounds with atmospheric oxidants (e.g., OH, O_3, and NO_x). The effect of SOA on climate forcing, however, is poorly understood due to the complexity of chemical compositions of SOA, limitation in product analysis, and the lack of measurement methods for aerosol optical properties.

To date, there is a discrepancy between mode treatment and observation for light absorption properties of SOA. Most direct radiative forcing models consider the light absorption of organic carbon as negligible (Forster, 2007). In contrast, laboratory and field studies have shown that SOA potentially would contribute to brown carbon as an important light-absorbing particulate matter. For example, laboratory studies (Bones et al., 2010b;Laskin et al., 2010a) suggest that SOA formed from the ozonolysis of terpenes can be transformed to brown carbon in the presence of ammonium ion or ammonia gas. In the recent study of $PM_{2.5}$ sampled from fifteen southeastern monitoring sites in the United States, Hecobian et al (2010) has reported that SOA is the one of the major sources of chromophores, contributing 20% to 30% of the light absorption coefficient for the total water soluble OC at 365nm.

The determination of the mass absorption cross section (*MAC*) of SOA is essential to develop a predictive model for radiative forcing of organic aerosol. However, conventional methods for measuring *MAC* of aerosol are limited in either

wavelength or the aerosol sample preparing procedure. For example, typical optical instruments such as an optical photoacoustic spectrometer (Moosmuller et al., 1998), a particle soot absorption photometer (Radiance Research, Seattle, WA), an aethalometer (Magee Scientific, Berkeley CA), an integrating plate photometer (Lin et al., 1973), and an integrating sphere photometer (Campbell et al., 1995), are able to measure *MAC* of aerosol filter samples or the aerosol suspended in the air but operated only at a fixed wavelength (e.g., one to seven wavelengths). Light absorption of actual atmospheric organic aerosol is wavelength dependent due to various functional groups present in the aerosol. Thus, it is necessary to determine *MAC* of organic aerosol over UV-visible wavelengths covering the sunlight spectrum.

As an alternative approach, an aerosol filter sample has been extracted with different solvents and measured for light absorbance using a UV-visible spectrometer covering a wide range of wavelengths. The weakness of the solvent extraction method is the modification of the chemical and physical properties of the aerosol. For example, the esterification of humic-like aerosol products stored in alcohol solvents has been reported (McIntyre and McRae, 2005). Researchers have also shown that carbonyls in SOA react with an alcohol (e.g., methanol) which is used as a solvent forming hemiacetals and acetals (Bateman et al., 2008). It is known that organic compounds react with sulfuric acid and produce organosulfates in aerosol (Iinuma et al., 2007;Surratt et al., 2008;Liggio et al., 2005a). Acetals, hemiacetal, and organosulfates present in aerosol can also return to original parent compounds during the solvent extraction. In addition, the solubility of aerosol products varies depending upon types of solvents. Therefore, a technique for measuring the light absorption coefficient of

aerosol directly using filter samples covering the full spectrum of UV-visible light is needed.

We proposed here to evaluate the feasibility of a UV-visible spectrometer equipped with an integrating sphere for measuring *MAC* of SOA collected on the filter. UV-visible spectrometry is not new, but is a user friendly technique based on a fundamental light absorption theory. The use of a filter for collecting aerosol is also very common and efficient. Yet, it is acknowledged that the UV-visible spectroscopic technique associated with the aerosol filter sample has not been fully developed for the study of an aerosol absorption coefficient. In this study, both the transmittance mode (TUV-IS) and reflective mode (RUV-IS) have been demonstrated for the measurement of *MAC* of chamber generated SOA covering a wide range of wavelengths (280-800nm). Toluene (TOL) as a major anthropogenic precursor hydrocarbon and *d*-limonene (DL) and α-pinene (AP) as major biogenic precursor hydrocarbons, were photochemically oxidized in the presence of NO_x and inorganic seed aerosol using a 2 m^3 Teflon indoor chamber. The influence of the precursor hydrocarbon types, seed acidity, and light source (no light vs. light) on light absorption spectra of SOA has also been investigated.

Experimental Section

SOA Formation

SOA was generated using a 2 m^3 Teflon film chamber equipped with UV and visible lamps. The indoor chamber operation has been reported previously (Cao and Jang, 2007). The chamber is surrounded by 16 lamps with total light emission between 280-900nm. Seed aerosol was generated using a constant output atomizer (TSI, model 3076). Inorganic seed aerosol was made from 0.01M aqueous solution of $(NH_4)_2SO_4$ and a mixture of 1:1 volume ratio of 0.01M solution of H_2SO_4 and NH_4HSO_4 solutions.

After injection of the seed, a known amount of NO_x and HC were injected into the chamber using a gentle stream of the clean air through a manifold and the lights were turned on, marking the starting point of the SOA experiment. For the ozonolysis experiment, ozone was introduced into the chamber by passing clean air through a photolytic ozone generator (Jelight Model 600, Irvine, CA).

The particle population was measured using a scanning mobility particle sizer (TSI, SMPS Model 3080, Shoreview, MN) together with a condensation nuclei counter (TSI, Model 3025A). The gas phase concentrations of hydrocarbons were measured with an HP 5890 GC-FID. The experimental conditions and the resulting data for SOA formed from the oxidation of TOL, AL and AP are shown in Table 2-1 and Table 2-2.

For light absorption analysis, the aerosol was collected on a 13mm diameter filter (Borosilicate microfibers reinforced with a woven glass cloth and bonded with Teflon, Gelman Science Pallflex, Type: TX40H120-WW) using a pump (Gast, DOA-P704-AA) at 13 L/min. To determine the aerosol density, the aerosol volume was measured with SMPS data and the aerosol mass collected on the filter was obtained by weighing the filter mass before and after sampling using an analytical balance (MX5 Mettler-Toledo Ltd., England).

Light Absorption Measurement

The light absorption spectra of aerosol collected on the filter were measured using a Perkin-Elmer lambda 35 UV-visible spectrophotometer equipped with a Labsphere RSA-PE-20 diffuse reflectance accessory. The deuterium lamp generated light between 190 -1100 nm. The wavelength interval of UV-visible spectral data was 1.0 nm and the slit width was 1.0 nm. The filter sample was supported by an in-house developed holder. For the TUV-IS mode, the particle sample filter was placed at the

entrance of the integrating sphere, and a barium sulfate packet for the reflection of transmitted light was attached at the exit of the integrating sphere as shown in Figure 2-1A. For the RUV-IS mode, the filter sample was located at the exit of the integrating sphere (Figure 2-1C). A blank filter was used to establish a zero baseline.

In order to calibrate the measured light absorption coefficients of SOA, the reference aerosol made of Metanil yellow (MY, Aldrich) or the internal mixture of NaCl and MY was introduced into the chamber using a constant output atomizer. MY aerosol was made from 3.5×10^{-5} M aqueous solution of MY. The internal mixed MY-NaCl aerosol is made of the 2:8 volume ratio of 3.5×10^{-4} M MY solution to 0.01 M NaCl solution. The absorption cross section of the reference aerosol was determined from the MY solution of various concentrations. The resulting data for the MY aerosol is summarized in Table A-1.

Results and Discussion

Methodology Development

Theory of transmittance for the particle filter sample

The attenuation of a light beam that passes through a solution can be traditionally expressed by the Beer-Lambert Law as:

$$abs(aq) = \varepsilon cd = \alpha d \,, \qquad (2\text{-}1)$$

where *abs(aq)* is the absorbance of solution, ε is the molar absorptivity of an analyte, c is the concentration of an analyte, α is the attenuation coefficient and d is the beam path length through the cuvette.

For the particle filter sample, light scattering, however, arises from both the filter matrix and particles which have discontinuity for the refractive index among the fibers of the filter materials, the air void, and the aerosol (Figure 2-1B). This light scattering

between interfaces contributes to the light attenuation. A mathematical formula for the light attenuation (*OD*) of the particle in the matrix, as a sum of the optical density (OD_{scat}) by scattering and the optical density (OD_{abs}) by absorption, is expressed as the following form (Anderson and Sekelj, 1967):

$$OD = \log\left(\frac{I_0}{I}\right) = OD_{abs} + OD_{scat} \ , \tag{2-2}$$

$$OD_{abs} = ad \ , \tag{2-3}$$

$$OD_{scat} = -\log_{10}[10^{-edH(1-H)} + q(1-10^{-edH(1-H)})] , \tag{2-4}$$

where I_0 and I are intensity of the incident light and the transmitted light, e and q are constants depending on particle size, wavelength, instrument, filter fiber and aerosol, H is the volume fraction of aerosol in the filter sample, d is the beam path depth, and a is the attenuation coefficient as shown in equation 2-1. OD_{abs} which is treated by the traditional Beer-Lambert Law is linear to the concentration of absorbers. Equations 2-2 decouple the total *OD* into two distinct and independent parts, OD_{abs} and OD_{scat}. Thus, we can evaluate the contribution of aerosol scattering to the total light attenuation.

In our aerosol filter sample, H is very small compared to the filter volume fraction and is almost negligible. OD_{scat} in equation 2-4 is then close to zero when H and $edH(1-H)$ approach zero. The calculated H values for most aerosol samples in our study were less than 1×10^{-3}. Thus, the measured transmittance ($T=I/I_0$) bears an exponential relationship to the aerosol mass on the filter as an analog of the aerosol concentration (equations 2-2 and 2-3):

$$OD = log\left(\frac{I_0}{I}\right) \approx OD_{abs} \ . \tag{2-5}$$

In this study, the MY aerosol and the internally mixed MY-NaCl particles were used as reference particles to test the feasibility of both TUV-IS and RUV-IS. The strong linear relation (R^2: 0.95-0.97) appears in plotting of ln (1/*T*) vs. the mass of MY aerosol in the TUV-IS mode at different wavelengths as shown in Figure 2-2. This result suggests that aerosol absorption coefficient can be mainly expressed by OD_{abs} (Equation 2-3).

Calibration of TUV-IS data

Absorption spectra for the aerosol collected on the filter require a calibration for the increase in path length caused by multiple scattering in the filter fiber. In this study, MY was used for the calibration. In general, the atmospheric organic aerosol could absorb visible light up to 500 nm (Baduel et al., 2009). The absorbing peak of MY is near 422 nm and can cover the light absorption of atmospheric organics in the visible range. The reference absorbance of MY aerosol is obtained as follows:

$$ln(1/T) = L \times n \times \sigma \,, \tag{2-6}$$

where σ is the cross-section (m^2) for absorption of MY, *L* is the length (m) of the tube of the air sample, which is estimated from *V/A*. *n* is the molecular number concentration (#/m^3) of MY suspended in the air and calculated as:

$$n = \frac{V_a \rho \ f}{Mw} \times N_A \tag{2-7}$$

where V_a is the aerosol volume concentration (nL/m^3) obtained from SMPS data, ρ is the density of the MY aerosol(1.43 μg/nL) or MY-NaCl aerosol mixture (2.11 μg/nL in this study), *f* is the mass fraction of MY in the MY-NaCl aerosol , N_A is Avogadro's number and *Mw* is the molecular weight of MY (375.38 g/mol).

σ is related to its molar absorptivity ε ($M^{-1}cm^{-1}$) described as (Lakowicz, 2006):

$$\sigma = 3.82 \times 10^{-25} \varepsilon \,, \qquad (2\text{-}8)$$

where ε is obtained from a plot of the aqueous MY absorbance vs the concentrations using equation 2-1 (when d = 1 cm). Figure A-1 illustrates the ε value of the MY as a function of λ.

The resulting σ values obtained from the MY aqueous solution using equation 2-8 are then used to calculate ln(1/T) in equation 2-6. Figure 2-3A illustrates both the estimated ln(1/T) and the measured ln(1/T) for the MY-NaCl aerosol when MY-NaCl aerosol mass is 29.18 µg. The maximum absorption wavelength (λ_{max}), which occurred at 434nm for the reference aerosol, is 422nm for the measured aerosol as shown in Figure 2-3A. This difference between two λ_{max} indicates that the solvent (water) used for the MY solution can induce the bathochromic shift. Figure 2-3B shows the plot of the theoretically estimated ln(1/T) at λ_{max} = 434 nm using equation 2-6 vs. the measure ln(1/T) at λ_{max} = 422 nm with various aerosol sample mass: slope = 1.4845 with a strong linearity (R^2 = 0.9511). The resulting slope was used as correction factor, C in equation 2-11, to correct the measured ln(1/T) for SOA.

Relationship between TUV-IS and RUV-IS

Since transmittance bears an exponential relationship to the molar absorptivity (ε) of the absorber, it follows that reflectance also has the same relationship to ε. The filter material used in this study has a fabric texture. The beam through a filter medium can travel typically by the diffuse-reflectance mode (Figure 2-1B). The decrease in diffusion reflectance of the filter sample is caused by the absorption of the sample. The linear relationship between reflectance (R) and transmittance (T) may be expressed by (Anderson and Sekelj, 1967):

$$R = C_1 T + C_2 \ . \tag{2-9}$$

C_1 and C_2 are constants at a given aerosol constituent and sample depth. Rearrange equation 2-9, then

$$-log(R - C_2) = log(1/T) - log\, C_1 \ . \tag{2-10}$$

The MY-NaCl aerosol with different sample mass (e.g., 14.5, 29.18 and 41.86 μg) was used to test the relation between *R* and *T*. Plotting of *R* against *T* between 422 nm to 600 nm shows a strong linearity (R^2 = 0.9935, Figure 2-4) using equation 2-9. The resulting C_2 value is -0.0038 and is negligible which can be demonstrated by showing no change in slope and R^2 when C_2 = 0. The resulting C_1 value was 1.01 at both C_2 = -0.0038 and C_2 = 0. C_1 is very close to one, indicating that only a slight difference appears in measured *T* and *R*. The C_1 and C_2 are measurement method dependent constants mainly depending on the reflection of the filter surface. Since the integrating sphere is able to collect most of the reflected and scattered light from the filter sample, the spectrum originated from *RUV-IS* that measures log (1/*R*) is more robust and less sensitive to environmental errors, compared to the *TUV-IS* data. Consequently, *RUV-IS* data includes a smaller error contribution than *TUV-IS*. Hence, in this study, the *RUV-IS* data was used to calculate the absorption coefficient of SOA.

Aerosol Mass Absorption Cross Section Calculation

The volume absorption coefficient (b_v, in unit of m^{-1}) of aerosol in the filter is generally calculated in the transmittance mode following as:

$$b_v = \frac{1}{C}\frac{A}{V}\ln\left(\frac{I_0}{I}\right) = \frac{1}{C}\frac{1}{L}abs\ln(10) \ . \tag{2-11}$$

Here *C* is the correction factor and obtained from the calibration experiment, *A* is the aerosol sampling area (7.85×10^{-5} m^2 in this sampling system) on the filter, *V* is the volume (m^3) of the air sample passing through the filter during a given sampling time, *L* is the length (m) of the tube of the air sample, which is estimated from *V/A*. I_0 and *I* are the transmitted intensity for the blank filter with no aerosol and the filter loaded with aerosol, respectively. *abs* is the absorbance typically measured from a spectrophotometer. In this study, *abs* is measured in both TUV-IS and RUV-IS modes.

In order to compare TUV-IS data among different SOA samples, the mass absorption cross section (m^2/g), *MAC*, can be estimated by normalizing b_v with the aerosol mass concentration (M_V) (g/m^3):

$$MAC = \frac{b_v}{M_V} \quad . \tag{2-12}$$

MAC is also described as (Patterson and Marshall, 1982)

$$MAC = \frac{m_a}{\rho} \quad , \tag{2-13}$$

where m_a is the absorption coefficient (m^{-1}) of a bulk material, ρ is the density (g/m^3) of the absorbing material. The density of SOA is estimated from the aerosol mass and the SMPS aerosol volume data, assuming that the measured aerosol density is similar to the density of the absorbing matter in aerosol. The density of the aerosol is 1.07 g/cm^3 for AP-SOA, 1.27 g/cm^3 for DL-SOA and 1.34 g/cm^3 for TOL-SOA. The imaginary component *k* for a refractive index, which is used for the Mie-scattering calculation, is proportional to m_a at a given wavelength, λ, shown in the following equation:

$$k = \frac{m_a \lambda}{4\pi} \tag{2-14}$$

Application on SOA

Absorption spectra and *MAC* of SOA

The chamber SOA generated from the photooxidation of three different precursors (TOL, DL, and AP) in both the absence and the presence of seed aerosol was collected on the filter and analyzed to measure the absorption spectrum between 280 nm and 800 nm. Figure 2-5 illustrates the absorption spectra of various SOA. Because there was no significant absorption beyond 580 nm for all SOA, absorption spectra were mainly focused on the wavelengths between 280 and 580 nm. All SOA filter samples strongly absorb UV light and the absorption intensities dramatically increase as the wavelength becomes shorter. In the visible range, the intensity of SOA light absorption varies with the types of precursors. The color of the TOL-SOA filter sample was yellowish indicating that TOL- SOA can absorb visible light while no color was observed for the AP-SOA in this study. The fresh DL- SOA showed no color for the first 20 minutes after collection on the filter, but it gradually turned to yellow during the next three hours standing in room air. The absorption spectra of DL- SOA were shown in Figure A-2.

The UV-visible spectrum of SOA is originated from a variety of oxygenated products. The chemical functional groups present in SOA provide useful insight for SOA spectra. For example, both AP- SOA (Jang and Kamens, 1999;Camredon et al., 2010) and DL- SOA (Grosjean et al., 1993;Glasius et al., 2002;Leungsakul et al., 2005) contain non-conjugated oxygenated compounds. AP-SOA includes pinonaldehyde, norpinonic acid and hydroxyl pinonadehydes, pinonic acid, and pinic acid and DL-SOA includes keto-limononaldehyde, keto-limonomic acid and keto-limonalic acid. The $n \rightarrow \pi^*$ transitions absorption of such non-conjugated carbonyl and carboxylic acid products

typically appears between 280 and 300nm. The absorption of TOL-SOA (Figure 2-5A) between 400 and 500 nm is most likely contributed from $\pi \rightarrow \pi^*$ transitions from conjugated double bond (e.g. aromatic ring) and $n \rightarrow \pi^*$ transitions from chromophoric groups (e.g., NO_2, C=O) and auxochromic groups (e.g., OH,). For example, 4,6-dinitro-o-cresol, one of the major TOL-SOA products (Jang and Kamens, 2001b) can show a yellow color corresponding with the visible absorption spectrum beyond 400nm (Howard, 1991).

Figure 2-5D shows the UV-visible spectrum of the DL-SOA produced from the ozonolysis of DL in the absence of inorganic seeds. The absorption peak at 428nm gradually increased for 7 hours during the experiment. A possible explanation for such an absorption peak is the formation of conjugated products through particle phase reactions. A proposed scheme is shown in Figure 2-8. Both limononaldehyde and 5-oxo-limononaldehyde are major products from ozonolysis of *d*-limonene and can produce colored products through the acid-catalyzed aldol condensation between these two products, followed by dehydration and a double bond rearrangement.

Figure 2-6 illustrates the comparison of the mass absorption cross section (*MAC*) at 350 nm and 450 nm among three different SOA (TOL-, DL- and AP-SOA). Overall, photooxidation of TOL gives the highest *MAC*, followed by DL-SOA and AP-SOA for both neutral and acid seeds. Since the SOA absorption property is directly related to oxygenated products originated from the oxidation of precursors, the chemical structure of precursors are expected to affect *MAC* of SOA. TOL is expected to produce SOA with more conjugated functional groups and higher *MAC* due to three double bonds in TOL. AP has an endocyclic double bond and DL has two non-conjugated double bonds.

Data in Figure 2-6 shows that *MAC* of TOL-SOA at 350nm is 15 times higher than that of fresh DL-SOA and 20 times higher than AP SOA.

Effect of inorganic seeds

The effect of the preexisting inorganic seed on SOA absorption coefficients is shown in Figure 2-6. In the UV range, the presence of both neutral and acidic inorganic seeds considerably increases light absorption of TOL-SOA and DL-SOA. For example, with $(NH_4)_2SO_4$ seed aerosol, *MAC* of TOL-SOA at 350 nm increased by 3.1 times compared to a no seed condition. In the same way, *MAC* of TOL-SOA with acidic seed aerosol (NH_4HSO_4:H_2SO_4 = 1:1) is 2.1 times higher than that of TOL-SOA without seeds. The effect of the seed aerosol on *MAC* is the highest with TOL. For both TOL-SOA and DL-SOA, the *MAC* value is higher in the presence of $(NH_4)_2SO_4$ than that in the presence of acidic seed aerosol. No significant difference appears between the seed and no seed condition for AP-SOA.

The brown or yellow color products have been reported for SOA from ozonolysis of *d*-limonene in the presence of amino acids, $(NH_4)_2SO_4$, or the mixed vapor of NH_3 and HNO_3 (Bones et al., 2010b;Laskin et al., 2010a). Brown color products have also been reported by reaction between glyoxal aerosol and amino acids (Galloway et al., 2009). Such studies suggest that light absorbing materials would be originated from C-N containing compounds (Galloway et al., 2009). The possible pathways to form the light absorbing species include aldol condensation, imidazole formation, Leuckart / Mannich reactions and pyridinim ions formation (Nozie`re and Esteve 2007;De Haan et al., 2009;Bones et al., 2010b). However, explanations for the SOA color change due to inorganic species are still unclear and require the future investigation.

Effect of light source

To investigate the effect of light source on SOA light absorption, several sets of SOA experiments have been conducted with and without light for both TOL and AP systems. Figure 2-7 summarizes the impact of light exposure on *MAC* of SOA under various experimental conditions of different oxidation, precursor HCs and preexisting seed aerosol. For DL-SOA, the time profiles of *MAC* (λ= 428nm) of the photoirradiated SOA in the presence of NO_x were compared to those of the SOA produced through ozonolysis under no light (Figure 2-7A). *MAC* values of DL-ozone-SOA at 428 nm (the small peak in the visible range, shown in Figure 2-5D) continuously increases, while those of photochemically irradiated DL-NO_x-SOA gradually decrease. For TOL-SOA, to determine the effect of light source on *MAC* values, the *MAC* value at 120 minutes (photooxidation with light) was subtracted from *MAC* values at 240 minutes (oxidation both with and without light) under the same experimental conditions. For oxidation experiments without light, the light source had been turned off immediately after SOA was sampled at 120min. The reduction of *MAC* (λ= 350nm) for TOL-SOA was observed with light exposure compared with the *MAC* without a light source, as shown in Figure 2-7B.

We conclude that the light source influences the light absorption of atmospheric organic compounds in two opposite ways. One is the formation of light absorbing products from the atmospheric oxidation of precursor HCs. For example, the colored products such as nitrophenols in TOL-SOA are formed from toluene photooxidation with OH radicals in the presence of NO_x. Opposite to the color production in SOA, the bleaching effect of the light source progresses in SOA through further photoirradiation of light absorbing organics. For example, the π-conjugated organic compound as an

oxygenated SOA product can be further photodissociated with the UV-visible light which excites organic compounds through a π-π^* transition. The n-π^* transitions in carbonyls is also able to decompose carbonyls *via* Norrish type-I and -II mechanisms (Calvert and Pitts, 1966.). As previously reported by Mang et al (2008, photodegradation of the DL-SOA collected on a glass fiber filter produced large amounts of small molecules such as CO, CH_4, acetaldehyde, acetaone and other VOCs, resulting in off-gassing of those organics from SOA into the air.

Conclusion and Atmospheric Implication

In this study, light absorption of a variety of SOA (equation 2-12) generated using the indoor chamber has been measured using the TUV-IS and the RUV-IS. The resulting *MAC* value enables estimation of absorption coefficient (m_a in equation 2-13) of SOA. Consequently, the imaginary part k of the reflective index of SOA can be estimated from m_a values using equation 2-14. For the chamber generated SOA, k values are in the order of 10^{-4} to 10^{-2} at 350 nm. The k values of SOA are relatively smaller than those for black carbon which ranges between 0.63~0.79 at 550 nm (Bond and Bergstromb, 2006), and atmospheric brown carbon which is about 0.27 at 550 nm (Alexander et al., 2008). Compared with black carbon and brown carbon, the light absorption of freshly chamber-produced SOA of this study is relatively weak even in the UV range.

This study has focused on *MAC* values of SOA formed within 1-7 hours after the reaction began using the 2 m^3 chamber that facilitates the artificial UV-visible light source. However, *MAC* values of the ambient SOA that is photoirradiated under actual sunlight for longer time (on average 6 days of aerosol life) would be different than those of the indoor chamber SOA. In the future, the outdoor chamber or the ambient field

studies using TUV-IS and the RUV-IS methods are necessary to investigate the light absorption of aged SOA

Both TUV-IS and the RUV-IS techniques are simple because they do not require solvent extraction and allow direct measurement of the *MAC* value of aerosol filter samples. The TUV-IS and the RUV-IS techniques are reproducible and sensitive even to a small amount of aerosol mass. The detection limit of this method not only depends on molar absorptivity of a variety of analytes but also is a function of wavelength showing a higher detection limit in the longer wavelength. For example, the lowest detectable aerosol mass is 5 ng at 422 nm for MY aerosol, 6 μg at 350nm for chamber-generated toluene SOA, and 14 μg at 350 nm for ambient particle collected at the sampling site at Gainesville, FL. The major uncertainty in both the TUV-IS and the RUV-IS methods is the scattering of light caused by the filter material. Different filter materials can produce different scattering effects on the calibration curve (Figure 2-3).

Table 2-1. Experimental conditions and the resulting SOA data for photooxidation of toluene using the 2 m^3 Teflon film chamber [a]

Precursor HCs	No.	Seed	RH %	Initial NO_x (ppb)	Initial O_3 (ppb)	Initial HC (ppb)	Δ HC ($\mu g/m^3$)	f [b]	SOA mass conc. ($\mu g/m^3$)	L [c] (m)	ln(1/R) $_{\lambda = 350}$	$b_{v\,\lambda=350}$ (Mm^{-1})	$MAC_{\lambda=350}$ (m^2g^{-1})	$m_{\lambda=350}$ ×10
Toluene	T1	None	42	62	NA	207	149	NA	46.0	4377	7.5E-02	26.43	0.574	0.214
	T2	AS	70	62	NA	291	197	0.54	37.6	3925	1.7E-01	66.43	1.767	0.660
	T3	Acid	40	70	NA	193	155	0.60	34.5	4118	1.1E-01	41.62	1.208	0.451
	T4	None	43	70	NA	202	188	NA	47.2	5045	8.9E-02	27.23	0.577	0.215
	T5	AS	72	69	NA	195	322	0.63	44.1	4304	1.9E-01	66.73	1.514	0.565
	T6	Acid	35	68	NA	193	131	0.65	30.9	4503	1.0E-01	34.85	1.128	0.421

a. Temperature: 294 –298 K.

b. The seed fraction of SOA was calculated from SMPS data at a given reaction time, 2h for T1-T6.

c. The length of the tube for the air sample that includes the suspended aerosol is obtained by dividing the air sample volume with the sample area on a filter.

Table 2-2. Experimental conditions and the resulting SOA data for oxidation of *d*-limonene and *a*-pinene using the 2 m^3 Teflon film chamber [a]

Precursor HCs	No.	Seed	RH (%)	Initial NO_x (ppb)	Initial O_3 (ppb)	Initial HC (ppb)	Δ HC ($\mu g/m^3$)	f [b]	SOA mass conc. ($\mu g/m^3$)	L [c] (m)	ln(1/R) $_{\lambda = 350}$	$b_{v\,\lambda=350}$ (Mm^{-1})	$MAC_{\lambda=350}$ (m^2g^{-1})	$m_{\lambda=350}$ ×10
d-Limone	L1	None	35	62	NA	188	1058	NA	409.9	1047	1.06E-02	15.69	0.038	0.014
	L2	AS	70	70	NA	183	803	0.64	362.5	924	2.25E-02	37.82	0.104	0.037
	L3	Acid	37	72	NA	193	986	0.49	308.7	706	8.82E-03	19.39	0.063	0.022
	L4	None	56	NA	126	189	1061	NA	588.5	936	8.73E-03	14.48	0.025	0.009
	L5	AS	69	NA	107.3	158	708	0.48	243.6	1539	8.20E-03	8.26	0.034	0.012
	L6	Acid	49	NA	140	207	1163	0.46	449.2	1698	1.27E-02	11.64	0.026	0.009
α-Pinene	A1	None	37	68	NA	142	710	NA	133.5	2078	5.18E-03	3.86	0.029	0.009
	A2	AS	70	71	NA	159	772	0.5	164.6	1030	5.42E-03	8.15	0.05	0.015
	A3	Acid	38	62	NA	142	685	0.68	140.7	1059	3.71E-03	5.44	0.039	0.012

a. Temperature: 294 –298 K.

b. The seed fraction of SOA was calculated from SMPS data at a given reaction time, 1h 40 min for L1-L6, 2h for A1-A3.

c. The length of the tube for the air sample that includes the suspended aerosol is obtained by dividing the air sample volume with the sample area on a filter.

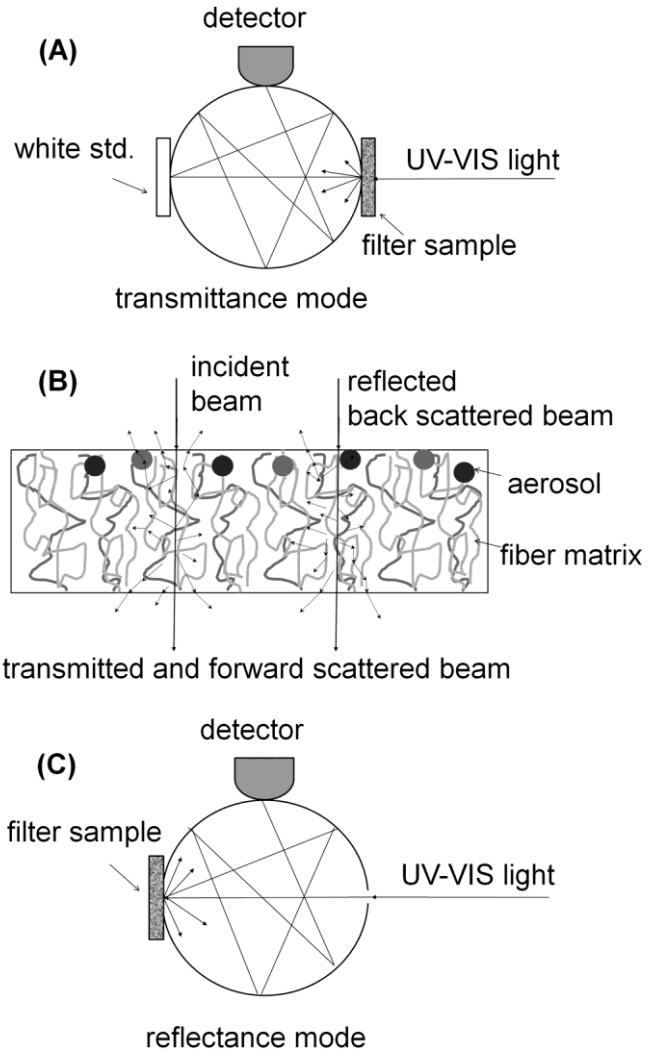

Figure 2-1. Schematic diagram for the beam pathway in both transmittance and reflectance mode: A) transmittance mode B) beam interaction with particles and filter matrix, and C) reflectance mode.

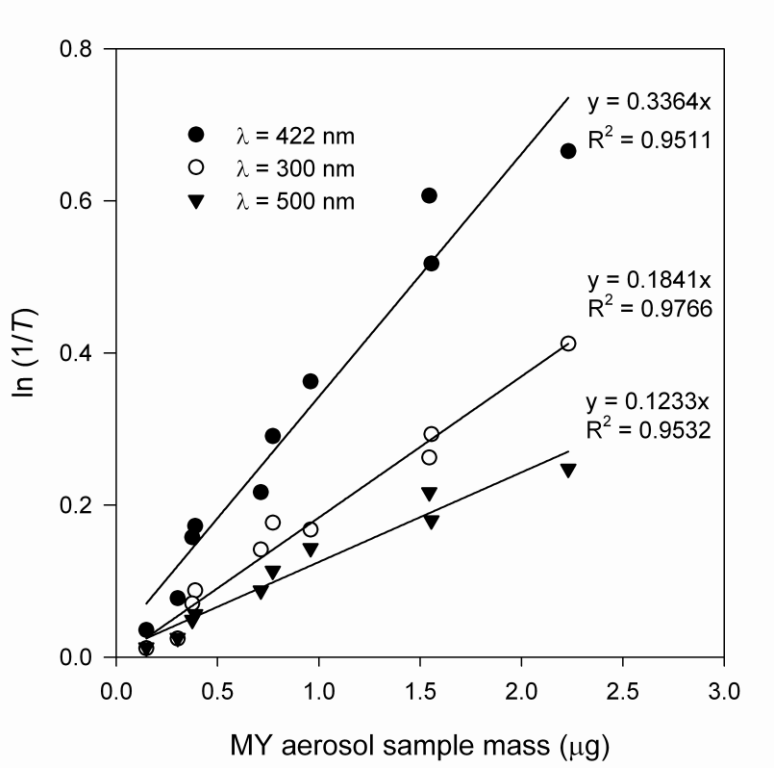

Figure 2-2. ln(1/T) plotted vs. metanil yellow aerosol mass collected on filter at three different wavelengths (422 nm, 300 nm, and 500 nm).

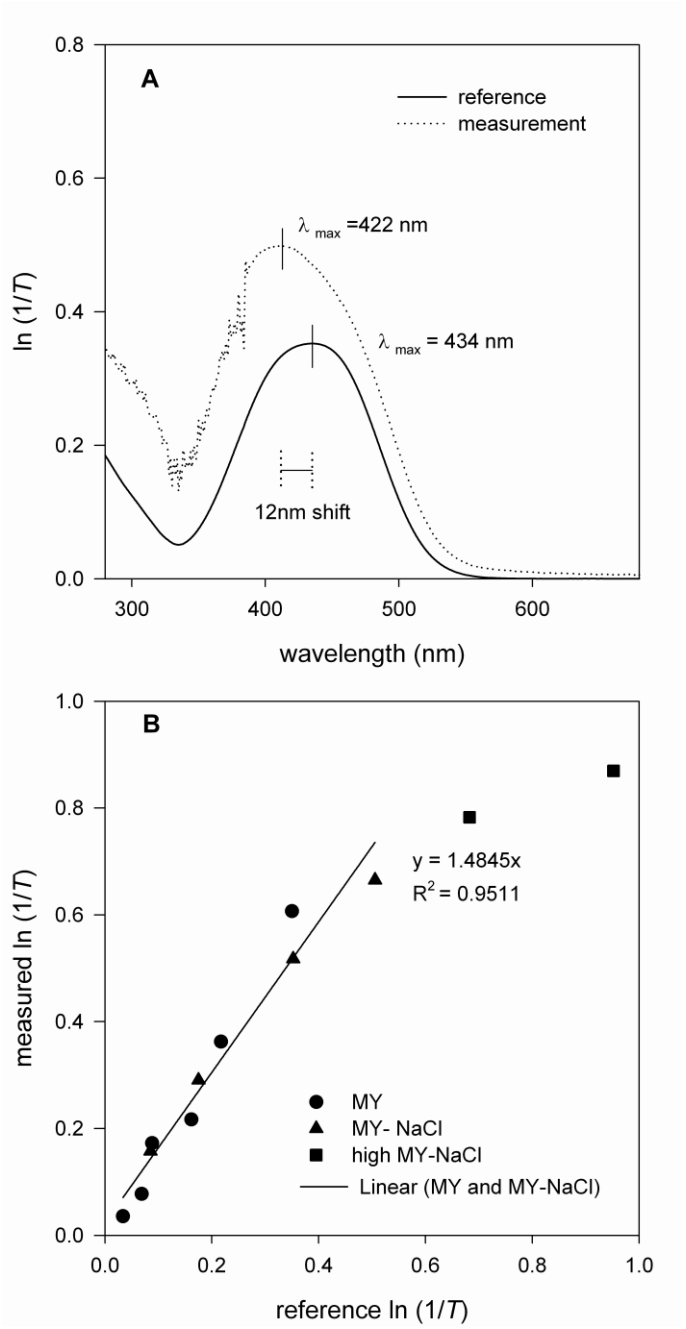

Figure 2-3. Measured ln(1/*T*) vs theoretical ln(1/*T*): (A) for the MY-NaCl aerosol as a function of wavelength, (B) for different MY-NaCl mixture at 434 nm.

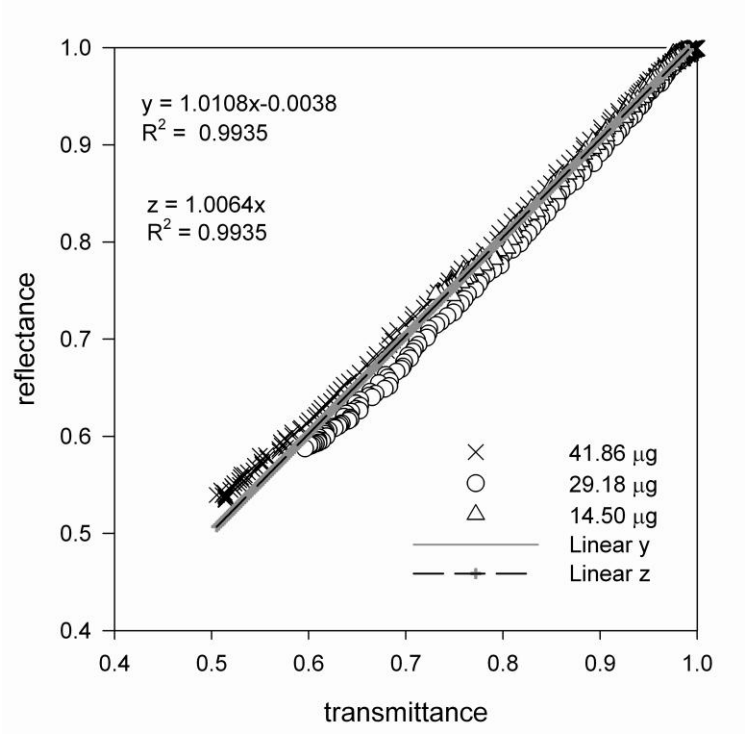

Figure 2-4. Reflectance is plotted against transmittance at 422~680 nm for MY-NaCl aerosol with different particle mass (41.86, 29.18, and 14.5). The linear regression lines with an intercept (C1 = 1.0108) and with intercept = 0 (C1 = 1.0064).

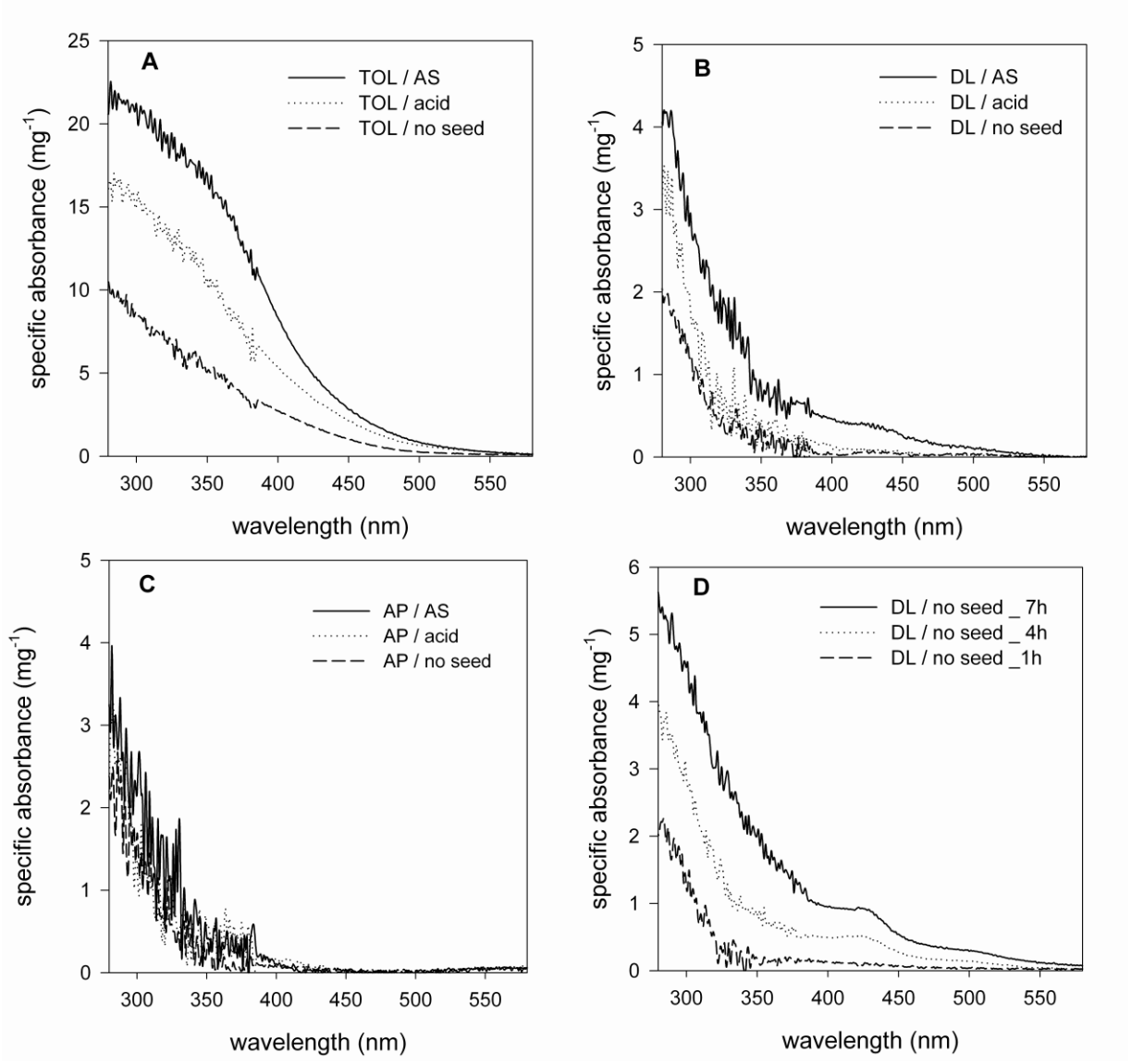

Figure 2-5. UV-visible spectra of SOA freshly generated from photooxidation of different hydrocarbons: (A) toluene using data T1-T3 in Table 2-1 , (B) *d*-limonene using data L1-L3 in Table 2-2, and (C) *α*-pinene using data A1-A3 in Table 2-2 (C). AS denotes the $(NH_4)_2SO_4$ seed condition and acid denotes the acidic seed (NH_4HSO_4:H_2SO_4=1:1) condition. UV-VIS spectra of DL-SOA (L4 in Table 2-2) formed from ozonolysis of *d*-limonene without seed at different oxidation time (D). For comparison, the specific absorbance is reported by dividing ln(1/*R*) with the mass of organic aerosol collected on the filter.

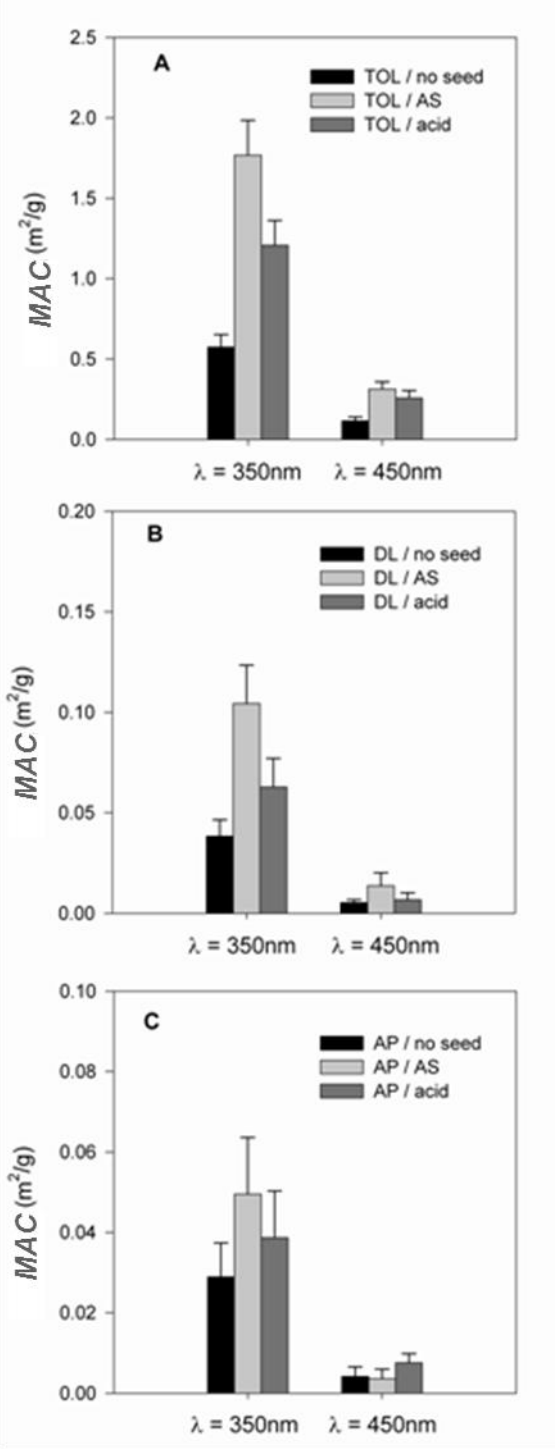

Figure 2-6. *MAC* values of SOA formed from three hydrocarbon precursors at λ=350 nm and 450 nm: (A) toluene, (B) *d*-limonene, and (C) α-pinene, under different seed conditions. AS: $(NH_4)_2SO_4$. Acid: seed aerosol made of NH_4HSO_4: H_2SO_4=1:1

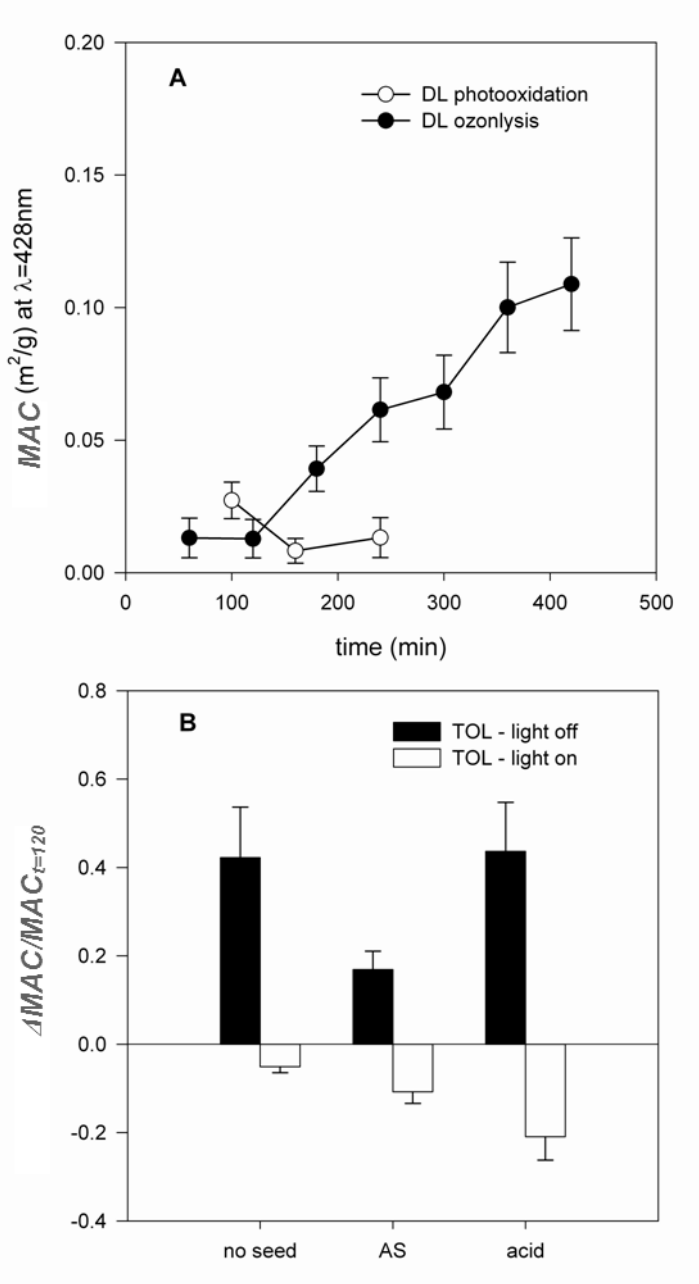

Figure 2-7. Effect of light on MAC of *d*-limonene and toluene SOA. (A) The time profile of *MAC* (at λ=428 nm) for DL-SOA formed from ozonolysis and phorooxidation of *d*-limonene in the presence of NO_x without seed (L4). (B) The reduction ratio of *MAC* for TOL-SOA due to the exposure to light source at different seed conditions (T1-T6). The reduction ratio is obtained by dividing the *ΔMAC* (*ΔMAC* = *MAC*.at 240 minutes oxidation - *MAC* at 120 minutes photooxidation) with *MAC* at 120 min photooxidation.

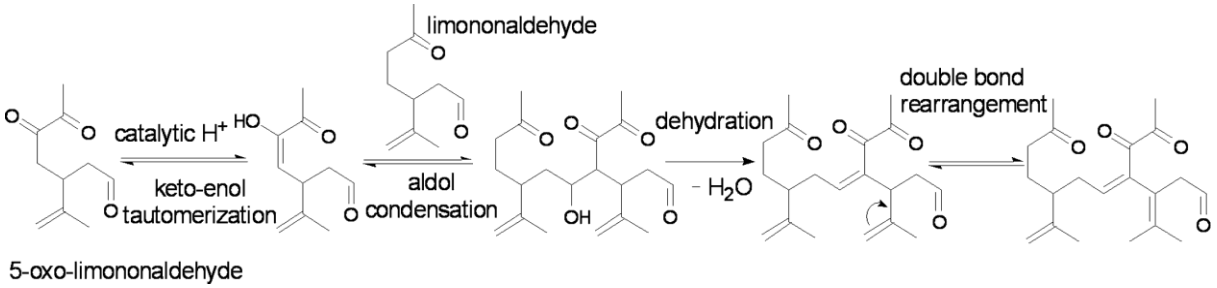

Figure 2-8. Proposed example of conjugated compound formation through aerosol-phase reaction in d-limonene SOA

CHAPTER 3
THE SOA FORMATION MODEL COMBINED WITH SEMIEMPIRICAL QUANTUM CHEMISTRY TO PREDICT UV-VIS ABSORPTION OF SECONDARY ORGANIC AEROSOLS

Background

Light absorption of aerosol is mainly determined by its chemical composition. The chemical composition of SOA is complex due to the multi-generational gas phase reactions of VOCs with atmospheric oxidants (e.g., O_3, OH, NO_2 and NO_3) and aerosol phase reactions. Very few SOA products have been identified, although much effort has been expended in this direction. For example, in a study by Forstner et al.(1997), identified SOA products from the photooxidation of aromatic hydrocarbons were only 15~30% of the total extractable SOA. Also, in a recent study by Sato et al. (2007), using liquid chromatography-mass spectrometry (LC-MS), only ~1wt% of the total mass of aerosol products from the photooxidation of toluene were identified. For α-pinene SOA, relatively complete product identification has been achieved. Jaoui and Kamens (2001) have identified more than 80wt% of α-pinene SOA products. The possible difficulty in characterizing SOA products is the unidentified aerosol phase reactions which lead to the formation of oligomeric compounds. High molecular weight structures are ubiquitous in SOA's compositions and they may account for a significant portion of the SOA mass (Gao et al., 2004;Tolocka et al., 2004;Kalberer et al., 2004). The great complexity of the SOA composition inhibits an improved understanding of the light absorption properties of SOA. Thus, the development of a model to overcome this difficulty would enhance our knowledge of how the composition of SOA affects its optical properties.

A few modeling approaches have been developed to predict the light absorption spectrum of organic aerosols. Lund Myhre and Nielsen (2004) calculated the absorption index of synthetic organic aqueous mixtures by an empirical approach using the measured absorption index of individual acids. Sun et al.(2007) employed the Band-gap and Urbach tail relationships to predict UV-visible absorption spectra of various organic aerosols. Moosmuller et al.(2011) calculated the absorption index of brown carbon using a damped simple harmonic oscillator model. However, to the best of our knowledge, development of a model for light absorption of SOA based on the chemical composition has not yet been explored.

The prediction of the UV-visible absorption spectrum of SOA on the basis of first principles begins with spectra of individual organic compounds. To calculate the light absorption spectra of organic compounds, quantum chemistry has been frequently employed. Popular computational approaches include *ab initio* quantum chemistry methods (Runge and Gross, 1984) and semiempirical methods (Zerner, 1991;Dewar et al., 1985). In this study, prediction of UV-visible spectra of a variety of organic compounds was approached with the AM1 (Austin Model 1) method (Dewar et al., 1985) based on the NDDO (Neglect of Diatomic Differential Overlap) semiempirical quantum chemistry approximation since it provides spectral predictions with reasonable accuracy and inexpensive computation. The NDDO based methods have been proven to be a useful tool using configuration interaction to calculate the spectroscopic properties of many organic compounds (Fabian et al., 2002;Matsuura et al., 2008).

The SOA chemical composition used for the SOA light absorption model was predicted from the SOA formation model by explicitly analyzing the gas phase kinetics

of a precursor VOC. Jang et al. (2006) in their recent study incorporated both heterogeneous reactions of organic products and gas-particle partitioning into a SOA formation model named PHRCSOA (Partitioning Heterogeneous Reaction Consortium Secondary Organic Aerosol Model). The PHRCSOA model has been evaluated for both α-pinene ozonolysis (Jang et al., 2006) and toluene photooxidation (Cao and Jang, 2010) in the presence of inorganic seeds. This model tends to reasonably predict precursor hydrocarbon decay, NO-NO_2 conversion, ozone formation and SOA mass.

In this study, an NDDO based semi-empirical quantum chemistry method and the PHRCSOA model are implemented to predict the UV-visible absorption spectrum of SOA. The absorption spectrum of SOA is calculated by taking the summation of spectrum of each individual SOA product. The model was tested and evaluated by chamber generated SOA. Toluene, which is a major anthropogenic precursor, or α-pinene, a major biogenic precursor, was photochemically oxidized in the presence of inorganic seed aerosol using a 2 m^3 indoor Teflon chamber. The influence of NO_x on light absorption of SOA was also investigated.

Experimental Section

SOA Formation

All experiments were conducted in a 2 m^3 indoor Teflon film chamber under UV-visible light. A detailed description of the procedures for chamber experiments and sample measurements has been provided elsewhere (Cao and Jang, 2010). The chamber is surrounded by 16 lamps with light emission in a range between 280nm and 900nm. Prior to each SOA experiment, the chamber was flushed with clean air from a clean air generator. The inorganic seed aerosols were injected into the chamber by nebulizing an inorganic aqueous solution using a Constant Output Atomizer (TSI, Model

3076, Shoreview, MN). The inorganic seed was made from a 0.01mol L^{-1} aqueous solution of $MgSO_4$. After injection of the seed, a known amount of NO was added into the chamber from a certified NO tank. Once the NO_x concentration became stabilized, a known volume of volatile hydrocarbon (HC) precursor was injected and the lamps were turned on, which marked the starting point of the SOA experiment. The HCs used in this study include toluene (99%, Aldrich) and α-pinene (98%, Aldrich).

The particle population was measured continuously using a scanning mobility particle sizer (TSI, SMPS Model 3080, Shoreview, MN) together with a condensation nuclei counter (TSI, Model 3025A). The gas phase concentrations of HCs were measured with a HP 5890 GC-FID. Ozone and NO_x concentrations were monitored using a photometric ozone detector analyzer (model 400E, Teledyne Instruments, San Diego, CA) and a chemiluminescence NO_x detector (model 200E, Teledyne Instruments, San Diego, CA). Temperature and humidity were measured with an electronic thermo-hygrometer (Hanna Instruments, Italy). The humidity of the chamber experiments ranged between 43~47%, while temperature was 294–298 K with an increase of around 4K for the duration of the SOA experiment.

SOA UV-Visible Spectra Recording

The resulting aerosol was collected on a 13mm diameter filter (Borosilicate microfibers reinforced with woven glass cloth and bonded with Teflon, Gelman Science Pallflex, Type: TX40H120-WW) using a pump (Gast, DOA-P704-AA). The UV-visible spectra of aerosols collected on the filter were directly measured using a Perkin-Elmer lambda 35 UV-visible spectrophotometer equipped with a Labsphere RSA-PE-20 diffuse reflectance accessory. The deuterium lamp generated light between 190–1100 nm. The wavelength interval of UV-visible spectral data was 1.0 nm. The filter sample

was supported in a home-made filter holder and was located at the exit of the integrating sphere upon which light absorptions measurements were performed (see Figure 3-1). For the zero baseline, a blank filter was used. The aerosol absorption measurement using filter samples is simple because this technique does not require solvent extraction. The detection limit of this method not only depends on molar absorptivity of a variety of analytes but also is a function of wavelength showing a higher detection limit in the longer wavelength. The lowest detectable aerosol mass is 6 μg at 350 nm for chamber-generated toluene SOA. The detailed measurement procedure of SOA light spectra can be found in our previous study (Zhong and Jang, 2011). The experimental conditions and the resulting data are shown in Table 3-1.

Results and Discussion

Measurement of SOA UV-Visible Spectra

The light absorbance of organic aerosol, A_{SOA}, is defined as:

$$A_{SOA} = \ln\left(\frac{I_0}{I}\right)_{SOA}, \tag{3-1}$$

where I_0 and I are the transmitted intensities of light at a specific wavelength (λ) without and with aerosol, respectively. A_{SOA} can be obtained by converting the experimentally measured absorbance, abs_{SOA}:

$$A_{SOA} = \frac{1}{C} abs_{SOA} \ln(10), \tag{3-2}$$

where C is a correction factor with a value of 1.4845 obtained from our previous study (Zhong and Jang, 2011) for the purpose of eliminating the absorbance caused by filter material scattering.

Theoretical Calculations of SOA UV-Visible Spectra

The light absorbance of SOA (A_{SOA}) can also be calculated by taking the sum of each individual spectrum of a SOA product and described as:

$$A_{SOA} = \sum A_k \ , \tag{3-3}$$

where A_k is the absorbance of individual species (k) of SOA. The light absorbance of individual species A_k is calculated as (Lakowicz, 2006),

$$A_k = \frac{V}{A} \times n_k \times \sigma = 3.82 \times 10^{-25} \frac{V}{A} \times n_k \times \varepsilon_k \tag{3-4}$$

In this expression, σ is the cross-section area for absorption in m^2, V is the volume (m^3) of air passing through the filter during a given sampling time, and A is the filter surface area exposed to the sample (7.85×10^{-5} m^2 in this sampling system). ε_k is the molar absorptivity (L $mol^{-1}cm^{-1}$), which is predicted using a semiempirical quantum chemistry method. n_k is the molecular number concentration(# m^{-3}), which is calculated from the mass percentage of component k:

$$n_k = \frac{OM_T \times F_k}{10^8 MW_k} \times N_A \, . \tag{5}$$

MW_k is the molecular weight (g mol^{-1}), N_A is the Avogadro's number and F_k is the mass percentage. F_k is determined by the mass balance of organic compounds in SOA. OM_T is the total SOA mass concentration and is predicted by the SOA formation model.

SOA Formation Model

The SOA formation model, (i.e., the PHRCSOA model), which includes a heterogeneous reaction model and a partitioning model, is used to predict the SOA mass from heterogeneous reaction (OM_H) and partitioning (OM_P). The detailed description of the PHRCSOA model can be found in the work of Cao and Jang(Cao and

Jang, 2010). The model starts from the gas-phase oxidation of VOCs described by the master chemical mechanism (MCM 3.2, http://mcm.leeds.ac.uk/MCM). A chemical kinetic solver (Morpho) was used to run the gas phase kinetic reaction model (Jeffries et al., 1998). The comparisons between model simulations and experimental data for toluene or α-pinene decay, ozone formation and NO_x consumption at different NO_x levels are shown in Figures B-1and B-2 (supporting information). Among the products predicted from the MCM model (Figure 3-2), the oxygenated products that can significantly contribute SOA mass are chosen. A total of 147 products from the oxidation of toluene and 129 products from the oxidation of α-pinene were used to predict the SOA mass.

The selected gas products are lumped into 20 groups according to their vapor pressures and reactivity in the aerosol phase. The vapor pressure (bar) is estimated by the following equation (Schwarzenbach et al., 1993):

$$\ln P^0 = \frac{\Delta S_{\text{vap}}(T_{\text{b}})}{R}\left[1.8\left(1-\frac{T_{\text{b}}}{T}\right)+0.8\left(\ln\frac{T_{\text{b}}}{T}\right)\right], \quad (3\text{-}6)$$

where ΔS_{vap} is the entropy of vaporization ($Jmol^{-1}K^{-1}$) which is calculated by the Trouton's rule modified by Zhao et al. (1998) with parameters related to molecular geometry. T_b is the boiling point (K) which is estimated from a group contribution method originally developed by Joback and Reid (1987) with a modified equation and group contribution parameters (Stein and Brown, 1994). T is the ambient temperature (K). R is the gas constant (8.314 $JK^{-1}mol^{-1}$).

The vapor pressures of gas phase organic products are categorized into five groups labeled by *i*, with *i* = 1 through 5 corresponding to 1.3×10^{-4}, 1.3×10^{-3}, $1.3\times10^{-}$

^{2} , 1.3×10^{-1} and 1.3 Pa respectively. Each group is then divided into four subgroups (*j*) according to the reactivity in the aerosol phase; *j* = PO, H-s, H-m, and H-f correspond to partitioning only, slow reactivity, middle reactivity and fast reactivity. The reactivity can be ranked by the order of functional groups: multifunctional aldehydes > aldehydes > ketones > carboxylic acids. The photochemical reactions then can be expressed as,

$$\text{Precursor} + OH \rightarrow \alpha_{1,PO} S_{1,PO} + \alpha_{2,PO} S_{2,PO} + \ldots + \alpha_{1,H\text{-}f} S_{1,H\text{-}f} + \alpha_{2,H\text{-}f} S_{2,H\text{-}f} + \ldots + \alpha_{1,H\text{-}m} S_{1,H\text{-}m} + \alpha_{2,H\text{-}m} S_{2,H\text{-}m} + \ldots + \alpha_{1,H\text{-}s} S_{1,H\text{-}s} + \alpha_{2,H\text{-}s} S_{2,H\text{-}s}$$

where $\alpha_{i,j}$ is the mass-based stoichiometric coefficient for the lumped group $S_{i,j}$.

The aerosol phase reactions producing OM_H through dimerization of organic compounds are assumed to be second-order reactions and the reaction rate is estimated from the semiempirical model which has been addressed in the previous study (Jang et al., 2006). The resulting OM_H is then taken as the preexisting absorbing material and integrated into a SOA partitioning model to calculate OM_P. The SOA partitioning model employed in this study was developed by Shell et al. (2001) and has been used in the regional air quality model (CMAQ 4.7). The summation of OM_H and OM_P gives the total mass of SOA (OM_T):

$$OM_T = OM_H + OM_P \tag{3-7}$$

The detailed derivation and mathematical expressions for OM_H and OM_P can be found in the previous work (Cao and Jang, 2010) of our group. Figure B-3 shows the simulated OM_T levels under different NO_x conditions. The error range for the difference between the predicted and observed aerosol mass concentration is ±7.3% at the 95% confidence level for 20 samples (Cao and Jang, 2010).

SOA Products

Based on the contributions to the total SOA mass, major SOA species (*k*) are selected among the products predicted using the master chemical mechanism kinetic model. The distribution of the selected SOA products is presented in Table 3-2 for toluene SOA and in Table 3-3 for α-pinene SOA. In our calculation, the selected SOA compounds contribute more than 97% of total SOA mass for both toluene and α-pinene SOA. For calculating light absorption spectra of glyoxal (GLYOX) and methlyglyoxal (MGLYOX), their oligomeric forms are used based on the structures known in literature (Liggio et al., 2005b;Hu et al., 2007). 2-Dihydroxymethyl- [1,3]-dioxolane-4,5- diol is used for glyoxal, and 2-Dihydroxymethyl- 2,4-dimethyl-[1,3] -dioxolane -4,5-diol for methylglyoxal. For UV-visible spectra of other compounds that contribute to OM_H, their monomeric structures are used. The chemical structure of toluene SOA products and that of α-pinene SOA products can be found in Table B-1 and Table B-3.

UV-Visible Spectrum Prediction

All geometry optimizations and calculations of spectroscopic parameters for individual molecules were performed using the NDDO based AM1 Hamiltonian in conjunction with the pair excitation configuration interaction (PECI) method. The calculations were done with the semiempirical program VAMP (Clark et al., 2002) (Accelrys Inc). In the PECI method, excited states are calculated by including all single and double excitations in which a complete electron pair is promoted. The calculated wavelength of the maximum absorption (λ_{max}) and oscillator strength (*f*) were used to predict the UV-visible absorption intensity. *f* is related to the molar absorptivity, ε (L mol^{-1} cm^{-1}), by the following equation (Belay, 2010):

$$f = 4.32 \times 10^{-9} \int \varepsilon \, d\nu \,, \tag{3-8}$$

where ν (cm^{-1}) is wavenumber ($\nu = 1/\lambda$). UV-visible spectra generally have a Gaussian band shape (Barker and Fox, 1980). Using the Gaussian function, the spectrally integrated molar absorptivity can be expressed as:

$$\int \varepsilon \, d\nu = \frac{1}{2}\sqrt{\frac{\pi}{\ln 2}} \varepsilon_{max} \Delta\nu_{FWHM} \tag{3-9}$$

where ε_{max} (L $mol^{-1}cm^{-1}$) is the maximum molar absorptivity, and $\Delta\nu_{FWHM}$ (cm^{-1}) is the full width at half maximum. The values of $\Delta\nu_{FWHM}$ of many SOA products are not available because these compounds are either difficult to synthesize or chemically too unstable. The sensitivity analysis for the predicted spectrum due to variation of $\Delta\nu_{FWHM}$ (56~80nm) is performed for both toluene SOA and α-pinene SOA. The model is highly sensitive to $\Delta\nu_{FWHM}$ as shown in Figure 3-4. When the same or a similar structure with a SOA product is found in the spectral data base, literature values were used for $\Delta\nu_{FWHM}$. Otherwise, $\Delta\nu_{FWHM}$ values were fixed at 68 nm to minimize the difference between the calculation and observation.

For selected nine compounds, the predicted spectroscopic parameters using the DNNO-based AM1 method are compared with those known in the literature (see Table 3-4 and Figure 3-3). At the 95% confidence level, the margin of error for the difference between predicted and observed data is ±25.4% for ε_{max} and ±7.4% for λ_{max}. Matsuura et al. (2008) reported an error range of ±4.4% for λ_{max} by comparing the observations and calculations for 49 dyes.

Simulation Results

Light absorption spectra of toluene SOA

The measured and calculated UV-visible absorption spectra of toluene SOA under different NO_x are shown in Figure 3-5(a-c). NO_x concentrations can affect the preferred reaction pathway for toluene oxidation in the gas phase (Cao and Jang, 2008;Song et al., 2005;Ng et al., 2007b). For example, under low NO_x conditions, multifunctional carbonyls from toluene oxidation can contribute more to SOA mass. For high NO_x conditions, higher concentrations of organic nitrates and nitro compounds appear in SOA. When a nitro group is attached to an aromatic ring or a conjugated compound, the nitro group can be a chromophore increasing both λ_{max} and the intensity of the absorption spectrum of a molecule. Under the NO_x levels of this study, the light absorbance of toluene SOA tends to become gradually higher as the NO_x concentration increases, but the effect of NO_x on measured aerosol spectra is not substantial. The model simulation also supports experimental observations showing that the formation of nitrophenols as light absorbing compounds is not sensitive to NO_x levels. For example, the formation rate (2.08E-12 cm^3 $molecules^{-1}$ s^{-1} at 298K) of 3-methyl-6-nitro-1,2-benzenediol (MNCATECH in Table 3-2) increases with NO_x concentrations but it is also highly reactive with atmospheric oxidants such as OH (6.83E-12 cm^3 $molecules^{-1}$ s^{-1} at 298K) and NO_3 (5.03E-12 cm^3 $molecules^{-1}$ s^{-1} at 298K), resulting in a weak sensitivity to NO_x.

Within the errors associated with the measured UV spectrum, the model output reasonably agrees with the measured spectrum for low NO_x condition but underestimates the absorbance of toluene SOA for high and middle NO_x condition (Figure 3-5). One of the possible explanations for the difference between the model's

predictions and the experimental measurements is that the model has failed to account for some light absorbing species with high molecular weights. Some oligomeric compounds formed through the aerosol phase reactions such as hydration, esterification, hemiacetal/acetal formation, and aldol condensation (Jang et al., 2002), might contain a long conjugated structure that can increase the absorption intensity in the visible range. In addition to aerosol phase reactions of organic compounds, the dissociations of dinitrocresols can influence aerosol absorption spectra. The dissociated forms of dinitrocresols usually absorb light with longer wavelength (visible range) and stronger intensity than the undissociated forms depending on aerosol's acidity.

Figure 3-5d shows spectra of individual products of toluene SOA under middle NO_x condition (T2 in Table 3-1). Among toluene SOA products, MNCATECH as a nitrophenol contributes about 60% of aerosol UV light absorption and about 95% of visible light absorption at different NO_x levels. MNCATECH accounts for nearly one third of the total toluene SOA mass and it has a strong absorption band tailing in the visible region (yellow). Other light absorbing species such as MNNCATCOOH, NC4MDCO2H and GLYOX polymer contribute mainly to UV light absorption. Although GLYOX polymer has a high mass percentage in toluene SOA (23~37%), it absorbs only UV light with low absorbance values (2~5% of aerosol UV absorption).

Many laboratory studies have also reported the presence of nitrophenols in toluene SOA (Forstner et al., 1997;Jang and Kamens, 2001a;Hamilton et al., 2005;Sato et al., 2007;Fang et al., 2011). For example, in a recent study of characterization of toluene SOA using thermal desorption/tunable vacuum ultraviolet photoionization time-

of-flight aerosol mass, Fang et al. (2011) have identified 4-nitro-o-cresol and its isomers as major components in toluene SOA. The nitro substituent on a phenol ring enhances the ε_{max} value and also shifts the absorption spectrum to longer wavelengths. Jacobson (1999) has pointed out the importance of nitro substituted aromatic compounds in atmospheric aerosols due to their high absorption of UV light based on the literature absorption spectra. Nakayama et al. *(2010b)* have also reported that nitrocresols might be a plausible source of the light absorption for toluene SOA.

Light absorption spectra of α-pinene SOA

In a manner similar to the analysis of toluene SOA, the aerosol phase products in Table 3-3 were used to predict the light absorption spectra of α-pinene SOA. The calculated spectra are in good agreement with the measured spectra (Figure 3-6). In this study, no NO_x effect on light absorbing spectra was observed for α-pinene SOA although NO_x can influence the product distribution through the modification of gas phase reactions (Ng et al., 2007a;Presto et al., 2005). Both model simulations and experimental data show that the light absorbing intensity of α-pinene SOA is much lower than that of toluene SOA. For example, the light absorbance of toluene SOA is five times higher than that of α-pinene SOA at 300nm, but twenty times higher at 400nm. Unlike toluene SOA, α-pinene SOA products do not contain aromatic or long conjugated moieties, which along with nitro functional groups, can be potential chromophores.

The spectra of major α-pinene SOA products produced under high NO_x condition (A1 in Table 3-1) are shown in Figure 3-6c. These six products contribute about 80% of the total SOA light absorption. The most frequently found functional group of these products is the non-conjugated carbonyl group (C=O), which has a major absorption near 200nm corresponding to a $\pi \rightarrow \pi^*$ transition. The calculation of λ_{max} using the

DNNO-based AM1 method also shows that non-conjugated SOA carbonyl products have absorptions near 200nm, as shown in Table 3-3.

Conclusion

A model to predict UV-visible absorption of SOA has been developed using a SOA formation model (PHRCSOA) and semiempirical quantum chemistry (NDDO-AM1). For the first time, the feasibility of semiempirical quantum chemistry has been explored for SOA systems with complex chemical composition. Overall, the light absorption of toluene SOA is higher than that of α-pinene SOA. The predicted NO_x effects on toluene SOA and α-pinene SOA also agree with the experimental observations.

There are several uncertainties in the current model approach. For example, SOA products obtained from the MCM kinetic model need to be revised when an improved mechanism of SOA formation becomes available. The structure of SOA oligomers needs to be experimentally identified, although the PHRCSOA model is able to predict the fraction of oligomers in the total SOA mass. In addition to the SOA formation model, the selection of different quantum chemistry methods for spectroscopic parameters can influence the model structure and the spectrum of SOA. The current quantum chemistry model of this study does not account for the spectrum shift due to coexistence of other organic matter in SOA, which can act as a solvent.

Table 3-1. Experimental conditions and the resulting SOA data for photooxidation of toluene and α-pinene using the 2 m^3 Teflon film chamber [a]

HCs	No.	RH %	Initial NO_x (ppb)	Initial HC (ppb)	V_{seed} (μg m^{-3})	Δ HC[b] (ppb)	OM_T[b] (μg m^{-3})	Mass ratio of org to inorg	Sampling time[c] (min)	*V*/*A*[d] (m)	Sampled SOA mass[e] (μg)
Toluene	T1	44.3	104	233.5	27	81	53	1.96	27	5964	15.2
	T2	43.7	49	250	21	95	50	2.4	31	6749	17.4
	T3	44.8	24	244	26	79	38	1.42	42	9171	16.8
α-Pinene	A1	45.9	105	148.7	118	112	141	1.2	8	1682	14.3
	A2	46.7	26	150.3	123	99	90	0.73	11	2293	10.8

a: Temperature: 294 –298 K. b: The average consumed hydrocarbons (*ΔHC*) and formed OM_T during sampling. c: The SOA sampling started at reaction time of 120min. d: *V* is the volume of air drawn through the filter during a given sampling time and *A* is the area of the sample spot. e: the collected SOA mass in the filter.

Table 3-2. Selected products of toluene SOA and their mass percentages at different NO_x conditions

Group (i, j)	*k*	Products name[a]	MW_k	λ_{max}[b] (nm)	*f*[b]	F_k[c] (%) H NO_x (T1)	F_k[c] (%) M NO_x (T2)	F_k[c] (%) L NO_x (T3)
1, PO	1	MNCATECH	169	330, 228	0.05, 0.40	26.27	30.48	26.14
1, PO	2	MNNCATCOOH	281	270, 189	0.3, 0.31	2.95	6.36	6.47
1, PO	3	DNCRES	191	321, 222,	0.04, 0.82	2	0.88	0.32
1, H-m	4	TLEMUCOOH	190	177, 165	0.04, 0.05	1.04	3.04	4.41
1, H-m	5	TLEMUCNO3	190	177, 161	0.04, 0.03	2.4	1.57	1.1
2, PO	6	TLBIPEROOH	174	216, 213	0.19, 0.11	2.13	8.68	14
2, PO	7	TLBIPERNO3	174	415, 233	0.06, 0.07	3.85	3.46	2.78
2, H-s	8	NC4MDCO2H	159	228, 221	0.15, 0.21	6.71	3.19	1.38
2, H-f	9	TLEMUCCO	156	202, 148	0.35, 0.03	0.53	0.81	1.09
3, PO	10	TOL1OHNO2	153	316, 222	0.04, 0.17	0.77	0.51	0.23
3, H-f	11	ACCOMEPAN	207	187, 174	0.26, 0.25	2.29	10.34	7.67
4, H-m	12	MALDIALPAN	161	190, 176	0.27, 0.26	0.59	0.48	0.41
4, H-m	13	C5COO2NO2	175	227, 184	0.59, 0.22	0.99	1.03	1.17
5, H-m	14	MALANHY	98	230	0.17	2.26	1	1.01
5, H-m	15	C5DICARB	98	223, 162	0.65, 0.09	0.55	0.21	0.14
5, H-m	16	MGLYOX[d]	72	193, 171	0.11, 0.18	4.98	2.55	2.16
5, H-m	17	GLYPAN	135	213, 189	0.13, 0.04	1.12	0.53	0.33
5, H-f	18	GLYOX[d]	58	196, 182	0.09, 0.10	37.17	23.26	27.3

a: The names of chemicals are from MCM mechanism, only primary products which contribute more than 1% of SOA mass are shown in the table, the detailed composition can be found in supplementary materials. b: λ_{max} and *f* are calculated using NDDO based AM1 semiempirical quantum chemistry method. Up to two major oscillator strengths are selected. Detailed values are shown in supplementary materials. c: F_k is the mass percentage of the *k*th species, obtained by the mass balance of chemical compounds in toluene SOA. The sum of F_k values is 98.6% for T1, 98.4% for T2 and 98.1% for T3. d: MGLYOX and GLYOX are in the form of oligomers. Their spectra were estimated using their dimer structure. The spectra of other oligomers are assumed to be as same as their monomers.

Table 3-3. Representative products of α-pinene SOA and their mass percentages in SOA at different NO_x conditions

Group (i, j)	*k*	Products[a]	MW_k	λ_{max}[b] (nm)	*f*[b]	F_k[c] (%)	
						H NO_x (A1)	L NO_x (A2)
1, H-s	1	C811PAN	247	183, 161	0.27, 0.11	4.59	3.98
1, H-s	2	PINIC	186	181, 174	0.25, 0.06	0.02	1.98
1, H-s	3	C921OOH	204	192, 186	0.09, 0.12	0.09	1.3
1, H-s	4	C812OOH	190	187, 186	0.14, 0.10	0.04	0.92
1, H-s	5	HOPINONIC	200	176, 171	0.25, 0.22	0.04	1.19
1, H-m	6	C920PAN	261	196, 171	0.07, 0.06	8.4	3.91
1, H-m	7	C98OOH	204	201, 167	0.29, 0.14	2.72	10.43
1, H-m	8	C98NO3	233	188, 183	0.18, 0.03	6.46	2.62
1, H-m	9	C922OOH	220	204, 177	0.32, 0.17	0.09	1.34
1, H-f	10	C7PAN3	233	205, 192	0.08, 0.35	18.43	3.54
2, H-s	11	C10PAN2	245	187, 171	0.04, 0.08	16.3	5.97
2, H-s	12	C97OOH	188	197, 186	0.05, 0.05	0.49	6.13
2, H-f	13	C717NO3	203	184, 182	0.08, 0.19	5.28	3.12
2, H-f	14	C108OOH	216	202	0.26	4.39	14.88
3, PO	15	APINAOOH	186	160, 158	0.16, 0.13	0.07	2.32
3, PO	16	APINANO3	215	174151	0.07, 0.2	0.93	2.42
3, PO	17	APINBNO3	215	202, 153	0.05, 0.22	0.59	1.26
3, H-s	18	PINONIC	184	173, 169	0.31, 0.15	0.09	0.7
3, H-m	19	C89PAN	231	179, 169	0.05, 0.06	3.36	2.14
3, H-m	20	C107OH	200	182, 175	0.25, 0.06	0.36	3.53
3, H-m	21	C109OH	200	181, 173	0.25, 0.06	0.28	0.82
3, H-m	22	C5PAN9	191	199, 184	0.05, 0.22	2.6	0.6
4, H-f	23	CO235C6CHO	156	159	0.01	2.88	2.85
4, H-f	24	C109CO	182	200	0.25	0.09	0.42
5, H-m	25	PINAL	168	168, 164,	0.03, 0.15	20.12	19.46

a: The names of chemicals are from MCM mechanism, only primary products which contribute more than 1% of SOA mass are shown in the table, the detailed composition can be found in supplementary materials. b: λ_{max} and *f* are calculated using NDDO based AM1 semiempirical quantum chemistry method. Up to two major oscillator strengths are given, more can be found in supplementary materials. c: F_k is the mass percentage of the *k*th species, obtained by the mass balance of chemical compounds in α-pinene SOA. The sum of F_k values is 98.7% for A1 and 97.8% for A2

Table 3-4. Comparisions between model predicted absorbance and literature values. The literature absorbance data are from NIST webbook

Name	By NDDO-AM1 (PECI)			By literature		
	λ_{max} (nm)	ε_{max} ($M^{-1}cm^{-1}$)	f	λ_{max} (nm)	ε_{max} ($M^{-1}cm^{-1}$)	$\Delta\nu_{FWHM}$ (nm)
9,10-Anthraquinone	303	3575	0.072	325	5048	40
2-Nitro-Phenol	305	1158	0.028	346	1752	64
2,4-Hexadienal	275	44059	0.861	260	25527	32
2,3-Butanedione	465	8	0.0002	435	9	94
3-Methyl-2-Butenoic acid	247	13673	0.33	221	12162	32
Phenol	275	1920	0.023	271	2041	20
1-Octene	202	13552	0.337	177	13335	22
Muconic acid	267	28708	0.698	259	28973	38
1-Methyl-2,4-Dinitrobenzene	211	18778	1.275	240	28642	66

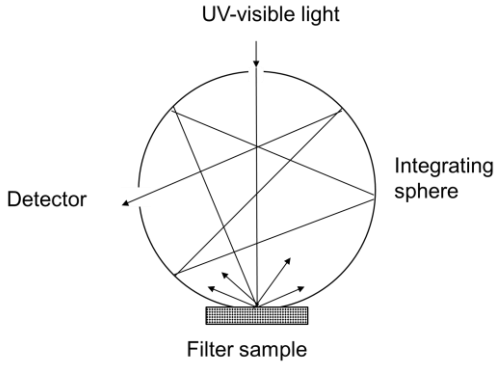

Figure 3-1. Schematic diagram for the measurement of UV-visible spectra of SOA.

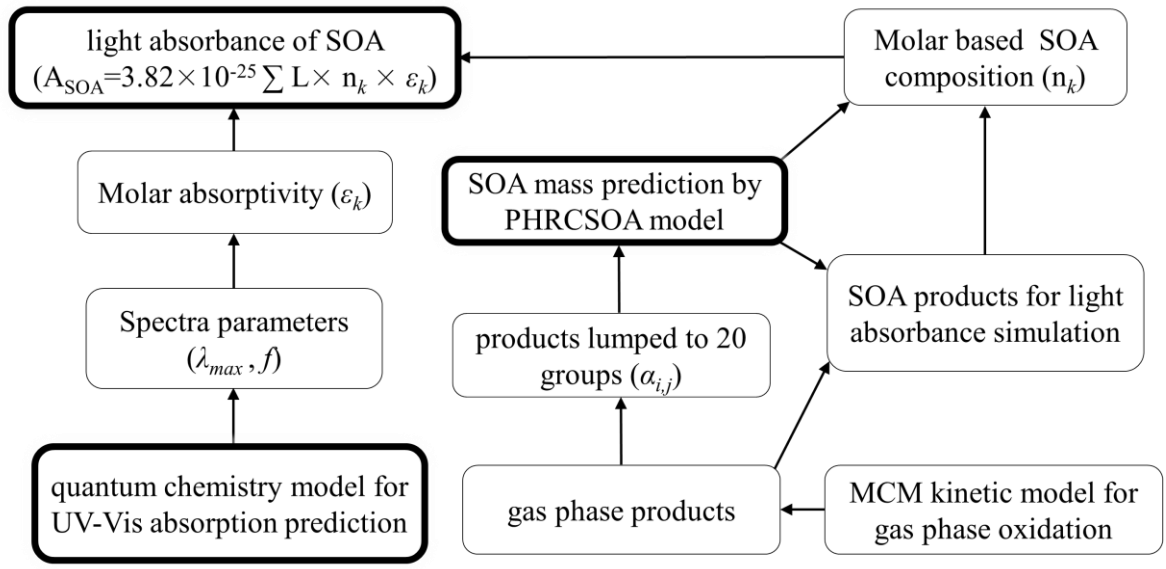

Figure 3-2. Structure of the SOA light absorption model.

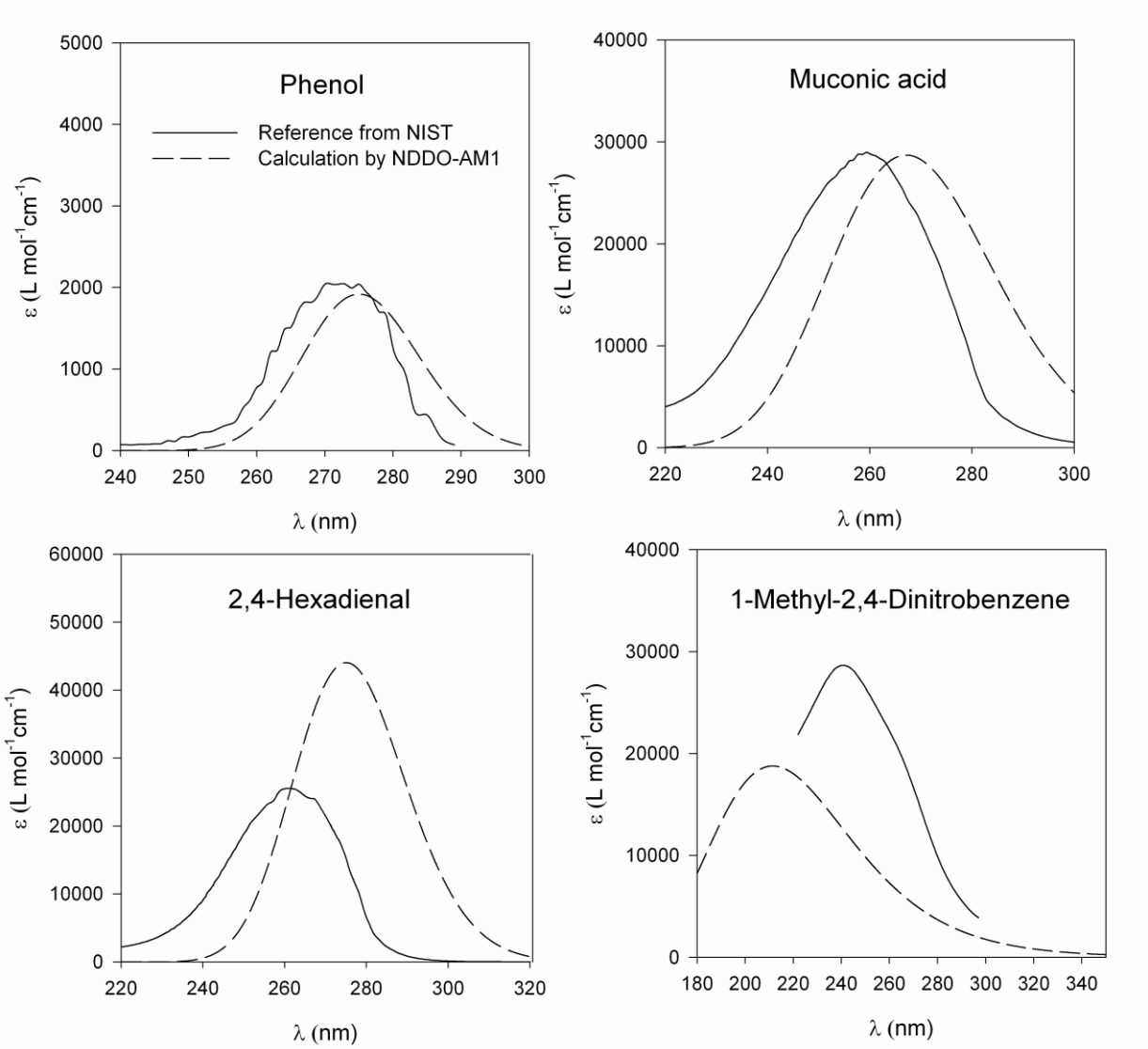

Figure 3-3. Comparisons of the observed and calculated spectra of testing compounds using Gaussian band shape function.

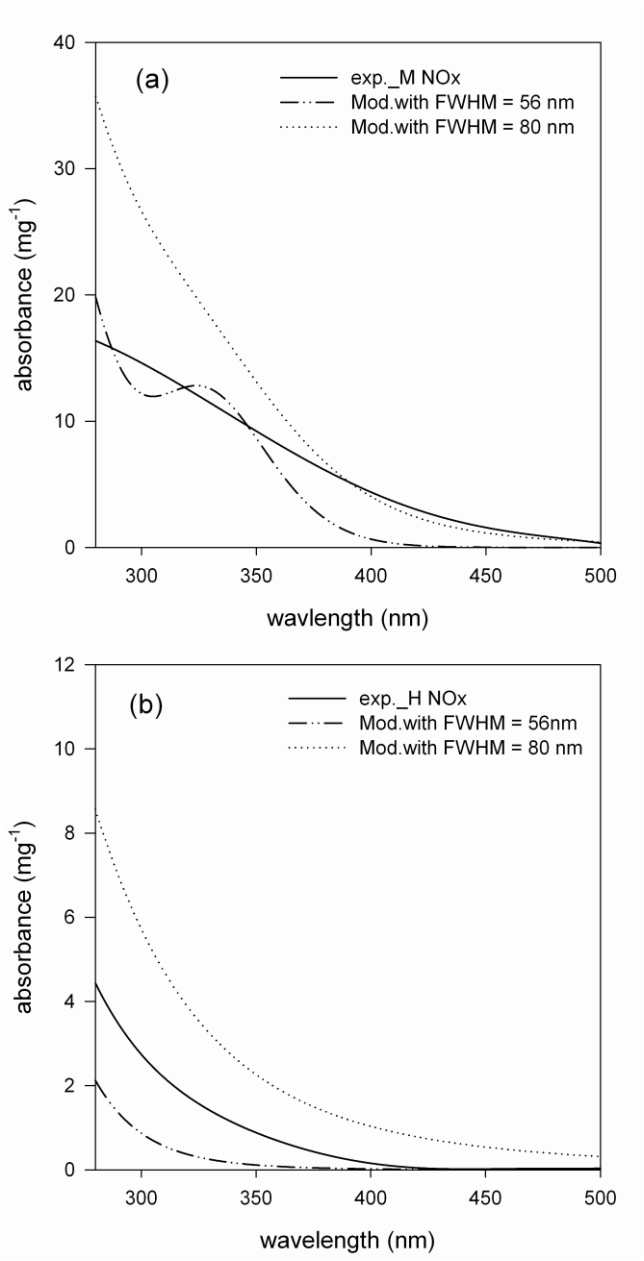

Figure 3-4. Sensitivity of the model to Δv_{FWHM} for two systems: (a) toluene and (b) α-pinene.

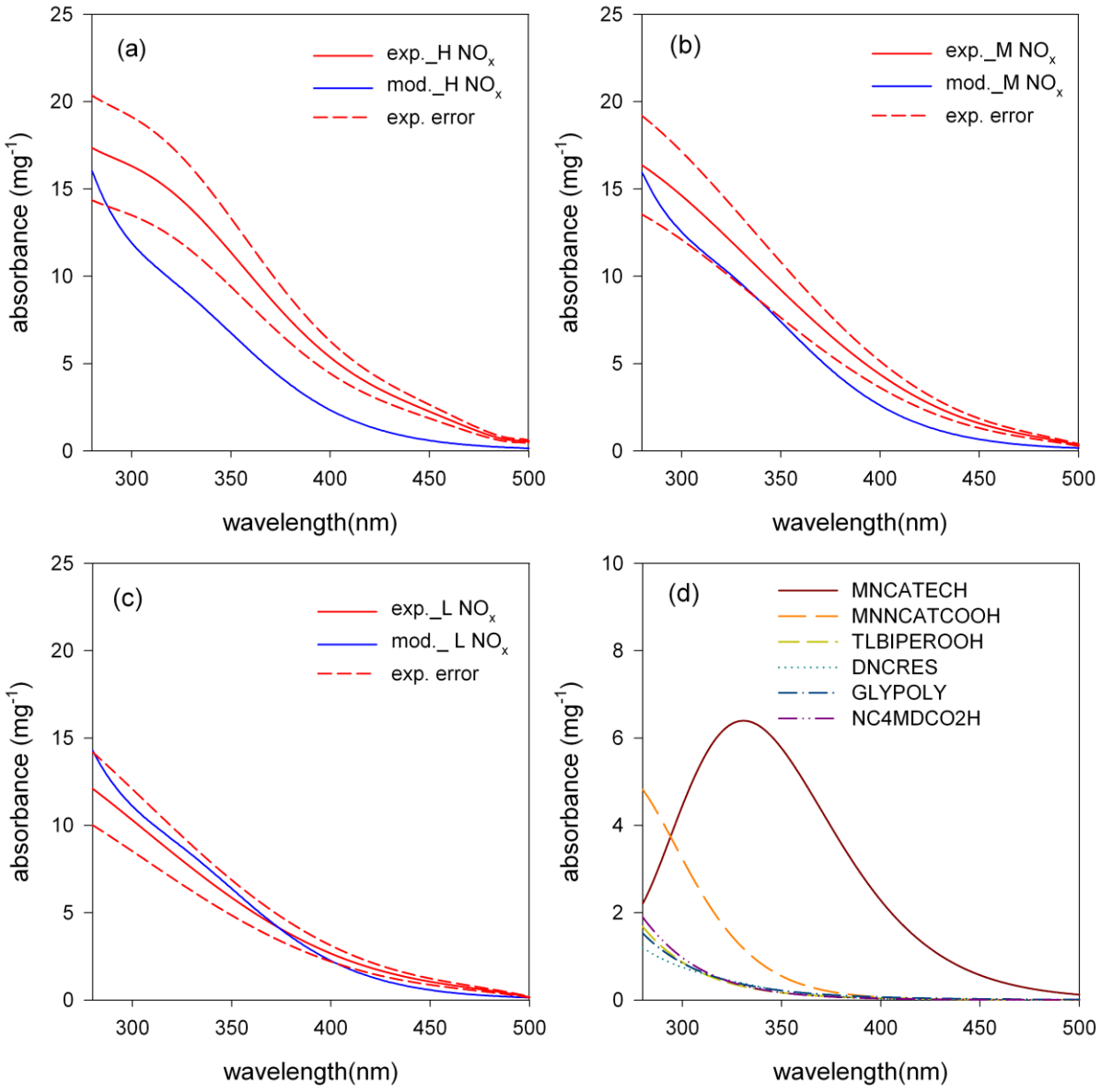

Figure 3-5. Comparison of the predicted absorption spectra and the measured absorption spectra of toluene SOA under three different NO_x conditions: (a) high NO_x, (b) middle NO_x, (c) and low NO_x. The spectra of individual products are shown in (d) for middle NO_x condition. The uncertainty of the mass normalized absorbance was calculated from the uncertainties of UV-visible absorbance and the aerosol mass through the propagation of uncertainty for divisions. Dash lines with the same color indicate upper and lower range.

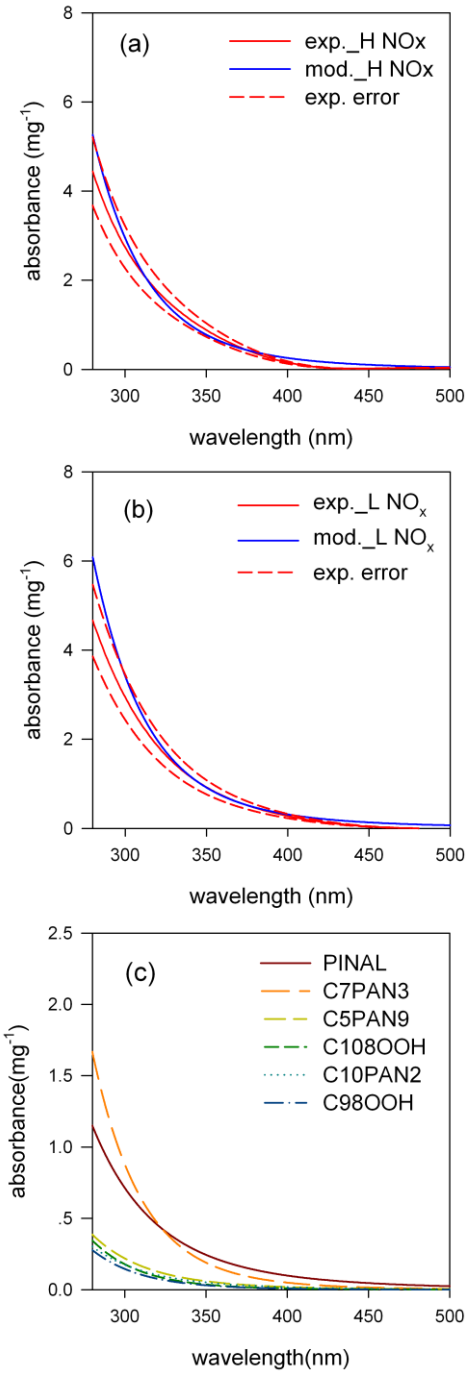

Figure 3-6. Comparison of the predicted absorption spectra and the measured spectra of α-pinene SOA under different NO_x conditions: (a) high NO_x and (b) low NO_x, using data A1and A2 in Table 2-1. The spectra of individual products are shown in (c) for high NO_x condition. The uncertainty of the mass normalized absorbance was calculated from the uncertainties of UV-visible absorbance and the aerosol mass through the propagation of uncertainty for divisions. Dash lines along the measured spectra indicate upper and lower range.

CHAPTER 4
DYNAMIC LIGHT ABSORPTION OF BIOMASS BURNING ORGANIC AEROSOL PHOCHEMICALLY AGED UNDER NATURAL SUNLIGHT

Background

Light absorption of organic carbon (OC) aerosol has been poorly understood mainly due to its complex chemical composition and dynamic evolution under atmospheric conditions. OC can be either primary (POA) or secondary (SOA) in origin. On a global scale, approximately 69% of POA and 23% of SOA are contributed by biomass burning (Hallquist et al., 2009). Considering the large source of biomass burning OC in the atmosphere, better understanding its light absorption properties is necessary.

Recently, there is growing evidence that biomass burning OC may be a nonnegligible contributor to light absorption in atmospheric aerosols, especially in the short wavelength visible and ultraviolet spectral regions (Hoffer et al., 2006;Kirchstetter and Thatcher, 2012;Lack et al., 2012). Kirchstetter and Thatcher (2012) analyzed the filter-based wood smoke aerosol from night-time ambient sampling, and estimated that OC accounted for 49% of total aerosol light absorption between 300nm and 400nm. Lack et. al (2012) measured light absorption of biomass burning aerosol originating from a wildfire event using a photo-acoustic aerosol absorption spectrometer. Their results suggested that primary OC contributed 27(±15) % of the total absorption at 404 nm.

Light absorption of OC is mainly determined by its chemical composition. Biomass burning OC has a yellowish to brown color, with absorption mainly at UV range, and decreasing absorption toward visible range (Kirchstetter et al., 2004;Schnaiter et al., 2005). Chen and Bond (2010) measured light absorption of solvent-extracted fresh primary OC generated in a nitrogen filled furnace. They proposed that chemicals with

large, polar, and conjugated aromatic rings would be the light absorbing materials. The study of Del Vecchio and Blough (2004) suggested that hydroxy-aromatic compounds and quinoid might be responsible for OC color.

In the atmosphere, the chemical composition of OC aerosol changes with aging through processes such as oxidation of organic gases, heterogeneous oxidation with atmospheric oxidants (e.g., ozone and OH radicals), and aerosol phase reactions. Recent laboratory experiments indicate that photochemical oxidation results in the dynamic evolution of chemical and physical properties of OC aerosol. The aged OC aerosol became less volatile and more oxygenated after a few hours of photochemical oxidation (Grieshop et al., 2009). Aging processes also change the hygroscopicity. The hygroscopic water content in OC aerosol may increase or decrease depending on wood burning conditions (Martin et al., 2012).

The aging effects on the light absorbing properties of OC have been varied among research reports due to the different aging times and oxidation conditions. For example, Adler et al.(2011) derived the effective broadband refractive index of biomass burning aerosol from a wood burning event using a white light optical counter. They found that the aged biomass burning aerosols were less absorbing than the freshly emitted aerosols, with the imaginary refractive index decreasing from 0.04 to 0.02. However, Saleh et al. (2013) recently reported that aged OC is more absorbing than fresh one due to SOA formation. In their study, the wood smoke aerosol was aged for only one hour in an indoor chamber. These conflicting results show that the influence of aging on light absorption of wood smoke OA needs further investigation.

The objectives of this study are: 1) to investigate the influence of photochemical oxidation on light absorption of wood smoke OC; 2) to explore the effects of relative humidity (RH) and NO_x on light absorption of wood smoke OC over the course of the photochemical aging process, and 3) to characterize the chemical evolution of OC aerosol. In order to focus on wood burning OC with minimum influence by BC, wood smoke was produced from smoldering-phase burning. Smoldering combustion has frequently been found in biomass burning situations including wildfires, prescribed burns and agriculture burning (Alves et al., 2011;Hille and Stephens, 2005;Hays et al., 2005). It has been reported to consume over 50% of biomass in temperate and boreal fires (Bertschi et al., 2003). In this study, the resulting wood burning OC was photochemically oxidized using outdoor dual chambers that exposed to natural sunlight. The large outdoor chamber allowed atmospheric aging conditions to be closely mimicked and aerosol samples to be collected for longer time periods.

Experimental Section

Outdoor Chamber Experimental Setup

The photooxidation of wood smoke was performed using the University of Florida Atmospheric Photochemical Outdoor Reactor (UF-APHOR) dual chambers (52 m^3 per chamber) which are located on the roof of Black Hall, UF. The UF-APHOR dual chambers with half-cylinder design are made of FEP Teflon film attached to metal frames. A detailed description of the UF-APHOR chambers can be found elsewhere (Im et al., 2013).

Prior to each experiment, the chambers were continuously flushed with clean ambient air for more than 12 hours and then purged overnight with clean air from an air cleaner (GC Series, IQAir Inc.). Commercial hickory hardwood logs were chopped into

pieces with approximate size of 3 cm × 4 cm × 33 cm. The wood pieces were burned under smoldering conditions using a wood grill stove. Before sunrise, smoke was introduced into the chambers through a 4 inch alumina tube (0.5 meter in length) connected to the stove. Immediately after injecting wood smoke, the chamber air was mixed for five minutes using mixing fans. The initial conditions for wood smoke particle concentration measured by an organic carbon (OC) analyzer are summarized in Table 1. For high NO_x experiments, NO gas from the tank was introduced into the chamber after the wood smoke injection.

Photochemical reactions started at sunrise. The sunlight intensity, chamber temperature and relative humidity (RH) dynamically changed over the course of chamber experiments. A typical time profile of these parameters is shown in Fig. S1. To study of the effect of humidity on photochemical aging of wood smoke, the dry condition (RH<30%) humidity was controlled one day prior to the experiment using a dehumidifier. To achieve the wet condition (RH>60%), the chamber air was humidified using a steam evaporator during the experiment. Sun light intensity and temperature-humidity were measured continuously with an ultraviolet radiometer (model TUVR, The Eppley Laboratory) and a Temp-RH sensor (CS2,Campbellscientific), respectively.

Wood Smoke Characterization

Gas and particles were sampled through manifolds that run directly to a laboratory just below the chambers. The wood smoke particles were collected on a 13mm diameter filter (Borosilicate microfibers reinforced with woven glass cloth and bonded with Teflon, Gelman Science Pallflex, Type: TX40H120-WW) at a flow rate of 17 L/min. The UV-visible light absorption spectrum of aerosols collected on the filter

was directly monitored using a Perkin-Elmer Lambda 35 UV-visible spectrophotometer equipped with a Labsphere RSA-PE-20 diffuse reflectance accessory. The detailed measurement procedure for light absorption spectra of aerosols can be found in our previous study (Zhong and Jang, 2011). OC and elemental carbon (EC) of the aerosol filter samples were analyzed with a semi-continuous OC/EC analyzer (Model 4, Sunset Laboratory Inc.). Levoglucosan obtained from the filter/acetonitrile extract was first derivatized with N,O-bis(trimethylsilyl) trifluoroacetamide(BSTFA) and then measured using a gas chromatograph/ion trap mass spectrometer (GC-ITMS) (CP-3800 GC, Saturn 2200 MS, Varian Inc.). The fluorescence spectra of extract of the filter sample with dichloromethane were measured by a fluorescence spectrophotometer (F-2500, Hitachi, Ltd.). The chemical functional group of particles impacted on a silicon disk was characterized using Fourier transform infrared spectroscopy (FTIR) (Nicolet Magna 560, SpectraLab Scientific Inc). To determine the water content of aerosols, the sampled silicon disk was installed in a miniature flow chamber which was located in the FTIR optical beam path. The relative humidity inside the flow chamber was controlled by passing wet air through the chamber. FTIR spectra of aerosols on the disk were obtained under varying relative humidity from 10% to 85%. Detailed descriptions of the methods can be found in the previous study by Jang et al. (2010). Particle concentrations and particle size distributions were monitored continuously using a scanning mobility particle sizer (Model 3080, TSI Inc.), together with a condensation nuclei counter (Model 3025A, TSI Inc.). Ozone was monitored using a photometric ozone analyzer (model 400E, Teledyne Instruments), and NO_x concentrations were

measured using a chemiluminescence NO/NO_x analyzer (model 200E, Teledyne Instruments).

Light Absorption of Ambient Organic Carbon

In April 2012, the County Line Fire located in Pinhook Swamp, Florida, 90 miles north of UF, burned more than ten thousand acres. Biomass burning aerosol was collected at the UF sampling site on April 9 -10, 2012. During the sampling day, the OC concentration in the morning was as high as 92 ug m^{-3} (measured at the sampling site) compared to a normal day in which the OC value is 2 to 4 ug m^{-3}. Thus, wildfire emission is the main source of the ambient aerosols in UF area during this episode. Fine particulate matter ($PM_{2.5}$) passing through a cyclone were collected on a 13mm diameter filter at a flow rate of 16.7 L/min. Light absorption spectra of the filter sample were directly measured using a UV-visible spectrometer equipped with an integrating sphere.

Results and Discussion

Light Absorption of OC

A wood burning particle contains a mixture of BC and OC. BC and elemental carbon (EC) are treated as equivalent. Due to its strong light absorption capacity, a small amount of BC may contribute significant spectral absorption depending upon wavelength. Hence, burning conditions were controlled as smoldering to generate less BC. The percentage of element carbon in smoldering smoke particles was near or less than 5% as shown in Table 1. A method introduced by Kirchstetter and Thatcher (2012) was used to separate light absorption by OC from the absorption of the smoke aerosol mixture (OC and BC). Light absorption of OC, Abs_{OC}, is obtained by subtracting the absorption of BC, Abs_{BC} from the mixture's absorption *Abs*:

$$Abs_{OC} = Abs - Abs_{BC} \quad (4\text{-}1)$$

Abs is directly measured from the filter sample. Abs_{BC} is estimated as:

$$Abs_{BC} = \frac{Abs(880nm)}{880nm^{-AAE}} \times \lambda^{-AAE}, \quad (4\text{-}2)$$

where AAE is the Absorption Angstrom Exponent and defined as :

$$AAE = \frac{-\ln(Abs(\lambda_1)/Abs(\lambda_2))}{\ln(\lambda_1/\lambda_2)} \quad (4\text{-}3)$$

For Abs_{BC} estimation, the measured *AAE* value was 1.03 for wavelengths between 360 and 900nm.

Figure 4-1a shows absorption spectra of the fresh smoke aerosol, the decoupled OC and the decoupled BC. Over the wavelength range of 280nm to 600nm, OC contributes 60~98% of the total sample absorption, while BC is dominate for longer wavelengths (>700nm). Light absorption of OC exhibits no distinct peaks, exponentially decreasing with increasing wavelength. In the visible range (400-700nm), the average *AAE* of OC is 4.74. This value accords with the *AAE* of ambient biomass burning OC (an average value of 5) reported by Kirchstetter and Thatcher (2012).

All samples were analyzed in a similar manner as described above. The main data reported here are mass absorption cross-section of OC (MAC_{OC}, m^2g^{-1}), which is wavelength (λ) dependent and determined by normalizing the absorption coefficient of OC ($b_{abs(OC)}$, m^{-1}) with thermal OC mass concentration, M_{OC} ($g\ m^{-3}$):

$$MAC_{OC} = \frac{b_{abs(OC)}}{M_{OC}} \quad (4\text{-}4)$$

In equation 4-4, $b_{abs(OC)}$ can be calculated from the measured absorbance of filter sample(abs):

$$b_{abs(OC)} = \frac{1}{\mathrm{C}} \frac{A}{V} Abs_{OC} \ln(10) \quad (4\text{-}5)$$

where *C* is the correction factor with a value of 1.4845 obtained from our previous study(Zhong and Jang, 2011), *A* is the filter surface area sampled (7.85×10^{-5} m^2 in this study), and *V* is the volume (m^3) of air passing through the filter during a given sampling time. Abs_{OC} is obtained from equation 4-1.

Effect of Photochemical Aging on Light Absorption of OC

Our chamber experimental data showed that light absorption of wood burning OC was significantly modified due to photochemical aging. Figure 4-1b shows the typical MAC_{OC} of wood smoke exposed to sunlight using the outdoor chamber at different daytime hours. Overall, MAC_{OC} increased with aging time in the morning. The total MAC_{OC}, which is estimated as the area under the MAC_{OC} spectrum curve between 280nm and 600nm, increased by 11% ~54% (26% on average) except data from the high RH condition (West chamber on Oct. 24, 2012). Saleh et al., (2013) have explained that the increment in aged OA absorption is caused by the formation of SOA, which absorbs more than fresh POA in the short wavelength visible and near-UV regions. Schauer et al.,(2001) reported that about 34% of identified organic compounds in the gas phase and 41% of organic compounds identified in POA were phenols, syringols and guaiacols. These phenols and methoxylated phenols in the gas phase or in the particle can rapidly react with atmospheric oxidants to form light brown substances (Gelencser et al., 2003;Chang and Thompson, 2010;Ofner et al., 2011).

Thus, the enhancement in light absorption would be caused by either oxidized POA or the SOA produced from oxidation of primary phenolic compounds.

However, the light absorption of OC in both the UV and visible ranges began to decrease with aging time. The total MAC_{OC} decreased by 19% ~ 68% (41% on average) compared to the fresh POA. The possible explanation for the decreases in MAC_{OC} is bleaching of colorant in POA and SOA by sunlight. The previous study by Zhong and Jang (2012) reported the bleaching effect of light on light absorption of SOA. In wood smoke POA and SOA, there are abundant of chromophores, such as conjugated aromatic rings and phenols, as well as nitro and hydroxyl groups. High energy photons in sunlight can excite electrons in colored molecules through π-π* or n-π* transitions and disrupt the conjugated structure of chromophores, resulting in the gradual fading of wood smoke color.

Effect of RH on Light Absorption of OC

In order to investigate the effect of humidity on MAC_{OC}, two sets of wet-dry dual chamber experiments were conducted: high RH (80-87%) vs low RH (11-27%) on Oct.24, 2012, and middle RH (56-75%) vs low RH (12-24%) on Nov.01, 2012. Figure 4-2 illustrates the time profile of the relative MAC_{OC} and MAC_{OC} at 550 nm. The relative MAC_{OC} was obtained by normalizing the total MAC_{OC} at a certain time by the initial total MAC_{OC}. As photooxidation progressed in the afternoon, the absorption decay at wet conditions became more rapid than the decay at dry conditions. For example, at the end of the experiment, the relative MAC_{OC} and MAC_{OC} at 550nm at the low RH were higher by 43% and 45% compared to those at the high RH. Unlike MAC_{OC} values in the middle or the low RHs, no increase appeared for MAC_{OC} values for the experiments at high RH in the morning. Elevated values of relative humidity can increase the water

content of wood smoke particles. Anastasio et al.(1996) reported that illumination of aqueous phase non-phenolic aromatic carbonyls in the presence of phenols can destroy phenols. In addition, this aqueous phase photooxidation produces a significant amount of H_2O_2, since both the aromatic carbonyls and phenols are major products from the combustion of wood (Rogge et al., 1998). In wet aerosols, H_2O_2 can photodisssociate to produce OH radicals (Zellner et al., 1990;Faust, 1994), which could decompose chromophores and lead to bleaching of wood OA.

Effect of NO_X on Light Absorption of OC

Controlled dual chamber experiments were also conducted to study the influence of NO_x on MAC_{OC} of wood aerosols, high NO_x (108 ppb) vs low NO_x (16 ppb) on Oct.30, 2012 and middle NO_x (43 ppb) vs low NO_x (16 ppb) on Oct. 11, 2012. Figure 4-3 shows the time profiles of the relative MAC_{OC} values and MAC_{OC} at 550nm under different NO_x concentrations. In the presence of high NO_x, the MAC_{OC} values are slightly higher than those at low NO_x concentration. NO_x is able to modify the reaction pathway for organic compounds in the gas phase. Nitro-phenols (e.g., nitrocatechols) and nitro compounds can be produced through the photooxidation of phenolic organic compounds and contribute SOA. Nitrophenols have been suggested to be strong candidates to represent light absorbing toluene SOA (Nakayama et al., 2010b;Zhong et al., 2012;Zhang et al., 2013). A higher NO_x level, the concentration of these chromophoric nitro-phenols can be greater, decelerating the decay of MAC_{OC} of wood smoke OA.

Chemical Evolution of Organic Carbon Aerosol

To investigate how the chemical composition of wood smoke aerosol influences light absorption, the aerosol introduced into the chamber was characterized as photooxidation progressed. In this study, levoglucosane, a major constituent in wood

smoke POA, was monitored by GC-ITMS. The intensity of fluorescence, which is mainly due to PAHs, was measured for solvent extracted aerosol samples. To study the alteration of the hygroscopic properties of wood smoke aerosol due to photooxidation, the aerosol water content was also measured by FTIR.

Levoglucosan decay

Levoglucosan is abundant in wood smoke POA, contributing 3~49% of total wood smoke aerosol carbon (Mazzoleni et al., 2007). Figure 4-4a illustrates the rapid degradation of both pure levoglucosan and levoglucosan in wood smoke after wall-loss correction of aerosols. The experiment method for the pure levoglucosan experiment is provided in the supplementary materials (Document C-1). The decay rate of the levoglucosan associated with wood smoke aerosol is similar to that of pure levoglucosan within an error range. The degradation of levoglucosan would be caused by wall loss of levoglucosan vapor and photochemical oxidation by OH radicals in the aerosol. According to Booth et al. (2011), the sub-cooled liquid vapor of levoglucosan is 1.9×10^{-4} pa at 298K, the wall loss of gas-phase levoglucosan is likely. In order to identify the products produced from the photooxidation of levoglucosan in the presence of HONO, aerosol filter samples were analyzed using GC-ITMS after silylation of the products. The mass fragments of the tentatively identified products are shown in Figure C-2 and the reaction pathways for the formation of the proposed products are illustrated in Figure C-3. However, the low amount of O_3 formation suggests that oxidation of levoglucosan occurred mainly *via* aerosol phase reaction.

PAHs decay

Although the mass percentage of PAHs in wood smoke is less than 1% (Schauer et al., 2001), PAHs can contribute to the color of wood smoke OA. The photooxidation of PAHs can therefore be examined by measuring the fluorescence as a function of time. The fluorescence spectra of OA (Figure 4-4b) show a rapid decrease in fluorescence emission when excited at 280 nm. Similar to levoglucosan, such decline can be caused by both evaporation combined with increased temperature after sunrise (Figure C-1) and photochemical oxidation of PAHs. PAHs can be transformed to oxy-PAHs *via* aerosol phase oxidation (e.g., reaction with singlet oxygen produced by a photosensitizing process or reaction with OH radicals and free radical reactions) (Jang and McDow, 1995). These oxy-PAHs generally have much lower fluorescence quantum yield compared to unoxidized PAHs.

FTIR spectra of wood burning aerosol

Figure 4-5a compares the characteristic FTIR spectra of fresh and aged wood burning particles at RH of 45%. For the fresh particles, the O-H stretching of alcohols is seen at 3500-3200cm^{-1}. The C=O stretching of carbonyls (e.g., aldehydes, ketones, and carboxylic acids) occurs at 1800-1680cm^{-1}, and the aromatic C=C stretching bands appear at 1610, 1517 and 1458cm^{-1}. After photochemical aging of wood smoke OA for 5 hours, the absorbance for both the O-H stretch of alcohols and the aromatic C=C stretch significantly decreased. The FTIR spectrum of aged particles also shows the formation of carboxylic acids confirmed by the broad O-H stretch at 3300-2500cm^{-1} and the increased absorbance at the C=O stretching frequency, suggesting oxidation of wood constituents.

Hygroscopic properties of wood burning aerosol

To investigate the hygroscopicity of wood smoke particles, the water content of wood burning OA was monitored using the FTIR equipped with a miniature flow chamber under varying RHs (Jang et al., 2010). In brief, the absorbance at 1650cm^{-1}, which is the characteristic frequency for O-H bending of water, was used to estimate the water content in the aerosol. The peak at 1650cm^{-1} was calibrated with the NaCl particle, which has a known water content obtained by an inorganic thermodynamic model at a given RH (e.g., AIM-III model, http://www.aim.env.uea.ac.uk/aim/aim.php) (Clegg et al., 1998). As shown in Figure 4-5b, the fresh particles were much more hygroscopic than the aged particles. The water content in fresh particles exponentially increased as a function of RH. No water was detected when the RH was lower than 25%. In the morning, fresh wood smoke particles contain a high amount of the sugar compounds such as levoglucosan, which is very hydrophilic and easily absorbs water. As described in section 3.4.1, the amount of primary sugars rapidly decayed due to photooxidation. Although the carboxylic acid content increased with aging, within aged wood aerosol (FTIR data in Figure 4-5a), the aerosol became less hygroscopic.

Conclusion and Atmospheric Implication

The dynamic changes in light absorption of biomass burning organic aerosol were investigated using the outdoor smog chamber under natural sunlight. The diurnal change in absorption of wood smoke aerosol is governed by two mechanisms: chromophore formation and sunlight bleaching. The colored products originating from photooxidation of phenolic SVOCs can increase wood smoke OA absorption in the morning while sunlight fades the color of both POA and SOA in the afternoon. Higher concentrations of NO_x help prolong the wood smoke aerosol color (Figure 4-3), but the

high RH accelerates the degradation of aerosol color (Figure 4-2). The decay of both PAHs and levoglucosan indicated dynamic changes in chemical composition of primary OC due to aging. The aged wood smoke OC became more oxidized but less hygroscopic as shown by FITR spectra measurement.

The ambient data obtained during the County Line Wildfire event on April 09 and 10, 2012, were analyzed using equation (4-5) with a measured AAE of 0.74 for ambient BC. Figure 6 shows the light absorption of ambient biomass burning OC after subtracting background OC. Compared to the MAC_{OC} sampled at 8:30am, the MAC_{OC} sampled at 9:36am on April 09 increased by 18%, but the MAC_{OC} decreased by 28% at 11:30am. The diurnal pattern in light absorption of the ambient biomass burning OA is consistent with the result obtained in the outdoor chamber.

There is increased emphasis on research pertaining to the climate forcing of OA, including both experimental studies and model simulations. Considering aerosol of lifetime (about six days), the results of both outdoor chamber studies (Figure 4-1) and ambient field data (Figure 4-6) suggest that biomass burning OA will absorb less light as photochemical reactions progress.

Table 4-1. Summary of experimental conditions of fresh wood smoke for photochemical oxidation

No	Date	Chamber	RH	Temp.	NO_x	Initial OC	EC/TC	Comments
			%	K	ppb	ug/m^3	%	
1	Oct.11, 2012	E	39-95	291-312	43	56	4.76	middle NO_x
2	Oct.11, 2012	W	51-95	291-311	16	40	5.56	low NO_x
3	Oct.30, 2012	E	21-87	275-300	108	58	4.17	high NO_x
4	Oct.30, 2012	W	26-88	275-297	16	68	3.33	low NO_x
5	Oct.24, 2012	E	10-26	291-311	5	58	3.23	low RH
6	Oct.24, 2012	W	80-87	291-310	6	58	3.57	high RH
7	Nov.01, 2012	E	12-23	281-306	5	111	4.35	low RH
8	Nov.01, 2012	W	56-75	283-304	6	77	2.78	middle RH
9	Nov. 21, 2012	W	67-87	285-305	10	144	2.50	chemical analysis

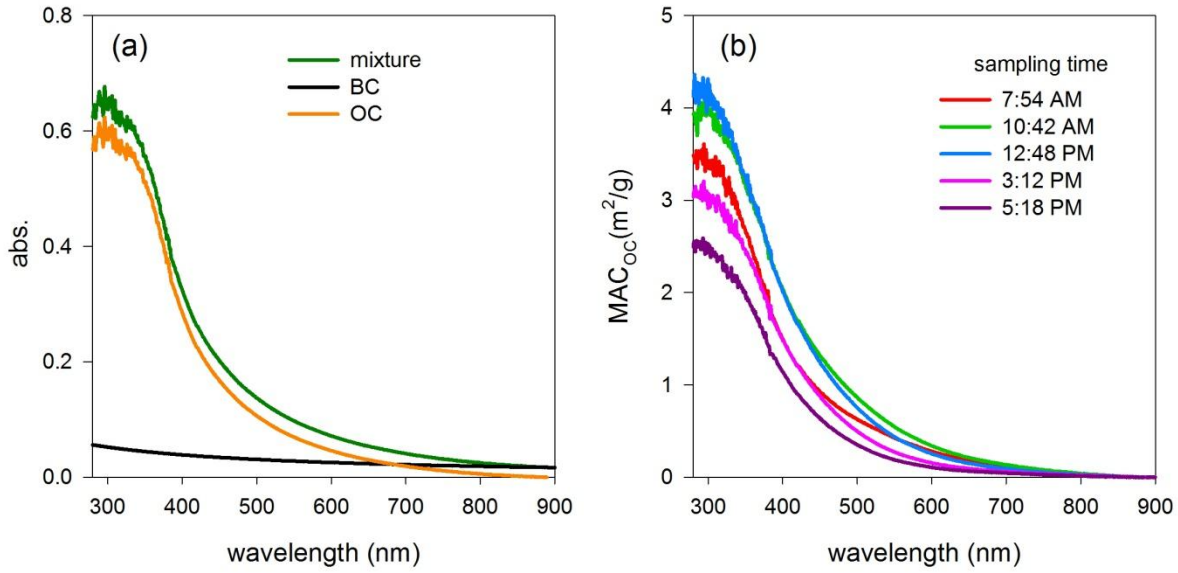

Figure 4-1. UV-visible light absorption spectra and MAC_{OC} of wood smoke OC. A) The absorption spectrum of wood smoke OC obtained by subtracting the BC absorbance from the total absorbance of wood burning particles. B) The diurnal pattern of MAC_{OC} of wood smoke OC photochemically aged under natural sunlight (Oct.11, 2012, middle NO_x).

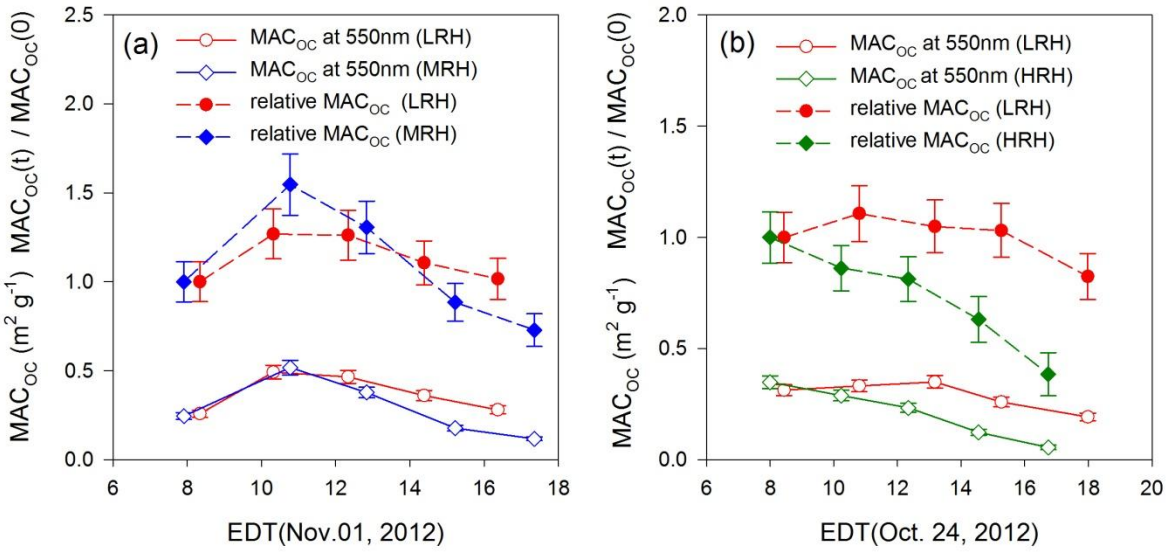

Figure 4-2. Comparison of light absorption of wood OA photochemically oxidized at different humidity conditions: A) low RH vs middle RH and B) low RH vs high RH. The open symbols are for MAC_{OC} at 550nm. The filled symbols are for the relative $MAC_{OC,}$ which is expressed as the total MAC_{OC} divided by the initial total MAC_{OC}. The error associated with MAC_{OC} was estimated based on the instrumental errors from OC/EC analyzer and UV-visible spectrometer as well as the uncertainty from the correction factor, *C* (see equation 5).

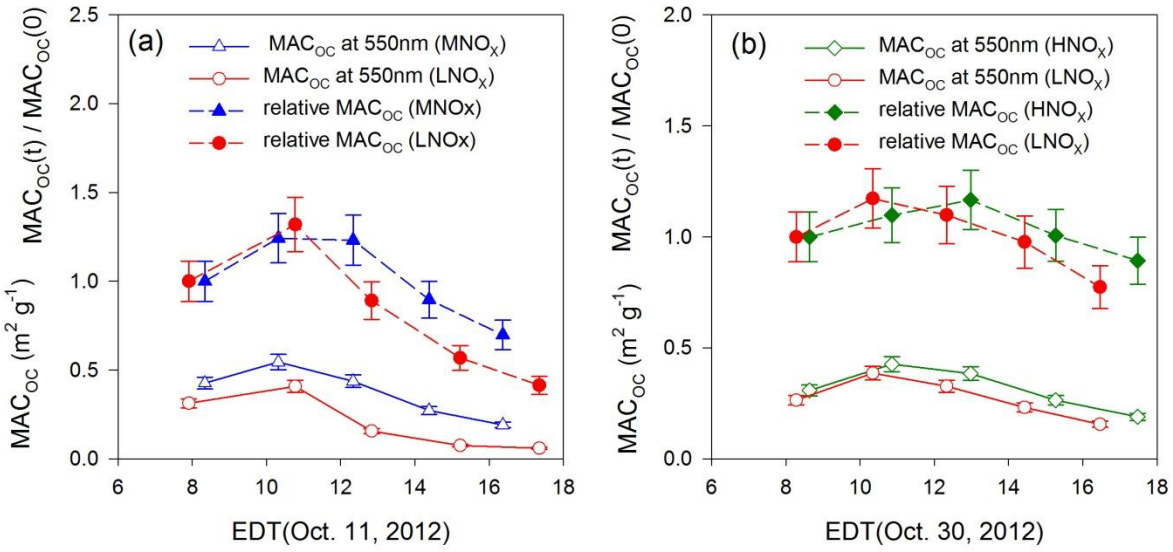

Figure 4-3. Comparison of light absorption of wood OA photochemically oxidized at different NO_x conditions: a) low NO_x vs middle NO_x and b) low NO_x vs high NO_x. The open symbols are for MAC_{OC} at 550nm. The filled symbols are for the relative MAC_{OC}, which is expressed as the total MAC_{OC} divided by initial total MAC_{OC}. The error associated with MAC_{OC} was estimated based on the instrumental errors from OC/EC analyzer and UV-visible spectrometer as well as the uncertainty from the correction factor, *C* (see equation 5).

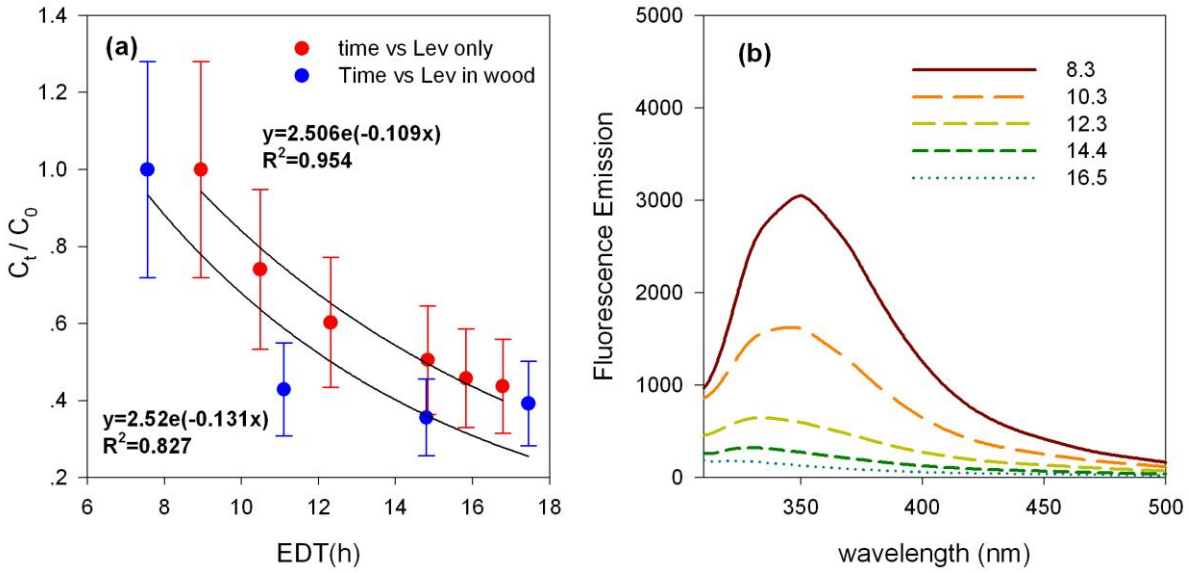

Figure 4-4. Decay of levoglucosan and PAHs. A) Time profile for the decay of pure levoglucosan (March 27, 2013) and levoglucosan in wood smoke OA (Nov. 21, 2012). The concentrations of levoglucosane (C_t) were corrected for wall-loss of particles and then normalized by the initial leveglucosan concentration (C_0). The associated error with the measured concentration of levoglucosan by GC-MS is ±20%. B) Fluorescence emission spectra of wood smoke particles collected at different times on Nov. 21, 2012. The excitation wavelength was 280nm. The error associated with the concentration of levoglucosan was estimated based on GC-MS.

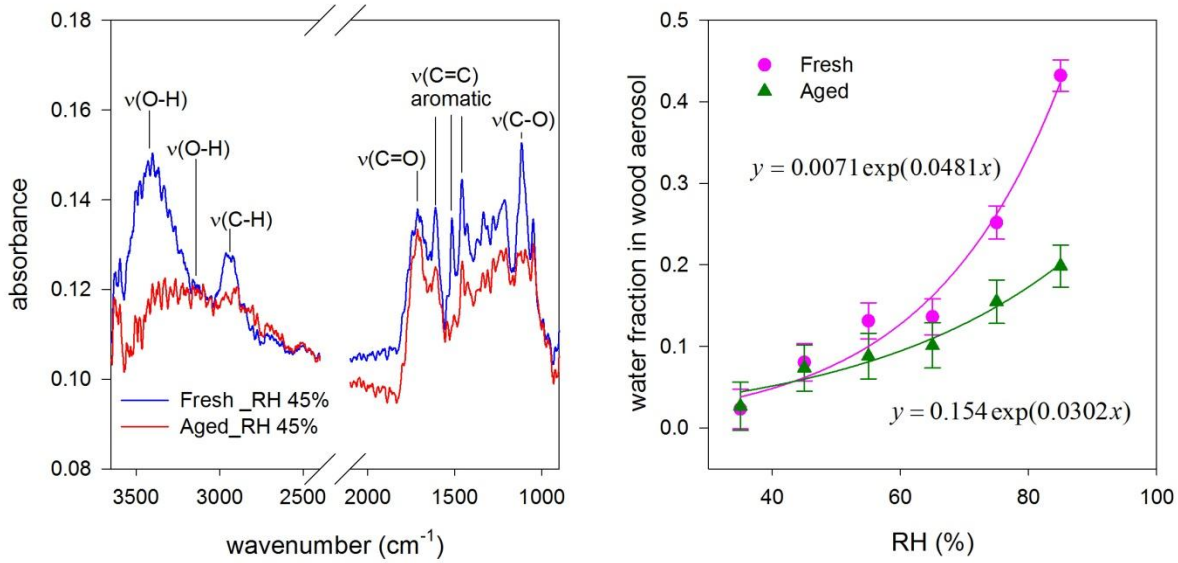

Figure 4-5. FTIR spectra and hygroscopic growth profile of fresh and aged wood burning particles. A) FTIR spectra of fresh and aged wood burning particles sampled on Nov.21, 2012. The spectra were recorded at RH of 45%. B) The water content of fresh particles and aged particles as a function of RH. The water content was measured with decreasing RH. The error associated with the water fraction in aerosol was estimated based on aerosol mass and FTIR absorbance at 1650cm^{-1}.

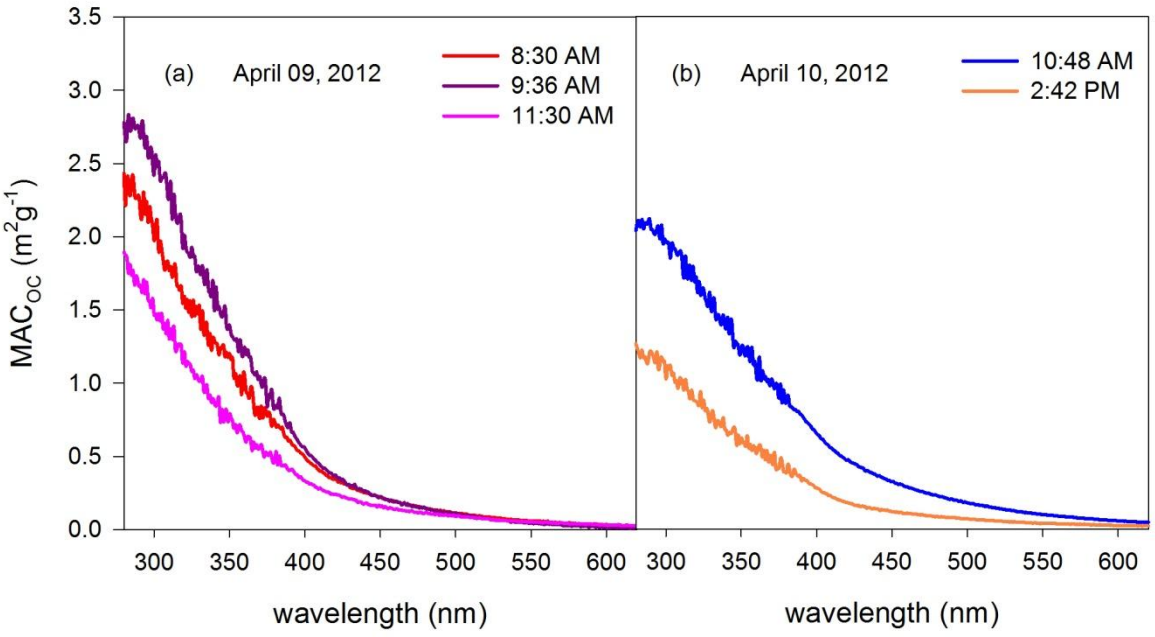

Figure 4-6. Light absorption of ambient biomass burning OA sampled during the country line wildfire event at different date: A) April 09, 2012 and B) April 09, 2012

CHAPTER 5
RADIATIVE IMPACT OF ORGANIC CARBON AEROSOL

Background

There are few studies available for the climate forcing of organic aerosols. Hoyle et al. (2009) calculated the climate forcing of SOA using the off-line aerosol chemistry transport model Oslo CTM2 and suggested a global average radiative forcing of -0.09~-0.06 w/m^2. This value was similar to that of POA. This study provides the first information about the anthropogenic influence of SOA climate impact. However, in their study, optical properties of SOA were taken to be similar to POA (Myhre et al., 2009). And the optical properties of POA were treated as same as those of sulfates.

What is the uncertainty caused by using sulfates as the surrogate of SOA? Is POA a good surrogate for SOA? The recent studies show that alpha-pinene SOA slightly absorbs UV light (Zhong and Jang, 2011), while POA from wood burning has much stronger absorption capability (Chen and Bond, 2010). The objective of this study is to calculate the radiative forcing of SOA and POA using the latest available measured optical data for the purpose of reducing uncertainties related to organic aerosol in the current climate model. To achieve the objective, the following steps will be followed: 1. calculate the single particle optical parameters of POA and SOA using Mie scattering model; 2. compute and compare radiative forcing of POA and SOA using a radiative transfer model.

Method

Optical parameters such as extinction cross-section area (Ext., $\sigma_{ext.}$), single scattering albedo (SSA, ω) and aerosol asymmetry factor(asym, g) were calculated using Mie scattering model with input of refractive index and particle size at certain RH.

A simple equation was then used to estimate the radiative forcing of organic carbon aerosol. The following section will describe the detailed procedure for each step.

Mie Scattering Model

The Lorenz -Mie solution to Maxwell's equation describes the scattering of electromagnetic radiation by a sphere. The Lorenz-Mie code from Dr. Tami Bond's research website (http://www.hiwater.org/), calculates absorption, scattering and backscattering for spherical, coated or uncoated particles of lognormal or measured size distributions. The only required input parameters are particle size and complex refractive index (RI, $n + ki$). In this study, the dry particle size is assumed to be lognormal distributed with count median diameter of 138 nm, geometric standard deviation of 2. The size parameter is taken from a study for ambient organic aerosol (Kaul et al., 2012).

The measured real part of RI (Kim and Paulson, 2013) is used for both SOA and POA. It is known that real RI is a function of wavelength. Since the measurement is only available at 550 nm, the fixed value (1.44) is used for the UV and visible wavelength range. The imaginary RI data of SOA and POA are from laboratory measurement in this work. Here SOA is represented by alpha-pinene SOA and POA by wood burning organic aerosol. In addition, sulfate droplet was simulated as reference for comparison purpose. The refractive index of sulfate droplet is taken from OPAC data base (http://ether.ipsl.jussieu.fr/etherTypo/?id=1058). Using the above input parameters, the Mie calculation was performed every 10 nm between 280 and 800 nm to provide scattering, absorption, and extinction cross section area. Table D-1 to D-5 summarizes the model experiments which were carried out.

Effect of RH on Particle Size

SOA can absorb water vapor at certain relative humidity. Consequently, the diameter of particle will depend on the relative humidity. The hygroscopic growth has immediate influence on the scattering of solar radiation. An empirical model (Birmili et al., 2009) was adopted to calculate the particle size change due to RH. The model is derived from ambient aerosols from a Finnish forest with OC fraction of 30% to 50%. It is used here for 100% organic aerosol since no better model is available. Growth factor (GF) is defined as follows:

$$GF\left(\mathrm{D}_p, RH\right) = \frac{D_p\left(RH = i\right)}{D_p\left(RH = 0\right)}, \tag{5-1}$$

where D_p is particle diameter. GF can be estimate using an empirical equation:

$$GF\left(\mathrm{D}_p, RH\right) = \left(1 - RH\right)^{-\alpha(D_p)}, \tag{5-2}$$

where $\alpha(D_p)$ is a function of dry particle diameter and estimated by:

$$\alpha\left(D_p\right) = 0.16215 - \frac{0.09177}{1 + e^{\frac{\ln Dp - 4.83217}{0.17168}}}. \tag{5-3}$$

According to the model developer, this empirical model can safely be applied for all particle size although the fit is only supported by data points between 60 nm and 350 nm.

Simple Radiative Efficiency Estimation

A simple forcing efficiency (SFE, W/cm^3 aerosol) was used here to provide a first estimate of climate impact of organic aerosols. The calculation was originated from Chylek and Wong (1995) equation that normalizes impact by particle volume. The wavelength dependent SFE is calculated as:

$$\mathrm{SFE} = -\frac{S(\lambda)}{4}\tau_{atm}^{2}(1-F_C)\left[2(1-\omega_s)^2\beta\sigma_{scat} - 4\omega_s\sigma_{abs}\right], \qquad (5\text{-}4)$$

where S(λ) is the solar irradiance, τ_{atm} is the atmospheric transmission (0.79), F_C is the cloud fraction(0.6), ω_s is the surface albedo(0.19), β is the backscatter fraction. σ_{scat} and σ_{abs} are the scattering and absorption cross sections per cm^3,respectively. The matlab code for this calculation is available on the website (http://www.hiwater.org/).

Results and Discussion

Optical Parameters

Figure 5-1 compares three optical parameters of SOA, POA and sulfates, extinction cross section area, aerosol asymmetry factor and single scattering albedo. The extinction cross section area is a measure of how strongly the aerosol absorbs and scatters light. The simulation result shows that extinction cross section area of the three types of aerosol is similar, decreasing with wavelength (Figure 5-1a). Aerosol asymmetry factor is a measure of the preferred scattering direction, forward or backward. In Figure 5-1b, the aerosol asymmetry factor is positive, indicating scattering is mainly in the forward direction. POA asymmetry factor is a little bit larger than SOA and sulfate in the UV range, but all are almost same in the visible range. Single scattering albedo (SSA) is the ratio of scattering to the extinction, ranging from 0 to 1. Values of SSA below 0.8 indicate that the aerosol could have a warming effect. Figure 5-1c shows SSA of SOA is near to 1 in the wavelength range between 280 nm and 800nm indicating SOA is mainly scattering, not active in absorbing light. SSA of POA gradually increases from 0.7 to 1, indicating the absorption of POA decrease with wavelength. This trend matches well with the trend of imaginary refractive index of POA.

Effect of RH on Optical Parameters

Relative humidity affects the optical properties of aerosol by changing particle size and adding water into particle. Figure 5-2 compares the dry SOA and wet SOA at RH of 50%. For Mie calculation, the water can be assumed to externally coat on the surface of aerosol. The simulation results show that higher humidity increases both extinction cross section area and aerosol asymmetry factor, but has little influence on aerosol single scattering albedo. Similar tread is also observed for POA, but not shown here.

Radiative Impact

Figure 5-3 shows forcing of SOA, POA and sulfate as a function of wavelength. The forcing of SOA is below zero in the studied wavelength, while that of POA is positive in the short UV range and negative in the visible range. Due to the significant difference in forcing of SOA and POA, it should be very cautious to replace POA and SOA with each other. The forcing of SOA is very similar to that of sulfate. Thus sulfate is a reasonable surrogate for SOA in terms of optical parameters. High RH increases the negative forcing for SOA and POA by adding non absorbing water. A full radiative transfer model would be necessary to determine the actual forcing of SOA.

Conclusion

The optical parameters of POA and SOA were estimated using measured refractive index by running the Mie scattering model. RH could change the particle size and thus the optical properties of organic aerosols. A simple estimation of radiative efficiency shows that POA has warming effect in the UV range, while SOA is a cooling aerosol, with similar radiative forcing to sulfate.

The estimation of the actual forcing of OC requires a full radiative transfer model with OC burden and meteorological data. OC burden can be estimated using a global model such as GEOS-Chem. A radiative transfer model such as Fu-Liou-Gu model (Gu et al., 2006) can be tested to produce the radiative forcing of OC.

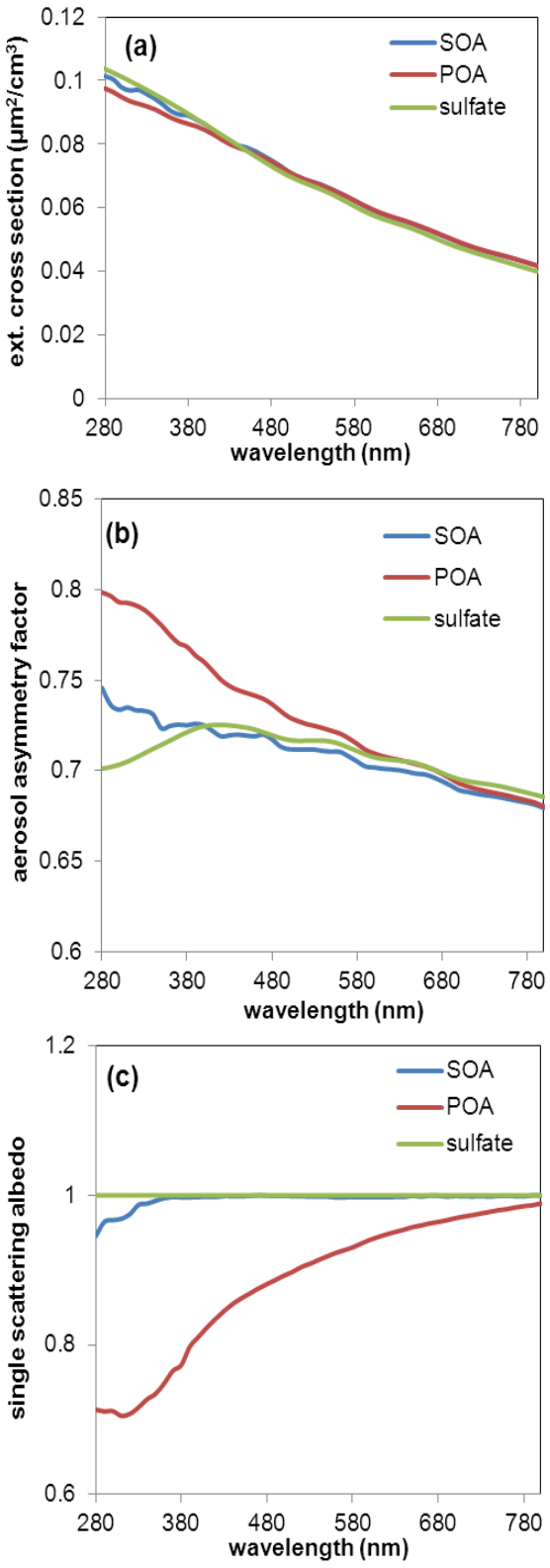

Figure 5-1. Optical parameters of SOA, POA and sulfate estimated using Mie code: (a) extinction cross section area, (b) aerosol asymmetry factor, and (c) single scattering albedo.

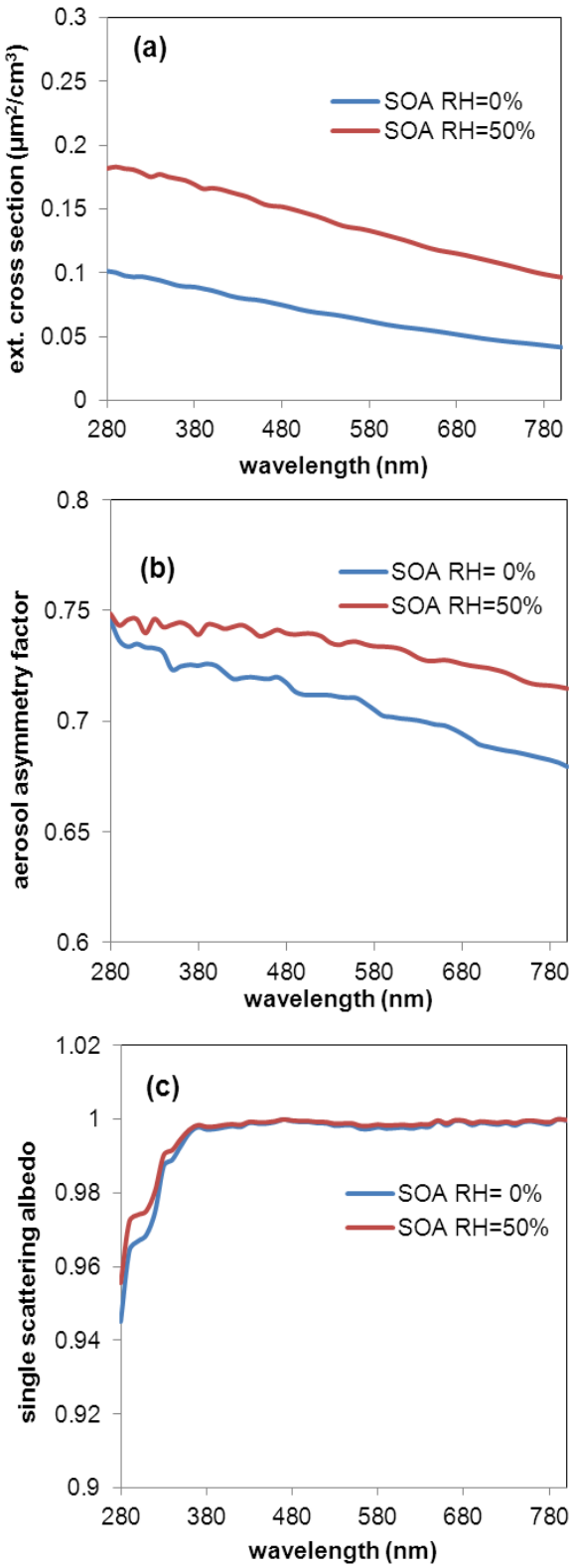

Figure 5-2. Effect of RH on optical parameters: (a) extinction cross section area, (b) aerosol asymmetry factor, and (c) single scattering albedo.

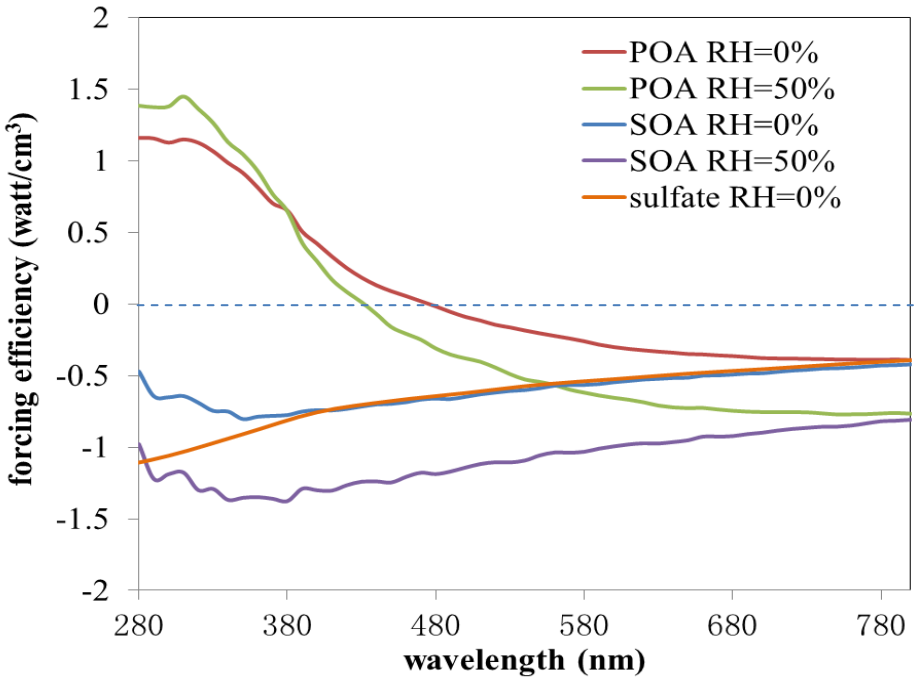

Figure 5-3. Comparison of radiative efficiency of SOA, POA and sulfate as a function of wavelength.

CHAPTER 6
CONCLUSIONS

A method for measuring the mass absorption cross section (*MAC*) of organic aerosol has been developed using a conventional UV-visible spectrometer equipped with an integrating sphere covering a wide range of wavelengths (280-800nm). The feasibility of the proposed method was evaluated using reference aerosols with known absorption cross section. This method directly measures *MAC* of organic aerosol on a conventional filter without solvent extraction.

The resulting method was applied to measure *MAC* of secondary organic aerosol (SOA) which was produced through photooxidation of different precursor hydrocarbons such as toluene, *d*-limonene and *α*-pinene using a 2 m^3 indoor Teflon film chamber. *MAC* value of toluene SOA (0.574 m^2g^{-1} at 350 nm) was the highest compared with *MAC* values for *α*-pinene SOA (0.029 m^2g^{-1}) and *d*-limonene SOA (0.038 m^2g^{-1}). When *d*-limonene SOA or toluene SOA was internally mixed with neutral [$(NH_4)_2SO_4$] or acidic inorganic seed (NH_4HSO_4:H_2SO_4 = 1:1 by mole), the SOA showed 2~3 times greater *MAC* values at 350 nm than the SOA with no seed. Aerosol aging with a light source for this study reduced *MAC* values of SOA (e.g., on average 10% for toluene SOA and 30% for *d*-limonene SOA within 4 hours).

The new model for UV-visible absorption spectrum of SOA in this work predicted that the light absorption of toluene SOA would increase with higher NO_x concentration, and that of alpha-pinene SOA is not affected by NO_x. The model results were in reasonably good agreement with the measurements. The model also predicted that the main light absorbing materials in toluene SOA were nitro-phenols and those in alph-pinene SOA were pinonaldehydes.

The method was also used to quantify *MAC* of primary organic aerosols (POA). POA produced under smoldering conditions was photochemically aged under different relative humidity and NO_x conditions using an outdoor chamber under natural sunlight. The measurement results suggest that *MAC* of POA changed under atmospheric conditions, increasing in the morning and decreasing in the afternoon, due to the competition between chromophore formation and sunlight bleaching. A similar trend in light absorption changes was observed in ambient smoke aerosol originating from the 2012 County Line Wildfire in Florida. We conclude that the biomass burning POA becomes less light absorbing after 8~9 hours sunlight exposure.

The simple estimation of radiative efficiency suggests that SOA is a cooling aerosol, having a similar value of radiative forcing to sulfate. Fresh POA has positive radiative forcing in the UV wavelength rang and negative forcing in the visible range. The net forcing is positive, thus fresh POA is warming aerosol.

CHAPTER 7
FUTURE STUDIES

The current study provides the experimental measured optical properties of organic carbon aerosols, contributing to reduce the uncertainties organic carbon aerosols in climate change. There are several directions for further study of the climate impact of aerosols:

1. Effect of high humidity on light absorption of SOA and POA This study has shown that RH at 85% will accelerate the decay of *MAC*. In the upper troposphere, RH usually reaches up to 100%. The study of optical properties of OC at high RH will benefit the modeling of OC which travel to the upper level of troposphere.

2. Light absorption of mixed aerosols. In atmosphere, organic aerosols usually mixed with other types of aerosols. For example, POA are always emitted together with black carbon. SOA can mix with dust or black carbon. Anthropogenic SOA may mix with biogenic SOA. Understanding the mixing rule in light absorption of different aerosols will make it possible to predict light absorption of aerosol mixture in atmosphere.

3. Identification of light absorbing materials This work suggests possible light absorbing materials in SOA and POA, such as nitrophenols. However, chemical analysis for these compounds has not been conducted. GC-MS or LCMS analysis is necessary in the future to identify these light absorbing chemicals in laboratory generated aerosols and field sampled ambient aerosols.

4. Hygroscopic properties of SOA and POA Hygroscopic growth of aerosol is directly related to cloud condensation nuclei. The indirect climate effect of organic aerosols associated with cloud formation is among the least understood factors in

climate system. The study of hygroscopic properties of fresh and aged organic aerosols is necessary to provide fundamental parameters for cloud formation.

5. Evaluate the radiative forcing of OC using radiative transfer model The current study uses a simple equation to estimate the radiative efficiency of OC without considering the mass budget of OC. As a further study of this research, the calculation of radiative forcing of OC using radiative transfer model and global chemical transport model needs to be achieved to have better evaluation of the role of OC in climate system.

APPENDIX A
SUPPLEMENTARY METERIALS FOR CHAPTER 2

Table A-1. Indoor Teflon film chamber experiments [a] involving the aerosol of known composition

No.	Aerosol	f [b]	Sample volume (m^3)	L [c] (m)	Aerosol vol. conc. (nL/m^3)	Density[d] (μg/nl)	Mass[e]$_{MY}$ (μg)	n [f] ($\#/m^3$)	$\ln(1/T)^g_{\lambda=434}$ Predicted	$\ln(1/T)^h_{\lambda=422}$ Measured
M1	MY	1.0	0.002	19.10	67	1.47	0.15	1.59E+17	0.034	0.036
M2	MY	1.0	0.003	38.20	69	1.47	0.30	1.63E+17	0.069	0.077
M3	MY	1.0	0.005	66.85	50	1.47	0.39	1.19E+17	0.088	0.173
M4	MY	1.0	0.010	127.32	49	1.47	0.71	1.14E+17	0.162	0.217
M5	MY	1.0	0.015	188.21	44	1.47	0.96	1.04E+17	0.217	0.363
M6	MY	1.0	0.015	190.99	70	1.47	1.54	1.65E+17	0.350	0.607
M7	MY-NaCl	0.0533	0.014	178.25	238	2.11	0.38	4.30E+16	0.085	0.158
M8	MY-NaCl	0.0533	0.028	358.29	244	2.11	0.77	4.41E+16	0.175	0.291
M9	MY-NaCl	0.0533	0.058	742.17	237	2.11	1.56	4.28E+16	0.352	0.518
M10	MY-NaCl	0.0533	0.083	1058.83	238	2.11	2.23	4.30E+16	0.506	0.665
M11	MY-NaCl	0.0533	0.112	1421.78	240	2.11	3.01	4.33E+16	0.682	0.783
M12	MY-NaCl	0.0533	0.160	2041.26	233	2.11	4.20	4.21E+16	0.952	0.869

a:Temperature and humidity are in the ranges of 294–298 K and 30.5-36.8%, respectively
b:F is the mass fraction of MY aerosol to total sampled aerosol
c:Length is obtained by sample air volume divided by the sample area of filter.
d:Density of MY aerosol is calculated by using molar weight divided by molar volume.
e:The estimated MY aerosol mass for each aerosol filter sample is obtained by multiplying sample volume to vol. conc., density and *f*.
f: *n* is estimated by equation (7).
g: Predicted $\ln(1/T)$ based on Equation (2-6) has a maximum value at λ=434 nm. Absorption cross section of MY at λ=434 nm is 1.12×10^{-20} m^2
h: Measured $\ln(1/T)$ is maximum at λ=422 nm

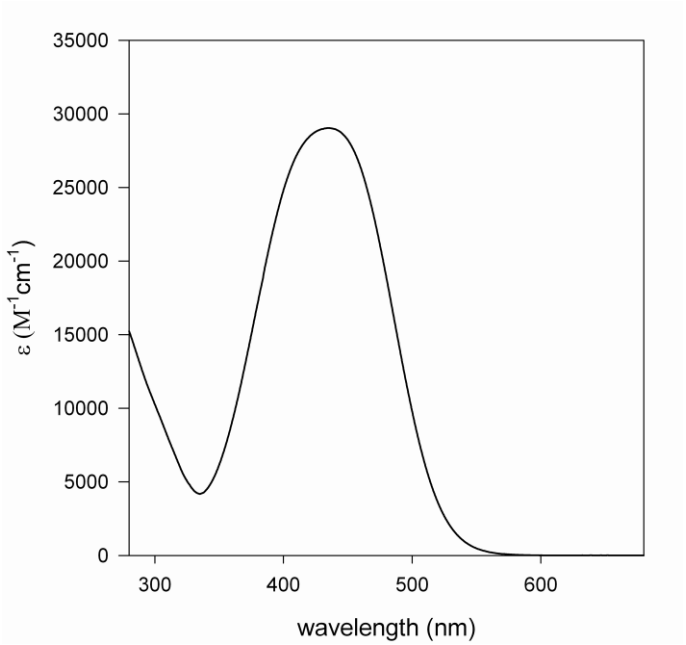

Figure A-1. Measured molar absorptivity of metanil yellow as a function of wavelength (280-680 nm).

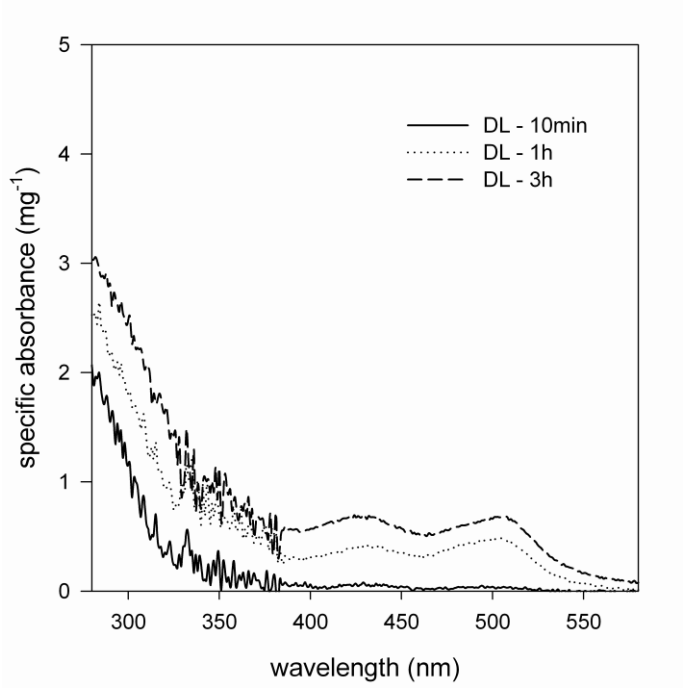

Figure A-2. UV-visible absorption spectra of *d*-limonene SOA collected on the filter at different exposure time in air. The SOA samples were stored in open air. SOA color turned to orange yellow in three hours corresponding to the growth of two absorption peaks at 428 nm and 505 nm.

APPENDIX B
SUPPLEMENTARY METERIALS FOR CHAPTER 3

Table B-1. Chemical structure of toluene SOA products

MCM name	IUPAC name	Structure
MNCATECH	3-methyl-6-nitrobenzene-1,2-diol	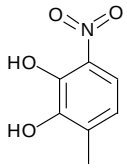
MNNCATCOOH	(2R)-2-hydroperoxy-2,3-dihydroxy-1-methyl-4-nitro-6,7-dioxabicyclo[3.2.1]oct-3-en-8-yl nitrate	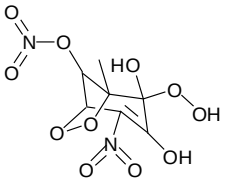
DNCRES	2-methyl-4,6-dinitro-phenol	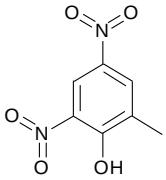
TLEMUCOOH	3-(2-hydroperoxy-1-hydroxy-3-oxo-butyl)-oxirane-2-carbaldehyde	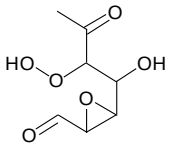
TLEMUCNO3	1-(3-formyloxiran-2-yl)-1-hydroxy-3-oxobutan-2-yl nitrate	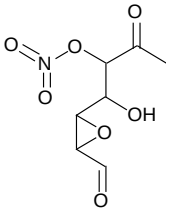
TLBIPEROOH	(1S,4S,5S)-4-hydroperoxy-1-methyl-6,7-dioxabicyclo[3.2.1]oct-2-en-8-ol	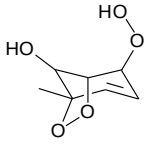

Table B-1. Continued

MCM name	IUPAC name	Structure
TLBIPERNO3	(1S,2S,5S)-8-hydroxy-5-methyl-6,7-dioxabicyclo[3.2.1]oct-3-en-2-yl nitrate	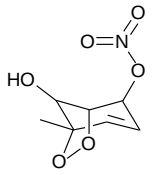
NC4MDCO2H	(Z)-2-methyl-3-nitro-4-oxobut-2-enoic acid	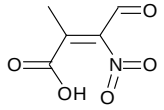
TLEMUCCO	3-(1-hydroxy-2,3-dioxobutyl)oxirane-2-carbaldehyde	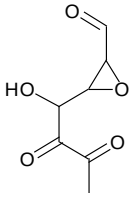
TOL1OHNO2	2-methyl-6-nitrophenol	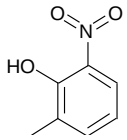
ACCOMEPAN	3-acetoxy-3-oxopropanoic nitric peroxyanhydride	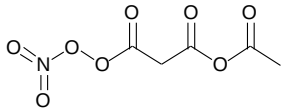
MALDIALPAN	nitric (E)-4-oxobut-2-enoic peroxyanhydride	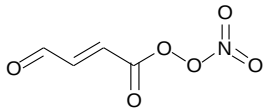
C5COO2NO2	nitric (E)-4-oxopent-2-enoic peroxyanhydride	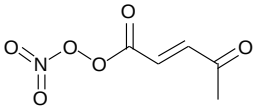

Table B-1. Continued

MCM name	IUPAC name	Structure
MALANHY	furan-2,5-dione	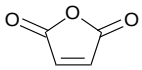
C5DICARB	4-Oxo-pent-2-enal	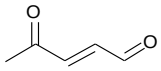
MGLYOX	2-oxopropanal	
GLYPAN	nitric 2-oxoacetic peroxyanhydride	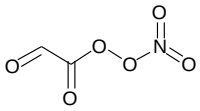
GLYOX	oxalaldehyde	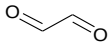
GLYOX oligomer	2-Dihydroxymethyl-[1,3]dioxolane-4,5-diol	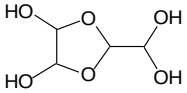
MGLYOX oligomer	2-Dihydroxymethyl-2,4-dimethyl-[1,3]dioxolane-4,5-diol	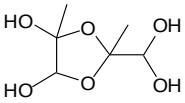

Table B-2. Representative products of toluene SOA and their mass percentages at different NO_x conditions

Group (*i*, *j*)	*k*	Products name[a]	MW_k	λ_{max}[b] (nm)	*f*[b]	F_k[c] (%)		
						H NO_x (T1)	M NO_x (T2)	L NO_x (T3)
1, PO	1	MNCATECH	169	330, 228	0.05, 0.40	26.27	30.48	26.14
	2	MNNCATCOOH	281	270, 199, 189, 188	0.3, 0.15, 0.31, 0.03	2.95	6.36	6.47
	3	DNCRES	191	321, 229, 227, 222, 203	0.04, 0.17, 0.40, 0.82, 0.08	2.00	0.88	0.32
1, H-m	4	TLEMUCOOH	190	177, 165, 161	0.04, 0.05, 0.03	1.04	3.04	4.41
	5	TLEMUCNO3	190	177, 165, 161	0.04, 0.05, 0.03	2.40	1.57	1.10
2, PO	6	TLBIPEROOH	174	216, 213, 163, 153, 143	0.19, 0.11, 0.13, 0.10, 0.05	2.13	8.68	14.00
	7	TLBIPERNO3	174	415, 233	0.06, 0.07	3.85	3.46	2.78
2, H-s	8	NC4MDCO2H	159	228, 226, 221, 202, 177, 172, 168	0.15, 0.08, 0.21, 0.26, 0.22, 0.19, 0.05	6.71	3.19	1.38
2, H-f	9	TLEMUCCO	156	202, 148	0.35, 0.03	0.53	0.81	1.09
3, PO	10	TOL1OHNO2	153	316, 222	0.04, 0.17	0.77	0.51	0.23
3, H-f	11	ACCOMEPAN	207	206, 187, 174	0.08, 0.26, 0.25	2.29	10.34	7.67
4, H-m	12	MALDIALPAN	161	208, 190, 176, 158	0.07, 0.27, 0.26, 0.05	0.59	0.48	0.41
	13	C5COO2NO2	175	227, 184, 176	0.59, 0.22, 0.26	0.99	1.03	1.17
5, H-m	14	MALANHY	98	230	0.17	2.26	1.00	1.01
	15	C5DICARB	98	223, 166, 162, 155	0.65, 0.06, 0.09, 0.42	0.55	0.21	0.14
	16	MGLYOX (oligomer)	72	193, 171, 160, 155	0.20, 0.34	4.98	2.55	2.16
	17	GLYPAN	135	213, 189, 183, 168	0.13, 0.04, 0.47, 0.53	1.12	0.53	0.33
5, H-f	18	GLYOX (oligomer)	58	196, 182, 163, 160	0.14, 0.06, 0.39, 0.11	37.17	23.26	27.30

a: The names of chemicals are from MCM mechanism; b: λ_{max} and *f* are calculated using NDDO based AM1 semiempirical quantum chemistry method; c: F_k is the mass percentage of the *k*th species, obtained by the mass balance of chemical compounds in toluene SOA.

Table B-3. Chemical structure of α-pinene SOA from MCM mechnism

MCM name	IUPAC name	Structure
C811PAN	2,2-dimethyl-3-(2-(nitroperoxy)-2-oxoethyl)cyclobutanecarboxylic acid	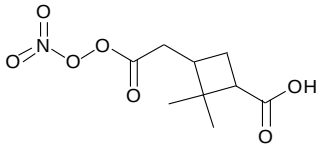
PINIC	3-(carboxymethyl)-2,2-dimethylcyclobutanecarboxylic acid	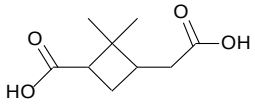
C921OOH	1-(1-hydroperoxy-3-(hydroxymethyl) -2,2-dimethylcyclobutyl)-2-hydroxyethanone	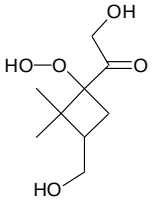
C812OOH	1-hydroperoxy-3-(hydroxymethyl)-2,2-dimethylcyclobutanecarboxylic acid	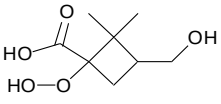
HOPINONIC	2-(3-(2-hydroxyacetyl)-2,2-dimethylcyclobutyl) acetic acid	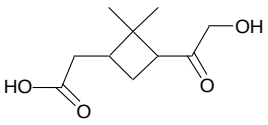
C920PAN	2-(3-(2-hydroxyacetyl)-2,2-dimethylcyclobutyl)acetic nitric peroxyanhydride	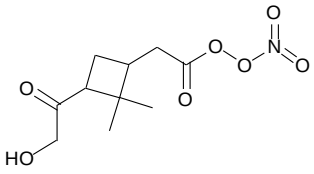

Table B-3. Continued.

MCM name	IUPAC name	Structure
C98OOH	6-hydroperoxy-5-(hydroxymethyl)-6-methylheptane-2,3-dione	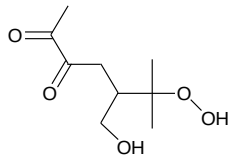
C98NO3	3-(hydroxymethyl)-2-methyl-5,6-dioxoheptan-2-yl nitrate	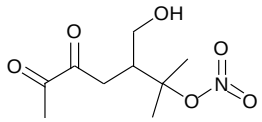
C922OOH	6-hydroperoxy-1-hydroxy-5-(hydroxymethyl)-6-methylheptane-2,3-dione	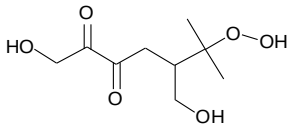
C7PAN3	nitric 3,5,6-trioxoheptanoic peroxyanhydride	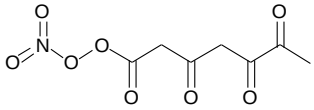
C10PAN2	2-(3-acetyl-2,2-dimethylcyclobutyl)acetic nitric peroxyanhydride	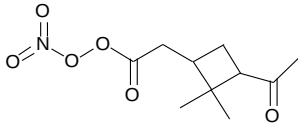
C97OOH	1-(1-hydroperoxy-3-(hydroxymethyl)-2,2-dimethylcyclobutyl)ethanone	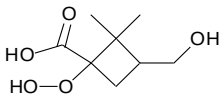
C717NO3	1,5,6-trioxoheptan-3-yl nitrate	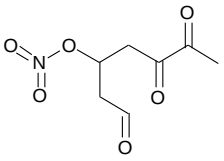

Table B-3. Continued.

MCM name	IUPAC name	Structure
C108OOH	3-(2-hydroperoxypropan-2-yl)-5,6-dioxoheptanal	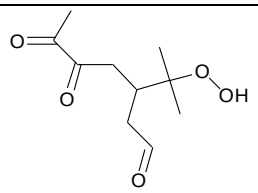
APINAOOH	2-hydroperoxy-2,6,6-trimethylbicyclo[3.1.1]heptan-3-ol	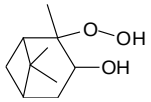
APINANO3	3-hydroxy-2,6,6-trimethylbicyclo[3.1.1]heptan-2-yl nitrate	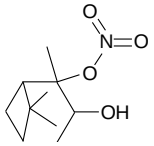
APINBNO3	2-hydroxy-2,6,6-trimethylbicyclo[3.1.1]heptan-3-yl nitrate	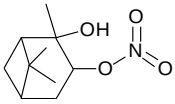
PINONIC	2-(3-acetyl-2,2-dimethylcyclobutyl)acetic acid	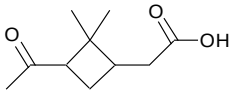
C89PAN	2,2-dimethyl-3-(2-oxoethyl)cyclobutanecarboxylic nitric peroxyanhydride	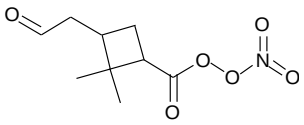
C107OH	2-(3-acetyl-3-hydroxy-2,2-dimethylcyclobutyl)acetaldehyde	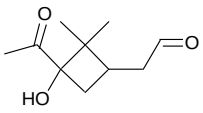

Table B-3. Continued.

MCM name	IUPAC name	Structure
C109OH	2-(3-(2-hydroxyacetyl)-2,2-dimethylcyclobutyl)acetaldehyde	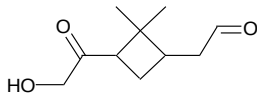
C5PAN9	nitric 3,4-dioxopentanoic peroxyanhydride	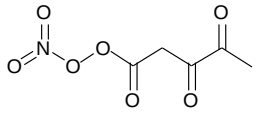
CO235C6CHO	3,5,6-trioxoheptanal	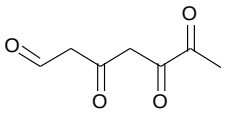
C109CO	2-(2,2-dimethyl-3-(2-oxoethyl)cyclobutyl)-2-oxoacetaldehyde	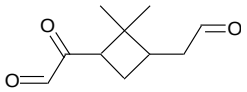
PINAL	2-(3-acetyl-2,2-dimethylcyclobutyl) acetaldehyde	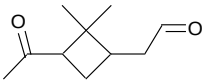

Table B-4. Representative products of α-pinene SOA and their mass percentages in SOA at different NO_x conditions

Group (i, j)	k	Products name[a]	MW_k	λ_{max}[b] (nm)	f[b]	F_k[c] (%)	
						H NO_x (A1)	L NO_x (A2)
1, H-s	1	C811PAN	247	183, 161	0.27, 0.11	4.59	3.98
	2	PINIC	186	181, 174, 164, 141, 135	0.25, 0.06, 0.03, 0.05, 0.09	0.02	1.98
	3	C921OOH	204	192, 186, 178, 167, 160, 156	0.09, 0.12,0.09, 0.08, 0.06, 0.07	0.09	1.30
	4	C812OOH	190	187, 186, 169, 164, 157	0.14, 0.10, 0.09, 0.05, 0.11	0.04	0.92
	5	HOPINONIC	200	176, 171, 169, 162, 139	0.25, 0.22, 0.12, 0.03, 0.07	0.04	1.19
1, H-m	6	C920PAN	261	196, 182, 171	0.07, 0.03, 0.06	8.40	3.91
	7	C98OOH	204	201, 167	0.29, 0.14	2.72	10.43
	8	C98NO3	233	188, 183	0.18, 0.03	6.46	2.62
	9	C922OOH	220	204, 177	0.32, 0.17	0.09	1.34
1, H-f	10	C7PAN3	233	205, 192	0.08, 0.35	18.43	3.54
2, H-s	11	C10PAN2	245	187, 171, 167	0.04, 0.08, 0.04	16.30	5.97
	12	C97OOH	188	197, 186, 180, 157, 142, 135	0.05, 0.05, 0.23, 0.05, 0.06, 0.09	0.49	6.13
2, H-f	13	C717NO3	203	184, 182, 177, 174, 165, 155	0.08, 0.19, 0.05, 0.06, 0.09, 0.06	5.28	3.12
	14	C108OOH	216	202	0.26	4.39	14.88
3, PO	15	APINAOOH	186	160, 158, 156, 153, 139, 137	0.16, 0.13, 0.07, 0.17, 0.09, 0.10	0.07	2.32
	16	APINANO3	215	174, 162, 151, 147, 146	0.07, 0.06, 0.2, 0.06, 0.08	0.93	2.42
	17	APINBNO3	215	202, 168, 158, 153	0.05, 0.04, 0.06, 0.22	0.59	1.26
3, H-s	18	PINONIC	184	173, 169, 165, 151	0.31, 0.04, 0.15, 0.08, 0.05	0.09	0.70
3, H-m	19	C89PAN	231	179, 169	0.05, 0.06	3.36	2.14
	20	C107OH	200	182, 175, 162, 145, 141	0.25, 0.06, 0.05, 0.06, 0.14	0.36	3.53
	21	C109OH	200	181, 173, 163, 140, 135	0.25, 0.06, 0.03, 0.05, 0.09	0.28	0.82
	22	C5PAN9	191	199, 184, 174, 168	0.05, 0.22, 0.25, 0.54	2.60	0.60
4, H-f	23	CO235C6CHO	156	159	0.01	2.88	2.85
	24	C109CO	182	200	0.25	0.09	0.42
5, H-m	25	PINAL	168	168, 164, 163, 157, 156, 152	0.03, 0.15, 0.06, 0.14, 0.05, 0.06	20.12	19.46

a: The names of chemicals are from MCM mechanism; b: λ_{max} and f are calculated using NDDO based AM1 semiempirical quantum chemistry method; c: F_k is the mass percentage of the kth species, obtained by the mass balance of chemical compounds in α-pinene SOA

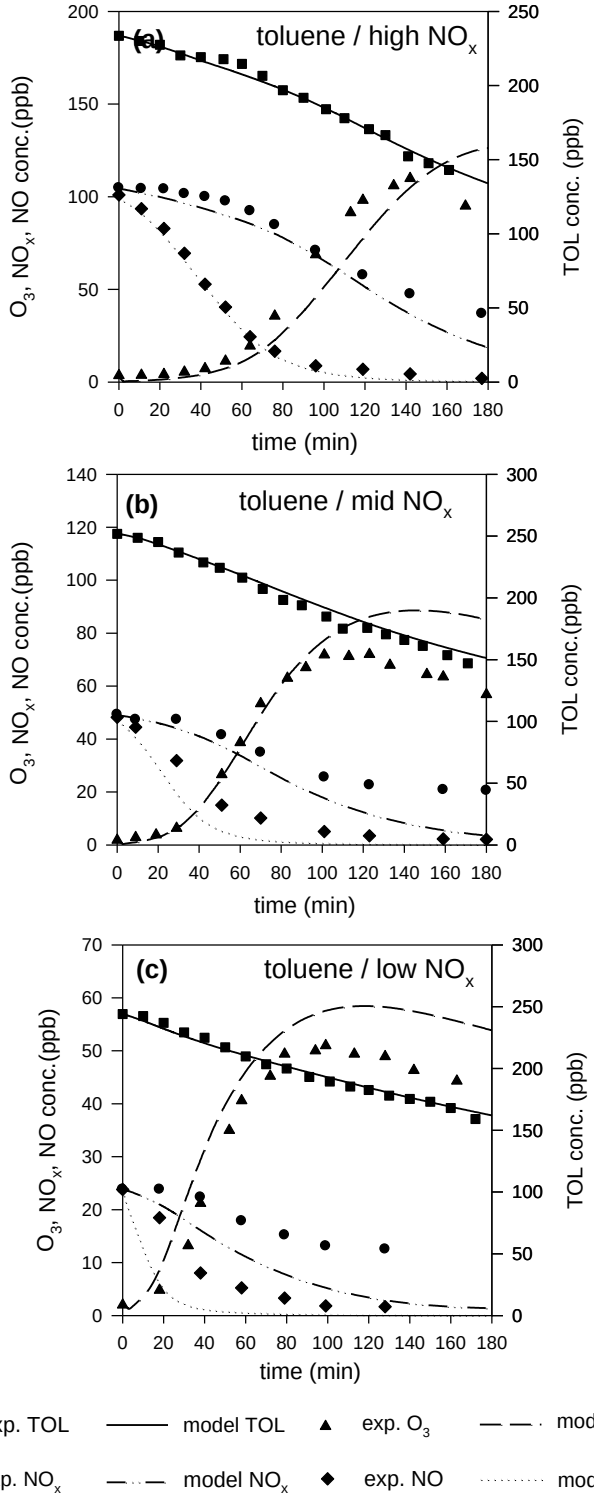

Figure B-1. Comparison of model simulated and measured concentrations of toluene, O_3, NO_x, and NO for experiments at different NO_x levels: A) high NOx, B) middle NOx, and C) low NOx levels (T1, T2 and T3).

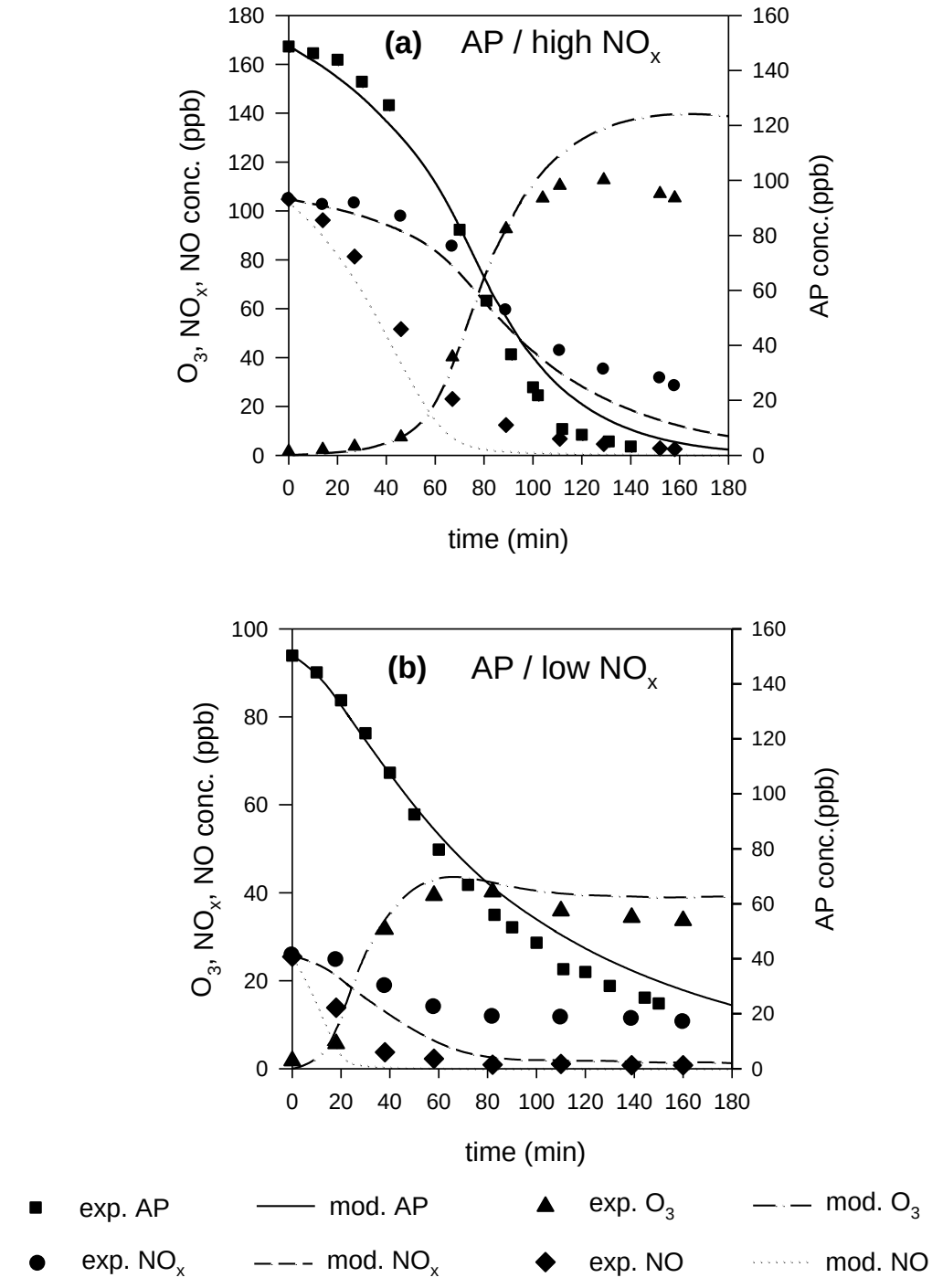

Figure B-2. Comparison of model simulated and measured concentrations of α-pinene, O_3, NO_x, and NO for experiments at different NO_x levels: A) high NO_x and B) low NO_x (A1and A2).

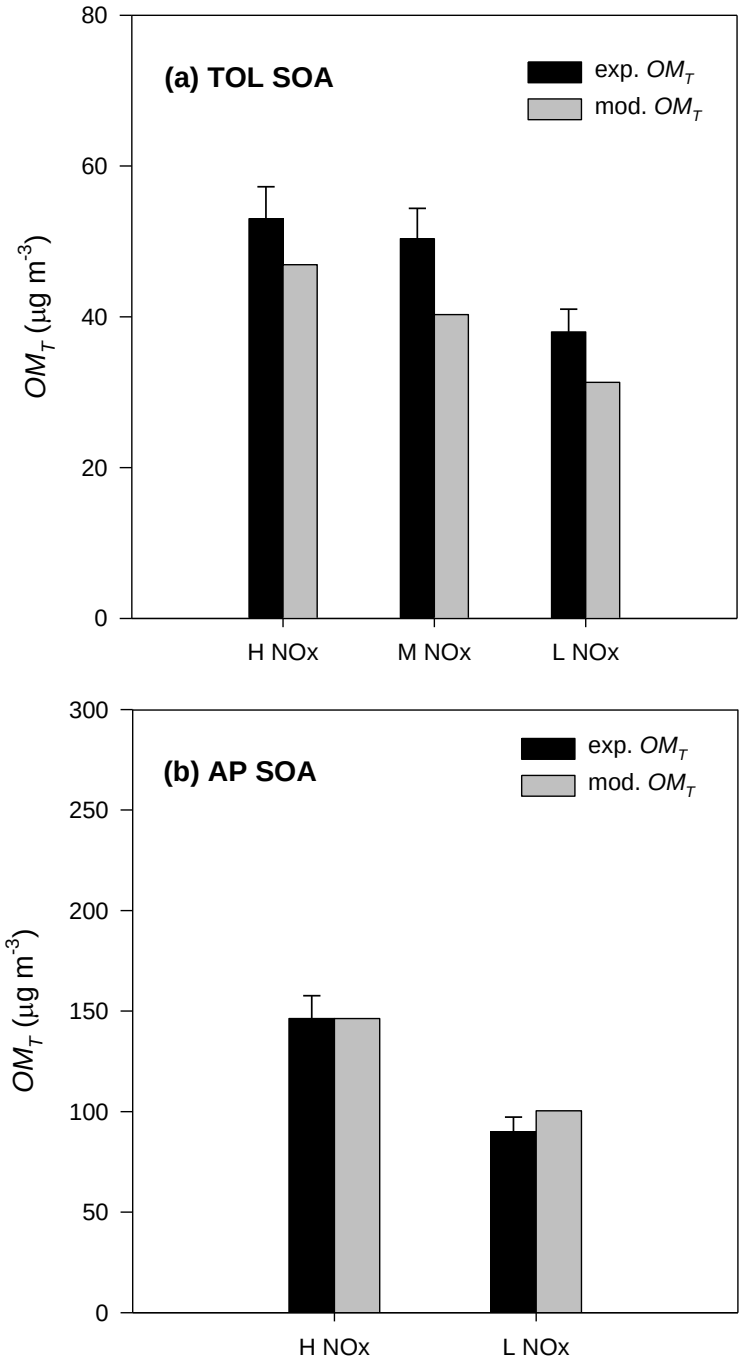

Figure B-3. Comparison of the predicted OM_T and the measured OM_T for different systems: (a) TOL SOA and (b) AP SOA, under different NO_x conditions. T1-T3 for TOL SOA and A1-A2for AP SOA (see Table 1)

APPENDIX C
SUPPLEMENTARY METERIALS FOR CHAPTER 4

Document C-1 Chamber operation and characterization of photooxidation of pure levoglucosan

Levoglucosan (99% purity, Aldrich) solid particles was dissolved in HPLC grade water to make 0.02M aqueous solution. Levoglucosan aerosol was generated from the aqueous solution using a constant output atomizer which is connected into the outdoor chamber. After the injection of levoglucosan, chamber air was mixed for five minutes using a mixing fan. HONO was introduced to the chamber by passing the clean air through a flask in which 10 mL of 0.1 M $NaNO_2$ and 10 mL of 10 % H_2SO_4 reacted to produce HONO. HONO was estimated as the difference in NO_x concentration which were measured by a NO_x analyzer with and without a base denuder (coated using 1% Na_2CO_3 + 1% glycerol in ethanol) (Febo and Perrino, 1991). The initial chamber concentration of levoglucosan was 121ug/m^3, HONO 50ppb, and NO_x 124ppb.

A filter sample was collected using a 13mm Teflon-coated borosilicate filter. For each filter sample, 5μL of bornyl acetate solution (2.4mg/mL in acetonitrile), an internal standard, was added. Both Levoglucosan and oxidation products were extracted by sonicating the filter sample with 5mL acetonitrile for one hour. The extracted solution was concentrated to 1ml and using a dry air stream and transferred to a GC vial. In order to derivatize alcol, phonol, and carboxylic acid, 35mL of N,O-Bis(trimethylsilyl)trifluoroacetamide (BSTFA) solution and 15mL pyridine were added to the GC vial. The solution was stood at 70℃ for 1 hour.

Gaseous products from oxidation of levoglucosan were collected using a XAD-coated denuder, which was located upstream the filter. After the sample collection, the

denuder was extracted using 125mL of acetonitrile. The extracted solution was concentrated to 1mL using a rotary evaporator, transferred to a GC vial, and derivertized with BSTFA as mentioned above.

The derivatized products were analyzed using a gas chromatography ion trap mass spectrometer (GC-ITMS). The GC temperature profile in this study was 80℃ for 1minute ramp to 100℃ at 5℃ $minute^{-1}$; ramp to 280℃ at 10℃$minute^{-1}$ and hold for 8 minutes. For the identification of new products, samples were analyzed in both electron impact (EI) and chemical ionization (CI) modes. Acetonitrile was used as the chemical ionization reagent.

References

Febo, A., and Perrino, C. Prediction and experimental evidence for high air concentration of nitrous acid in indoor environments, Atmospheric Environment. Part A. General Topics, 25, 1055-1061, http://dx.doi.org/10.1016/0960-1686(91)90147-Y, 1991.

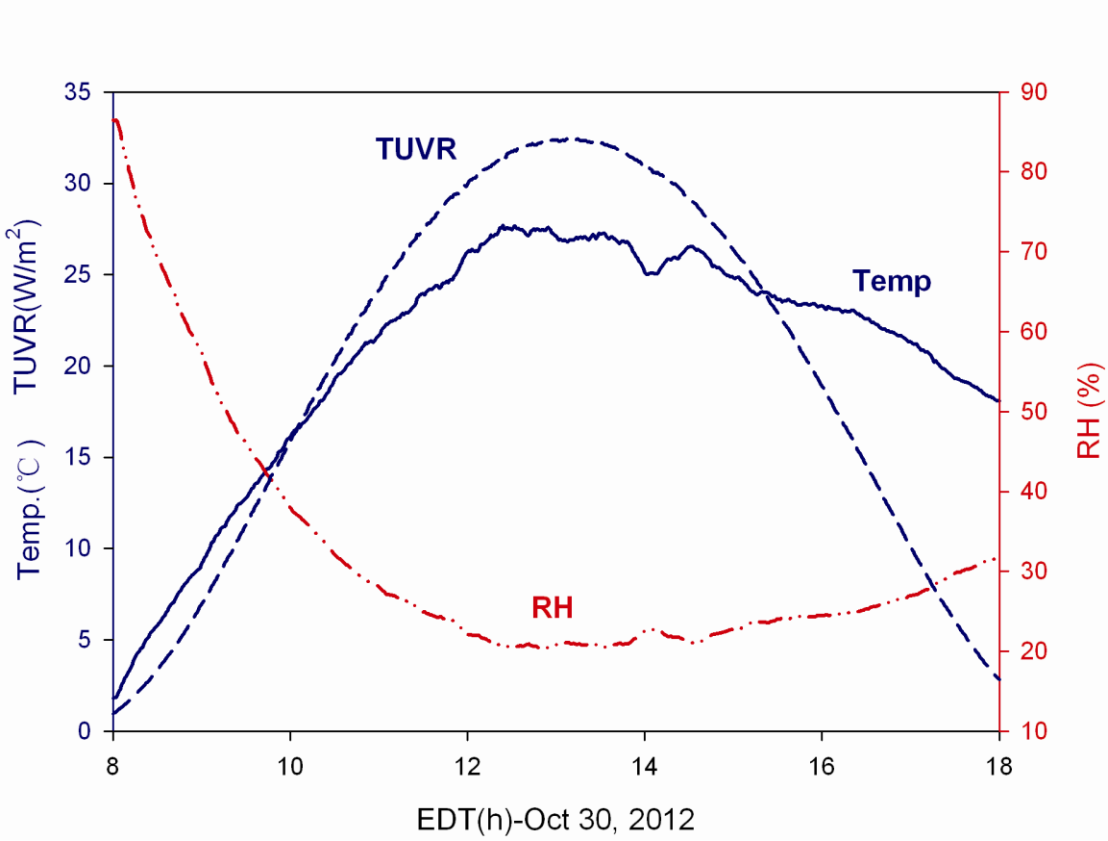

Figure C-1. Time profile of sunlight total ultra-violet radiation (TUVT), temperature and relative humidity measured in the UF-APHOR East chamber on October 30, 2012.

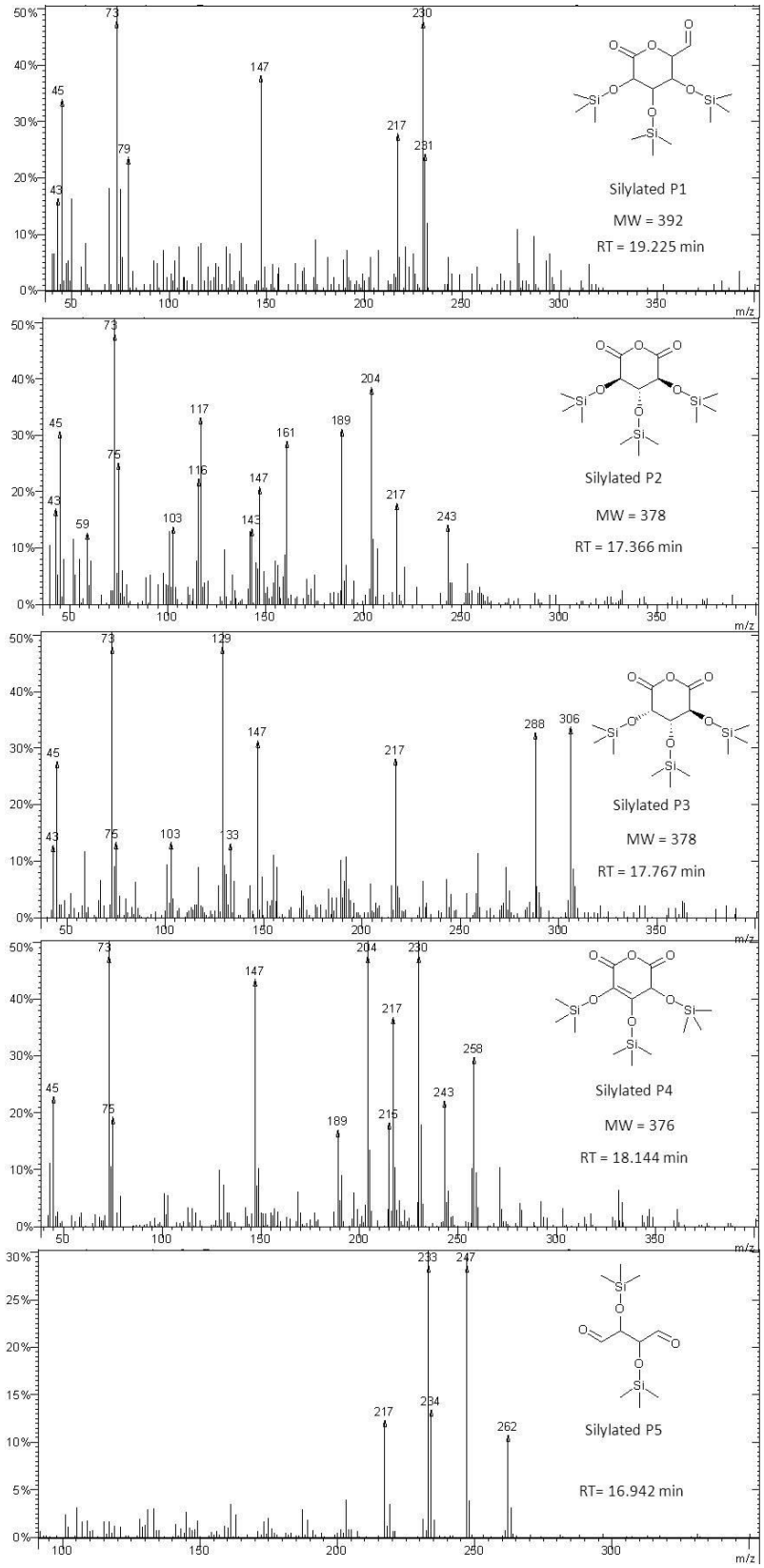

Figure C-2. Mass spectra of BSTFA-derivatives of levoglucosan oxidation products in EI mode. RT is retention time.

The mass peak at m/z = 217 and m/z=147 are the typical mass fragmentation pattern for sugar types of compounds. All products show these two peaks in mass fragmentation patterns.

P1. The molecular structure was tentatively identified based on the molecular ion peak shown in the CI spectrum in Figure S3.
P2. The mass peak at m/z = 243 corresponds with M-45 (~COOH)
P3. The mass peak at m/z = 306 and m/z = 288 originate from M-72 [~$Si(CH_3)_3$+1] and M-88(~$OSi(CH_3)_3$+1), respectively.
P4. The molecular structure was tentatively identified based on the molecular ion peak shown in the CI spectrum in Figure S3.
P 5. The mass peak at m/z = 262 is the molecular ion peak. The mass peaks at m/z=247 and m/z=233 correspond with M-15 (~CH_3) and M-29 (~CHO), respectively.

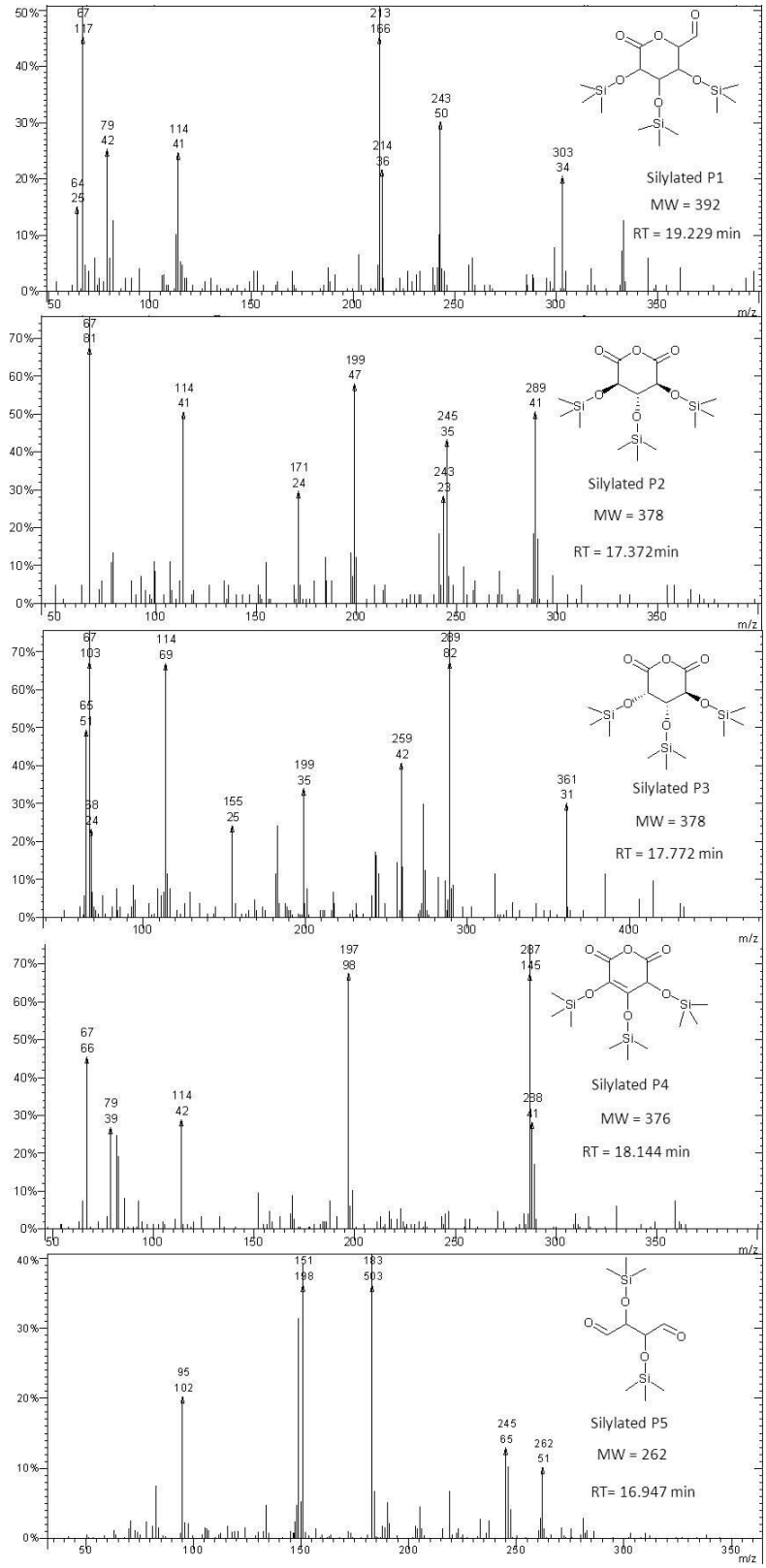

Figure C-3. Mass spectra of BSTFA-derivatives of levoglucosan oxidation products in CI mode. RT is retention time.

P1. The mass peak at m/z = 303 corresponds with M-89 [(~$OSi(CH_3)_3$].

P2. The mass peaks at m/z=289, m/z=245, and m/z=199 correspond with M-89 [~$OSi(CH_3)_3$], M-89-44 [~$OSi(CH_3)_3$ and ~CO_2] and M-89-90 [2 ~$OSi(CH_3)_3$-1], respectively.

P3. The mass peak at m/z = 289 and m/z=199 correspond with M-89 [~$OSi(CH_3)_3$] and M-89-90 [2 ~$OSi(CH_3)_3$-1], respectively. P3 is isomer of P2.

P4. The mass peak at m/z = 287 and m/z=197 correspond with M-89 [~$OSi(CH_3)_3$] and M-89-90 [2 ~$OSi(CH_3)_3$-1], respectively.

P 5. The mass peak at m/z = 262 is the molecular ion peak.

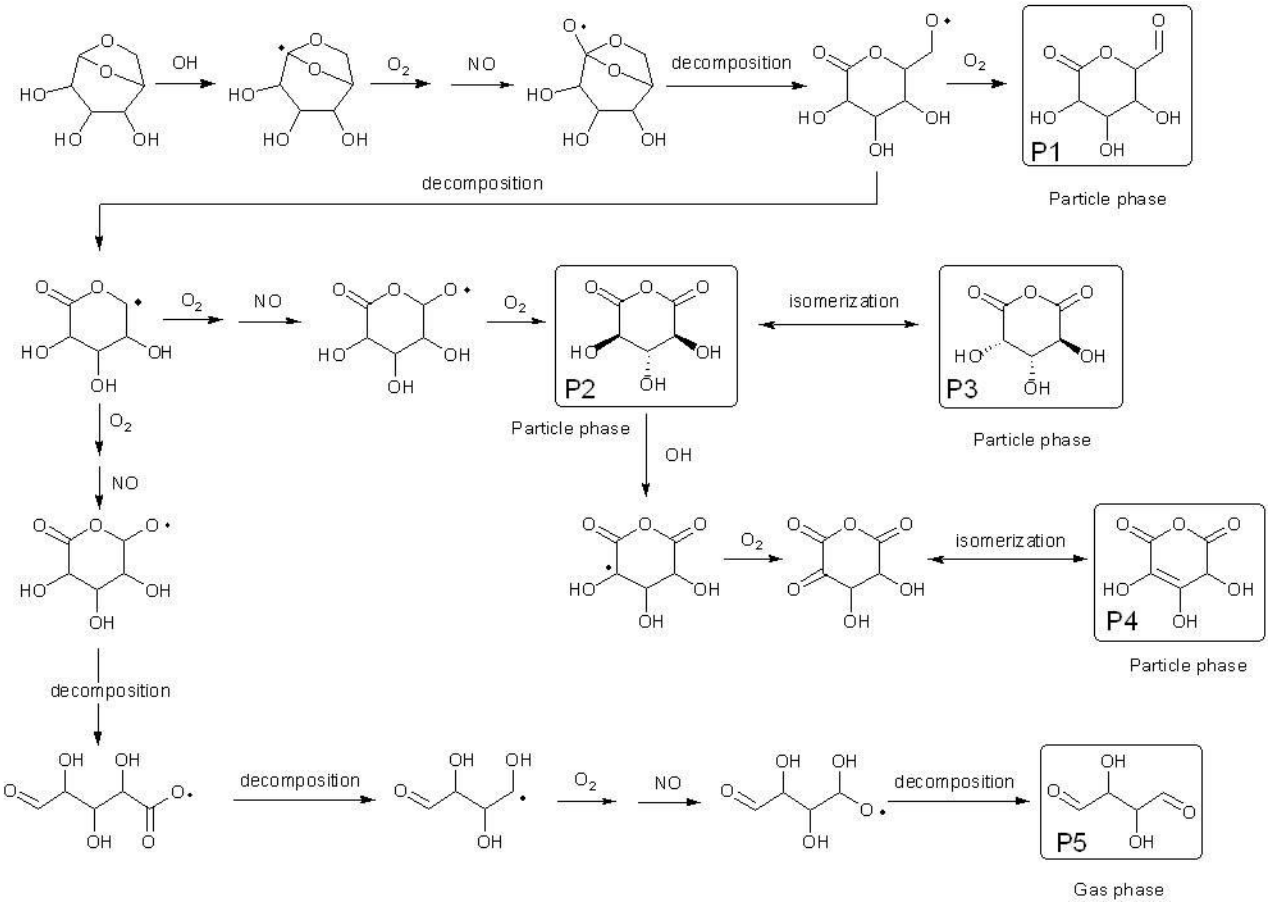

Figure C-4. Reaction pathways for levoglucosan decomposition in the presence of OH radical.

APPENDIX D
SUPPLEMENTARY METERIALS FOR CHAPTER 5

Table D-1. Input parameters in Mie code for dry SOA aerosol.

run	lambda	cmd	gsd	n_{core}	k_{core}	f_{coat}	n_{shell}	k_{shell}
1	280	138	2	1.44	6.36E-03	0.000	1.33	0.000001
2	290	138	2	1.44	3.98E-03	0.000	1.33	0.000001
3	300	138	2	1.44	3.81E-03	0.000	1.33	0.000001
4	310	138	2	1.44	3.74E-03	0.000	1.33	0.000001
5	320	138	2	1.44	2.96E-03	0.000	1.33	0.000001
6	330	138	2	1.44	1.51E-03	0.000	1.33	0.000001
7	340	138	2	1.44	1.33E-03	0.000	1.33	0.000001
8	350	138	2	1.44	8.63E-04	0.000	1.33	0.000001
9	360	138	2	1.44	4.68E-04	0.000	1.33	0.000001
10	370	138	2	1.44	2.69E-04	0.000	1.33	0.000001
11	380	138	2	1.44	3.47E-04	0.000	1.33	0.000001
12	390	138	2	1.44	3.42E-04	0.000	1.33	0.000001
13	400	138	2	1.44	2.79E-04	0.000	1.33	0.000001
14	410	138	2	1.44	2.41E-04	0.000	1.33	0.000001
15	420	138	2	1.44	2.74E-04	0.000	1.33	0.000001
16	430	138	2	1.44	1.32E-04	0.000	1.33	0.000001
17	440	138	2	1.44	1.59E-04	0.000	1.33	0.000001
18	450	138	2	1.44	1.60E-04	0.000	1.33	0.000001
19	460	138	2	1.44	1.07E-04	0.000	1.33	0.000001
20	470	138	2	1.44	1.21E-05	0.000	1.33	0.000001
21	480	138	2	1.44	7.29E-05	0.000	1.33	0.000001
22	490	138	2	1.44	1.02E-04	0.000	1.33	0.000001
23	500	138	2	1.44	1.08E-04	0.000	1.33	0.000001
24	510	138	2	1.44	1.53E-04	0.000	1.33	0.000001
25	520	138	2	1.44	1.62E-04	0.000	1.33	0.000001
26	530	138	2	1.44	2.56E-04	0.000	1.33	0.000001
27	540	138	2	1.44	2.36E-04	0.000	1.33	0.000001
28	550	138	2	1.44	2.39E-04	0.000	1.33	0.000001
29	560	138	2	1.44	3.78E-04	0.000	1.33	0.000001
30	570	138	2	1.44	3.78E-04	0.000	1.33	0.000001
31	580	138	2	1.44	3.11E-04	0.000	1.33	0.000001
32	590	138	2	1.44	3.65E-04	0.000	1.33	0.000001
33	600	138	2	1.44	3.47E-04	0.000	1.33	0.000001
34	610	138	2	1.44	3.28E-04	0.000	1.33	0.000001
35	620	138	2	1.44	3.72E-04	0.000	1.33	0.000001
36	630	138	2	1.44	2.99E-04	0.000	1.33	0.000001
37	640	138	2	1.44	3.04E-04	0.000	1.33	0.000001
38	650	138	2	1.44	8.02E-05	0.000	1.33	0.000001
39	660	138	2	1.44	2.45E-04	0.000	1.33	0.000001
40	670	138	2	1.44	6.25E-05	0.000	1.33	0.000001
41	680	138	2	1.44	8.52E-05	0.000	1.33	0.000001
42	690	138	2	1.44	2.32E-04	0.000	1.33	0.000001
43	700	138	2	1.44	1.34E-04	0.000	1.33	0.000001

Table D-1. Continued

run	lambda	cmd	gsd	n_{core}	k_{core}	f_{coat}	n_{shell}	k_{shell}
44	710	138	2	1.44	1.74E-04	0.000	1.33	0.000001
45	720	138	2	1.44	2.16E-04	0.000	1.33	0.000001
46	730	138	2	1.44	1.53E-04	0.000	1.33	0.000001
47	740	138	2	1.44	2.45E-04	0.000	1.33	0.000001
48	750	138	2	1.44	1.10E-04	0.000	1.33	0.000001
49	760	138	2	1.44	8.65E-05	0.000	1.33	0.000001
50	770	138	2	1.44	1.51E-04	0.000	1.33	0.000001
51	780	138	2	1.44	1.94E-04	0.000	1.33	0.000001
52	790	138	2	1.44	7.15E-06	0.000	1.33	0.000001
53	800	138	2	1.44	4.96E-05	0.000	1.33	0.000001

Table D-2. Input parameters in Mie code for SOA aerosol at RH of 50%.

run	lambda	cmd	gsd	n_{core}	k_{core}	f_{coat}	n_{shell}	k_{shell}
1	280	150.872	2	1.44	0.0064	0.235	1.33	0.000001
2	290	150.872	2	1.44	0.004	0.235	1.33	0.000001
3	300	150.872	2	1.44	0.0038	0.235	1.33	0.000001
4	310	150.872	2	1.44	0.0037	0.235	1.33	0.000001
5	320	150.872	2	1.44	0.003	0.235	1.33	0.000001
6	330	150.872	2	1.44	0.0015	0.235	1.33	0.000001
7	340	150.872	2	1.44	0.0013	0.235	1.33	0.000001
8	350	150.872	2	1.44	0.0009	0.235	1.33	0.000001
9	360	150.872	2	1.44	0.0005	0.235	1.33	0.000001
10	370	150.872	2	1.44	0.0003	0.235	1.33	0.000001
11	380	150.872	2	1.44	0.0003	0.235	1.33	0.000001
12	390	150.872	2	1.44	0.0003	0.235	1.33	0.000001
13	400	150.872	2	1.44	0.0003	0.235	1.33	0.000001
14	410	150.872	2	1.44	0.0002	0.235	1.33	0.000001
15	420	150.872	2	1.44	0.0003	0.235	1.33	0.000001
16	430	150.872	2	1.44	0.0001	0.235	1.33	0.000001
17	440	150.872	2	1.44	0.0002	0.235	1.33	0.000001
18	450	150.872	2	1.44	0.0002	0.235	1.33	0.000001
19	460	150.872	2	1.44	0.0001	0.235	1.33	0.000001
20	470	150.872	2	1.44	1E-05	0.235	1.33	0.000001
21	480	150.872	2	1.44	7E-05	0.235	1.33	0.000001
22	490	150.872	2	1.44	0.0001	0.235	1.33	0.000001
23	500	150.872	2	1.44	0.0001	0.235	1.33	0.000001
24	510	150.872	2	1.44	0.0002	0.235	1.33	0.000001
25	520	150.872	2	1.44	0.0002	0.235	1.33	0.000001
26	530	150.872	2	1.44	0.0003	0.235	1.33	0.000001
27	540	150.872	2	1.44	0.0002	0.235	1.33	0.000001
28	550	150.872	2	1.44	0.0002	0.235	1.33	0.000001

Table D-2. Continued

run	lambda	cmd	gsd	n_{core}	k_{core}	f_{coat}	n_{shell}	k_{shell}
29	560	150.872	2	1.44	0.0004	0.235	1.33	0.000001
30	570	150.872	2	1.44	0.0004	0.235	1.33	0.000001
31	580	150.872	2	1.44	0.0003	0.235	1.33	0.000001
32	590	150.872	2	1.44	0.0004	0.235	1.33	0.000001
33	600	150.872	2	1.44	0.0003	0.235	1.33	0.000001
34	610	150.872	2	1.44	0.0003	0.235	1.33	0.000001
35	620	150.872	2	1.44	0.0004	0.235	1.33	0.000001
36	630	150.872	2	1.44	0.0003	0.235	1.33	0.000001
37	640	150.872	2	1.44	0.0003	0.235	1.33	0.000001
38	650	150.872	2	1.44	8E-05	0.235	1.33	0.000001
39	660	150.872	2	1.44	0.0002	0.235	1.33	0.000001
40	670	150.872	2	1.44	6E-05	0.235	1.33	0.000001
41	680	150.872	2	1.44	9E-05	0.235	1.33	0.000001
42	690	150.872	2	1.44	0.0002	0.235	1.33	0.000001
43	700	150.872	2	1.44	0.0001	0.235	1.33	0.000001
44	710	150.872	2	1.44	0.0002	0.235	1.33	0.000001
45	720	150.872	2	1.44	0.0002	0.235	1.33	0.000001
46	730	150.872	2	1.44	0.0002	0.235	1.33	0.000001
47	740	150.872	2	1.44	0.0002	0.235	1.33	0.000001
48	750	150.872	2	1.44	0.0001	0.235	1.33	0.000001
49	760	150.872	2	1.44	9E-05	0.235	1.33	0.000001
50	770	150.872	2	1.44	0.0002	0.235	1.33	0.000001
51	780	150.872	2	1.44	0.0002	0.235	1.33	0.000001
52	790	150.872	2	1.44	7E-06	0.235	1.33	0.000001
53	800	150.872	2	1.44	5E-05	0.235	1.33	0.000001

Table D-3. Input parameters in Mie code for dry POA.

run	lambda	cmd	gsd	n_{core}	k_{core}	f_{coat}	n_{shell}	k_{shell}
1	280	138	2	1.44	0.0541	0.000	1.33	0.000001
2	290	138	2	1.44	0.0554	0.000	1.33	0.000001
3	300	138	2	1.44	0.0564	0.000	1.33	0.000001
4	310	138	2	1.44	0.0597	0.000	1.33	0.000001
5	320	138	2	1.44	0.0595	0.000	1.33	0.000001
6	330	138	2	1.44	0.057	0.000	1.33	0.000001
7	340	138	2	1.44	0.0537	0.000	1.33	0.000001
8	350	138	2	1.44	0.0518	0.000	1.33	0.000001
9	360	138	2	1.44	0.0485	0.000	1.33	0.000001
10	370	138	2	1.44	0.0443	0.000	1.33	0.000001
11	380	138	2	1.44	0.0425	0.000	1.33	0.000001
12	390	138	2	1.44	0.0363	0.000	1.33	0.000001

Table D-3. Continued

run	lambda	cmd	gsd	n_{core}	k_{core}	f_{coat}	n_{shell}	k_{shell}
13	400	138	2	1.44	0.0333	0.000	1.33	0.000001
14	410	138	2	1.44	0.0304	0.000	1.33	0.000001
15	420	138	2	1.44	0.0282	0.000	1.33	0.000001
16	430	138	2	1.44	0.0263	0.000	1.33	0.000001
17	440	138	2	1.44	0.0246	0.000	1.33	0.000001
18	450	138	2	1.44	0.0231	0.000	1.33	0.000001
19	460	138	2	1.44	0.0218	0.000	1.33	0.000001
20	470	138	2	1.44	0.0205	0.000	1.33	0.000001
21	480	138	2	1.44	0.0194	0.000	1.33	0.000001
22	490	138	2	1.44	0.0183	0.000	1.33	0.000001
23	500	138	2	1.44	0.0174	0.000	1.33	0.000001
24	510	138	2	1.44	0.0166	0.000	1.33	0.000001
25	520	138	2	1.44	0.0156	0.000	1.33	0.000001
26	530	138	2	1.44	0.0148	0.000	1.33	0.000001
27	540	138	2	1.44	0.0139	0.000	1.33	0.000001
28	550	138	2	1.44	0.013	0.000	1.33	0.000001
29	560	138	2	1.44	0.0122	0.000	1.33	0.000001
30	570	138	2	1.44	0.0115	0.000	1.33	0.000001
31	580	138	2	1.44	0.0109	0.000	1.33	0.000001
32	590	138	2	1.44	0.01	0.000	1.33	0.000001
33	600	138	2	1.44	0.0093	0.000	1.33	0.000001
34	610	138	2	1.44	0.0087	0.000	1.33	0.000001
35	620	138	2	1.44	0.0081	0.000	1.33	0.000001
36	630	138	2	1.44	0.0076	0.000	1.33	0.000001
37	640	138	2	1.44	0.0071	0.000	1.33	0.000001
38	650	138	2	1.44	0.0065	0.000	1.33	0.000001
39	660	138	2	1.44	0.0061	0.000	1.33	0.000001
40	670	138	2	1.44	0.0057	0.000	1.33	0.000001
41	680	138	2	1.44	0.0054	0.000	1.33	0.000001
42	690	138	2	1.44	0.005	0.000	1.33	0.000001
43	700	138	2	1.44	0.0046	0.000	1.33	0.000001
44	710	138	2	1.44	0.0042	0.000	1.33	0.000001
45	720	138	2	1.44	0.004	0.000	1.33	0.000001
46	730	138	2	1.44	0.0036	0.000	1.33	0.000001
47	740	138	2	1.44	0.0033	0.000	1.33	0.000001
48	750	138	2	1.44	0.003	0.000	1.33	0.000001
49	760	138	2	1.44	0.0027	0.000	1.33	0.000001
50	770	138	2	1.44	0.0024	0.000	1.33	0.000001
51	780	138	2	1.44	0.0021	0.000	1.33	0.000001
52	790	138	2	1.44	0.0019	0.000	1.33	0.000001
53	800	138	2	1.44	0.0016	0.000	1.33	0.000001

Table D-4. Input parameters in Mie code for POA at RH of 50%.

run	lambda	cmd	gsd	n_{core}	k_{core}	f_{coat}	n_{shell}	k_{shell}
1	280	150.872	2	1.44	0.0541	0.235	1.33	0.000001
2	290	150.872	2	1.44	0.0554	0.235	1.33	0.000001
3	300	150.872	2	1.44	0.0564	0.235	1.33	0.000001
4	310	150.872	2	1.44	0.0597	0.235	1.33	0.000001
5	320	150.872	2	1.44	0.0595	0.235	1.33	0.000001
6	330	150.872	2	1.44	0.057	0.235	1.33	0.000001
7	340	150.872	2	1.44	0.0537	0.235	1.33	0.000001
8	350	150.872	2	1.44	0.0518	0.235	1.33	0.000001
9	360	150.872	2	1.44	0.0485	0.235	1.33	0.000001
10	370	150.872	2	1.44	0.0443	0.235	1.33	0.000001
11	380	150.872	2	1.44	0.0425	0.235	1.33	0.000001
12	390	150.872	2	1.44	0.0363	0.235	1.33	0.000001
13	400	150.872	2	1.44	0.0333	0.235	1.33	0.000001
14	410	150.872	2	1.44	0.0304	0.235	1.33	0.000001
15	420	150.872	2	1.44	0.0282	0.235	1.33	0.000001
16	430	150.872	2	1.44	0.0263	0.235	1.33	0.000001
17	440	150.872	2	1.44	0.0246	0.235	1.33	0.000001
18	450	150.872	2	1.44	0.0231	0.235	1.33	0.000001
19	460	150.872	2	1.44	0.0218	0.235	1.33	0.000001
20	470	150.872	2	1.44	0.0205	0.235	1.33	0.000001
21	480	150.872	2	1.44	0.0194	0.235	1.33	0.000001
22	490	150.872	2	1.44	0.0183	0.235	1.33	0.000001
23	500	150.872	2	1.44	0.0174	0.235	1.33	0.000001
24	510	150.872	2	1.44	0.0166	0.235	1.33	0.000001
25	520	150.872	2	1.44	0.0156	0.235	1.33	0.000001
26	530	150.872	2	1.44	0.0148	0.235	1.33	0.000001
27	540	150.872	2	1.44	0.0139	0.235	1.33	0.000001
28	550	150.872	2	1.44	0.013	0.235	1.33	0.000001
29	560	150.872	2	1.44	0.0122	0.235	1.33	0.000001
30	570	150.872	2	1.44	0.0115	0.235	1.33	0.000001
31	580	150.872	2	1.44	0.0109	0.235	1.33	0.000001
32	590	150.872	2	1.44	0.01	0.235	1.33	0.000001
33	600	150.872	2	1.44	0.0093	0.235	1.33	0.000001
34	610	150.872	2	1.44	0.0087	0.235	1.33	0.000001
35	620	150.872	2	1.44	0.0081	0.235	1.33	0.000001
36	630	150.872	2	1.44	0.0076	0.235	1.33	0.000001
37	640	150.872	2	1.44	0.0071	0.235	1.33	0.000001
38	650	150.872	2	1.44	0.0065	0.235	1.33	0.000001
39	660	150.872	2	1.44	0.0061	0.235	1.33	0.000001
40	670	150.872	2	1.44	0.0057	0.235	1.33	0.000001
41	680	150.872	2	1.44	0.0054	0.235	1.33	0.000001

Table D-4. Continued

run	lambda	cmd	gsd	n_{core}	k_{core}	f_{coat}	n_{shell}	k_{shell}
42	690	150.872	2	1.44	0.005	0.235	1.33	0.000001
43	700	150.872	2	1.44	0.0046	0.235	1.33	0.000001
44	710	150.872	2	1.44	0.0042	0.235	1.33	0.000001
45	720	150.872	2	1.44	0.004	0.235	1.33	0.000001
46	730	150.872	2	1.44	0.0036	0.235	1.33	0.000001
47	740	150.872	2	1.44	0.0033	0.235	1.33	0.000001
48	750	150.872	2	1.44	0.003	0.235	1.33	0.000001
49	760	150.872	2	1.44	0.0027	0.235	1.33	0.000001
50	770	150.872	2	1.44	0.0024	0.235	1.33	0.000001
51	780	150.872	2	1.44	0.0021	0.235	1.33	0.000001
52	790	150.872	2	1.44	0.0019	0.235	1.33	0.000001
53	800	150.872	2	1.44	0.0016	0.235	1.33	0.000001

Table D-5. Input parameters in Mie code for dry sulfate.

run	lambda	cmd	gsd	n_{core}	k_{core}	f_{coat}	n_{shell}	k_{shell}
1	250	138	2	1.48	1E-08	0.000	1.33	0.000001
2	300	138	2	1.47	1E-08	0.000	1.33	0.000001
3	350	138	2	1.45	1E-08	0.000	1.33	0.000001
4	400	138	2	1.44	1E-08	0.000	1.33	0.000001
5	450	138	2	1.43	1E-08	0.000	1.33	0.000001
6	500	138	2	1.43	1E-08	0.000	1.33	0.000001
7	550	138	2	1.43	1E-08	0.000	1.33	0.000001
8	600	138	2	1.43	1E-08	0.000	1.33	0.000001
9	650	138	2	1.43	2E-08	0.000	1.33	0.000001
10	700	138	2	1.43	2E-08	0.000	1.33	0.000001
11	750	138	2	1.43	7E-08	0.000	1.33	0.000001
12	800	138	2	1.43	9E-08	0.000	1.33	0.000001

LIST OF REFERENCES

Adler, G., Flores, J. M., Abo Riziq, A., Borrmann, S., and Rudich, Y.: Chemical, physical, and optical evolution of biomass burning aerosols: a case study, Atmos. Chem. Phys., 11, 1491-1503, 10.5194/acp-11-1491-2011, 2011.

Alexander, D. T. L., Crozier, P. A., and Anderson, J. R.: Brown carbon spheres in east Asian outflow and their optical properties, Science, 321, 833-836, 2008.

Alves, C. A., Vicente, A., Monteiro, C., Gonçalves, C., Evtyugina, M., and Pio, C.: Emission of trace gases and organic components in smoke particles from a wildfire in a mixed-evergreen forest in Portugal, Science of The Total Environment, 409, 1466-1475, http://dx.doi.org/10.1016/j.scitotenv.2010.12.025, 2011.

Anastasio, C., Faust, B. C., and Rao, C. J.: Aromatic Carbonyl Compounds as Aqueous-Phase Photochemical Sources of Hydrogen Peroxide in Acidic Sulfate Aerosols, Fogs, and Clouds. 1. Non-Phenolic Methoxybenzaldehydes and Methoxyacetophenones with Reductants (Phenols), Environmental Science & Technology, 31, 218-232, 10.1021/es960359g, 1996.

Anderson, N. M., and Sekelj, P.: Light-absorbing and scattering properties of nonhaemolysed blood, Physics in Medicine and Biology, 12, 173-184, 1967.

Andreae, M., and Gelencser, A.: Black carbon or brown carbon? The nature of light-absorbing carbonaceous aerosols, Atmospheric Chemistry and Physics, 6, 3131-3148, 2006.

Andreae, M. O., and Crutzen, P. J.: Atmospheric Aerosols: Biogeochemical Sources and Role in Atmospheric Chemistry, Science, 276, 1052-1058, 10.1126/science.276.5315.1052, 1997.

Baduel, C., Voisin, D., and Jaffrezo, J. L.: Comparison of analytical methods for Humic Like Substances (HULIS) measurements in atmospheric particles, Atmospheric Chemistry and Physics, 9, 5949-5962, 2009.

Barker, B. E., and Fox, M. F.: Computer resolution of overlapping electronic absorption bands, Chemical Society Reviews, 9, 1980.

Bateman, A. P., Walser, M. L., Desyaterik, Y., Laskin, J., Laskin, A., and Nizkorodov, S. A.: The effect of solvent on the analysis of secondary organic aerosol using electrospray ionization mass spectrometry, Environmental Science & Technology, 42, 7341–7346, 2008.

Belay, A.: Measurement of integrated absorption cross-section, oscillator strength and number density of caffeine in coffee beans by integrated absorption coefficient technique, Food Chem, 121, 585-590, DOI 10.1016/j.foodchem.2009.12.052, 2010.

Bertschi, I., Yokelson, R., Ward, D., Babbitt, R., Susott, R., Goode, J., and Hao, W.: Trace gas and particle emissions from fires in large diameter and belowground biomass fuels, Journal of Geophysical Research-Atmospheres, 108, 10.1029/2002JD002100, 2003.

Birmili, W., Schwirn, K., Nowak, A., Petäjä, T., Joutsensaari, J., Rose, D., Wiedensohler, A., Hämeri, K., Aalto, P., Kulmala, M., and Boy, M.: Measurements of humidified particle number size distributions in a Finnish boreal forest: derivation of hygroscopic particle growth factors, Boreal Environ. Res., 14, 458–480, 2009.

Bond, T. C., and Bergstromb, R. W.: Light Absorption by carbonaceous particles: an investigative review, Aerosol Science and Technology 40, 27-67, 2006.

Bones, D. L., Henricksen, D. K., Mang, S. A., Gonsior, M., Bateman, A. P., Nguyen, T. B., and Cooper, W. J.: Appearance of strong absorbers and fluorophores in limonene-O_3 secondary organic aerosol due to NH_4^+ -mediated chemical aging over long time scales, Journal of Geophysical Research, 115, D05203, 10.1029/2009JD012864, 2010a.

Bones, D. L., Henricksen, D. K., Mang, S. A., Gonsior, M., Bateman, A. P., Tran B. Nguyen, and Cooper, W. J.: Appearance of strong absorbers and fluorophores in limonene-O_3 secondary organic aerosol due to $NH4^+$-mediated chemical aging over long time scales, Journal of Geophysical Research, 115, D05203, 2010b.

Booth, A. M., Montague, W. J., Barley, M. H., Topping, D. O., McFiggans, G., Garforth, A., and Percival, C. J.: Solid state and sub-cooled liquid vapour pressures of cyclic aliphatic dicarboxylic acids, Atmos. Chem. Phys., 11, 655-665, 10.5194/acp-11-655-2011, 2011.

Calvert, J. G., and Pitts, J. N.: Photochemistry, John Wiley & Sons: New York, 1966.

Campbell, D., Copeland, S., and Cahill, T.: Measurement of aerosol absorption coefficient from telfon on filters using integrating plate and integrating sphere techniques, Aerosol Science and Technology, 22, 287–292, 1995.

Camredon, M., Hamilton, J. F., Alam, M. S., Wyche, K. P., Carr, T., White, I. R., Monks, P. S., Rickard, A. R., and Bloss, W. J.: Distribution of gaseous and particulate organic composition during dark α-pinene ozonolysis Atmospheric Chemistry and Physics, 10, 2893–2917, 2010.

Cao, G., and Jang, M.: Secondary organic aerosol formation from toluene photooxidation under various NOx conditions and particle acidity, Atmos. Chem. Phys. Discuss., 8, 14467-14495, 10.5194/acpd-8-14467-2008, 2008.

Cao, G., and Jang, M.: An SOA model for toluene oxidation in the presence of inorganic aerosols, Environ Sci Technol, 44, 727-733, 10.1021/es901682r, 2010.

Chang, J. L., and Thompson, J. E.: Characterization of colored products formed during irradiation of aqueous solutions containing H2O2 and phenolic compounds, Atmospheric Environment, 44, 541-551, http://dx.doi.org/10.1016/j.atmosenv.2009.10.042, 2010.

Chen, Y., and Bond, T. C.: Light absorption by organic carbon from wood combustion, Atmos. Chem. Phys., 10, 1787, 10.5194/acp-10-1773-2010, 2010.

Chung, S., and Seinfeld, J.: Global distribution and climate forcing of carbonaceous aerosols, Journal of Geophysical Research-Atmospheres, 107, 10.1029/2001JD001397, 2002.

CHYLEK, P., and WONG, J.: EFFECT OF ABSORBING AEROSOLS ON GLOBAL RADIATION BUDGET, Geophysical Research Letters, 22, 929-931, 10.1029/95GL00800, 1995.

Clark, T., Alex, A., Beck, B., Burkhardt, F., Chandrasekhar, J., Gedeck, P., Horn, A. H. C., Hutter, M., Martin, B., Rauhut, G., Sauer, W., Schindler, T., Steinke, T., and Germany: Vamp 8.1, University of Erlangen, Erlangen, 2002.

Clegg, S. L., Brimblecombe, P., and Wexler, A. S.: Thermodynamic Model of the System H+−NH4+−Na+−SO42-−NO3-−Cl-−H2O at 298.15 K, The Journal of Physical Chemistry A, 102, 2155-2171, 10.1021/jp973043j, 1998.

De Haan, D., Corrigan, A., Smith, K., Stroik, D., Turley, J., Lee, F., Tolbert, M., Jimenez, J., Cordova, K., and Ferrell, A.: Secondary organic aerosol-forming reactions of glyoxal with amino acids, Environmental Science & Technology, 43, 2818–2824, 2009.

Del Vecchio, R., and Blough, N. V.: On the Origin of the Optical Properties of Humic Substances, Environmental Science & Technology, 38, 3885-3891, 10.1021/es049912h, 2004.

Dewar, M. J. S., Zoebisch, E. G., Healy, E. F., and Stewart, J. J. P.: The Development and Use of Quantum-Mechanical Molecular-Models .76. Am1 - a New General-Purpose Quantum-Mechanical Molecular-Model, Journal of the American Chemical Society, 107, 3902-3909, 1985.

EPA, U. S.: Air quality criteria for particulate matter, Washington, D.C., 2004.

Fabian, J., Diaz, L. A., Seifert, G., and Niehaus, T.: Calculation of excitation energies of organic chromophores: a critical evaluation, J Mol Struc-Theochem, 594, 41-53, Pii S0166-1280(02)00322-6, 2002.

Fang, W., Gong, L., Shan, X., Liu, F., Wang, Z., and Sheng, L.: Thermal Desorption/Tunable Vacuum–Ultraviolet Time-of-Flight Photoionization Aerosol Mass Spectrometry for Investigating Secondary Organic Aerosols in Chamber Experiments, Analytical Chemistry, 83, 9024-9032, 10.1021/ac201838e, 2011.

Faust, B. C.: Photochemistry of Clouds, Fogs, and Aerosols, Environmental Science & Technology, 28, 216A-222A, 10.1021/es00054a001, 1994.

Febo, A., and Perrino, C.: Prediction and experimental evidence for high air concentration of nitrous acid in indoor environments, Atmospheric Environment. Part A. General Topics, 25, 1055-1061, http://dx.doi.org/10.1016/0960-1686(91)90147-Y, 1991.

Forster, P.: Changes in Atmospheric Constituents and in Radiative Forcing

http://ipcc-wg1.ucar.edu/wg1/ wg1-report.html, 2007.

Forstner, H. J. L., Flagan, R. C., and Seinfeld, J. H.: Secondary organic aerosol from the photooxidation of aromatic hydrocarbons: Molecular composition, Environmental Science & Technology, 31, 1345-1358, 1997.

Galloway, M. M., Chhabra, P. S., Chan, A. W. H., Surratt, J. D., Flagan, R. C., Seinfeld, J. H., and Keutsch, F. N.: Glyoxal uptake on ammonium sulphate seed aerosol: reaction products and reversibility of uptake under dark and irradiated conditions, Atmospheric Chemistry and Physics, 9, 3331-3345, 2009.

Gao, S., Ng, N. L., Keywood, M., Varutbangkul, V., Bahreini, R., Nenes, A., He, J., Yoo, K. Y., Beauchamp, J. L., Hodyss, R. P., Flagan, R. C., and Seinfeld, J. H.: Particle phase acidity and oligomer formation in secondary organic aerosol, Environ Sci Technol, 38, 6582-6589, 2004.

Gelencser, A., Hoffer, A., Kiss, G., Tombacz, E., Kurdi, R., and Bencze, L.: In-situ formation of light-absorbing organic matter in cloud water, Journal of Atmospheric Chemistry, 45, 25-33, 10.1023/A:1024060428172, 2003.

Glasius, M., Lahaniati, M., Calogirou, A., Di Bella, D., Jensen, N. R., Hjorth, J., Kotzias, D., and Larsen, B. R.: Carboxylic acids in secondary aerosols from oxidation of cyclic monoterpenes by ozone, Environmental Science & Technology, 34, 1001–1010, 2002.

Grieshop, A. P., Donahue, N. M., and Robinson, A. L.: Laboratory investigation of photochemical oxidation of organic aerosol from wood fires 2: analysis of aerosol mass spectrometer data, Atmos. Chem. Phys. , 9, 2227-2240, 2009.

Grosjean, D., Williams, E. L., II., Grosjean, E., Andino, J. M., and Seinfeld, J. H.: Atmospheric oxidation of biogenic hydrocarbons:reaction of ozone with beta-pinene, D-limonene and trans-caryophyllene, Environmental Science & Technology, 27, 2754-2758, 1993.

Gu, Y., Liou, K., Xue, Y., Mechoso, C., Li, W., and Luo, Y.: Climatic effects of different aerosol types in China simulated by the UCLA general circulation model, Journal of Geophysical Research-Atmospheres, 111, 10.1029/2005JD006312, 2006.

Hallquist, M., Wenger, J. C., Baltensperger, U., Rudich, Y., Simpson, D., Claeys, M., Dommen, J., Donahue, N. M., George, C., Goldstein, A. H., Hamilton, J. F., Herrmann, H., Hoffmann, T., Iinuma, Y., Jang, M., Jenkin, M., Jimenez, J. L., Kiendler-Scharr, A., Maenhaut, W., McFiggans, G., Mentel, T. F., Monod, A., Prevot, A. S. H., Seinfeld, J. H., Surratt, J. D., Szmigielski, R., and Wildt, J.: The formation, properties and impact of secondary organic aerosol: current and emerging issues, Atmos. Chem. Phys., 9, 5155-5236, 2009.

Hamilton, J. F., Webb, P. J., Lewis, A. C., and Reviejo, M. M.: Quantifying small molecules in secondary organic aerosol formed during the photo-oxidation of toluene with hydroxyl radicals, Atmospheric Environment, 39, 7263-7275, 10.1016/j.atmosenv.2005.09.006, 2005.

Hays, M. D., Fine, P. M., Geron, C. D., Kleeman, M. J., and Gullett, B. K.: Open burning of agricultural biomass: Physical and chemical properties of particle-phase emissions, Atmospheric Environment, 39, 6747-6764, http://dx.doi.org/10.1016/j.atmosenv.2005.07.072, 2005.

Hecobian, A., Zhang, X., Zheng, M., Frank, N., Edgerton, E. S., and Weber, R. J.: Water-Soluble Organic Aerosol material and the light-absorption characteristics of aqueous extracts measured over the Southeastern United States, Atmos. Chem. Phys., 10, 5965-5977, 10.5194/acp-10-5965-2010, 2010.

Hille, M. G., and Stephens, S. L.: Mixed Conifer Forest Duff Consumption during Prescribed Fires: Tree Crown Impacts, Forest Science, 51, 417-424, 2005.

Hoffer, A., Gelencser, A., Guyon, P., Kiss, G., Schmid, O., Frank, G. P., Artaxo, P., and Andreae, M. O.: Optical properties of humic-like substances (HULIS) in biomass-burning aerosols, Atmos. Chem. Phys., 6, 3563-3570, 10.5194/acp-6-3563-2006, 2006.

Howard, P. H.: Handbook of Environmental Fate and Exposure Data for Organic Chemicals. Pesticides., Lewis Publishers, Chelsea, MI., 1991.

Hoyle, C., Myhre, G., Berntsen, T., and Isaksen, I.: Anthropogenic influence on SOA and the resulting radiative forcing, Atmospheric Chemistry and Physics, 9, 2715-2728, 2009.

Hu, D., Tolocka, M., Li, Q., and KamenS, R. M.: A kinetic mechanism for predicting secondary organic aerosol formation from toluene oxidation in the presence of NOx and natural sunlight, Atmospheric Environment, 41, 6478-6496, DOI 10.1016/j.atmosenv.2007.04.025, 2007.

Iinuma, Y., Müller, C., Berndt, T., Böge, O., Claeys, M., and Herrmann, H.: Evidence for the Existence of Organosulfates from β-Pinene Ozonolysis in Ambient Secondary Organic Aerosol, Environmental Science & Technology, 41, 6678-6683, 10.1021/es070938t, 2007.

Im, Y., Jang, M., and Beardsley, R. L.: Simulation of aromatic SOA formation using the lumping model integrated with explicit gas-phase kinetic mechanisms and aerosol-phase reactions, Atmos. Chem. Phys. Discuss., 13, 5843-5870, 10.5194/acpd-13-5843-2013, 2013.

IPCC: Changes in Atmospheric Constituents and in Radiative Forcing, in Climate Change, The Physical Science Basis. Contribution of Working Group I to the Fourth Assessment Report of the Intergovenmental Panel on Climate Change 129, 132, 2007.

Jacobson, M. Z.: Isolating nitrated and aromatic aerosols and nitrated aromatic gases as sources of ultraviolet light absorption, Journal of Geophysical Research-Atmospheres, 104, 3527-3542, 1999.

Jang, J., Jang, M., Mui, W., Delcomyn, C. A., Henley, M. V., and Hearn, J. D.: Formation of Active Chlorine Oxidants in Saline-Oxone Aerosol, Aerosol Science and Technology, 44, 1018-1026, 10.1080/02786826.2010.507612, 2010.

Jang, M., and McDow, S. R.: Benz[a]anthracene photodegradation in the presence of known organic constituents of atmospheric aerosols, Environmental Science & Technology, 29, 2654-2660, 10.1021/es00010a030, 1995.

Jang, M., and Kamens, R. M.: Newly characterized products and composition of secondary aerosols from the reaction of a-pinene with ozone, Atmospheric Environment, 33, 459-474, 1999.

Jang, M., and Kamens, R. M.: Characterization of Secondary Aerosol from the Photooxidation of Toluene in the Presence of NOx and 1-Propene, Environmental Science & Technology, 35, 3626-3639, 10.1021/es010676+, 2001a.

Jang, M., and Kamens, R. M.: Characterization of secondary aerosol from the photooxidation of toluene in the presence of NOx and 1-propene, Environmental Science & Technology, 35, 3626-3639, 2001b.

Jang, M., Czoschke, N. M., Northcross, A. L., Cao, G., and Shaof, D.: SOA formation from partitioning and heterogeneous reactions: model study in the presence of inorganic species, Environ Sci Technol, 40, 3013-3022, 2006.

Jang, M. S., Czoschke, N. M., Lee, S., and Kamens, R. M.: Heterogeneous atmospheric aerosol production by acid-catalyzed particle-phase reactions, Science, 298, 814-817, 2002.

Jaoui, M., and Kamens, R. M.: Modeling aerosol formation from alpha-pinene + NOx in the presence of natural sunlight using gas-phase kinetics and gas-particle partitioning theory, Environ Sci Technol, 35, 1394-1405, 2001.

Jeffries, H. E., Gary, M. W., Kessler, M., and Sexton, K. G.: Morphecule reaction mechanism, MORPHO, ALLOMORPHIC simulation software, , 1998.

Joback, K. G., and Reid, R. C.: ESTIMATION OF PURE-COMPONENT PROPERTIES FROM GROUP-CONTRIBUTIONS, Chemical Engineering Communications, 57, 233-243, 10.1080/00986448708960487, 1987.

Kalberer, M., Paulsen, D., Sax, M., Steinbacher, M., Dommen, J., Prevot, A. S. H., Fisseha, R., Weingartner, E., Frankevich, V., Zenobi, R., and Baltensperger, U.: Identification of polymers as major components of atmospheric organic aerosols, Science, 303, 1659-1662, 2004.

Kaul, D. S., Gupta, T., and Tripathi, S. N.: Chemical and microphysical properties of the aerosol during foggy and nonfoggy episodes: a relationship between organic and inorganic content of the aerosol, Atmos. Chem. Phys. Discuss., 12, 14483-14524, 10.5194/acpd-12-14483-2012, 2012.

Kim, H., and Paulson, S. E.: Real refractive indices and volatility of secondary organic aerosol generated from photooxidation and ozonolysis of limonene, α-pinene and toluene, Atmos. Chem. Phys. Discuss., 13, 1949-1977, 10.5194/acpd-13-1949-2013, 2013.

Kirchstetter, T. W., Novakov, T., and Hobbs, P. V.: Evidence that the spectral dependence of light absorption by aerosols is affected by organic carbon, Journal of Geophysical Research: Atmospheres, 109, n/a-n/a, 10.1029/2004jd004999, 2004.

Kirchstetter, T. W., and Thatcher, T. L.: Contribution of organic carbon to wood smoke particulate matter absorption of solar radiation, Atmos. Chem. Phys., 12, 6067-6072, 10.5194/acp-12-6067-2012, 2012.

Lack, D. A., Langridge, J. M., Bahreini, R., Cappa, C. D., Middlebrook, A. M., and Schwarz, J. P.: Brown carbon and internal mixing in biomass burning particles, Proceedings of the National Academy of Sciences, 10.1073/pnas.1206575109, 2012.

Lakowicz, J. R.: Principles of fluorescence spectroscopy, 3rd ed., Springer, New York, 2006.

Laskin, J., Laskin, A., Roach, P. J., Slysz, G., Anderson, G. A., Nizkorodov, S. A., Bones, D. L., and Nguyen, L. Q.: High-resolution desorption electrospray Ionization mass spectrometry for chemical characterization of organic aerosols, Analytical Chemisty, 82, 2010a.

Laskin, J., Laskin, A., Roach, P. J., Slysz, G. W., Anderson, G. A., Nizkorodov, S. A., Bones, D. L., and Nguyen, L. Q.: High-resolution desorption electrospray ionization mass spectrometry for chemical characterization of organic aerosols, Anal Chem, 82, 2048-2058, 10.1021/ac902801f, 2010b.

Leungsakul, S., Jaoui, M., and Kamens, R. M.: Kinetic mechanism for predicting secondary organic aerosol fromation from the reaction of d-limonene with ozone, Environmental Science & Technology, 39, 9583–9594, 2005.

Liggio, J., Li, S.-M., and McLaren, R.: Heterogeneous reactions of glyoxal on particulate matter: identification of acetals and sulfate esters, Environmental Science & Technology, 39, 1532–1541, 2005a.

Liggio, J., Li, S. M., and Mclaren, R.: Reactive uptake of glyoxal by particulate matter, J Geophys Res-Atmos, 110, -, Artn D10304

Doi 10.1029/2004jd005113, 2005b.

Lin, C.-I., Baker, M., and Charlson, R. J.: Absorption coeffcient of atmospheric aerosol: A method for measurement Applied Optics, 12, 1356-1363, 1973.

Maria, S. F., Russell, L. M., Gilles, M. K., and Myneni, S. C. B.: Organic Aerosol Growth Mechanisms and Their Climate-Forcing Implications, Science, 306, 1921-1924, 10.1126/science.1103491, 2004.

Martin, M., Tritscher, T., Jurányi, Z., Heringa, M. F., Sierau, B., Weingartner, E., Chirico, R., Gysel, M., Prévôt, A. S. H., Baltensperger, U., and Lohmann, U.: Hygroscopic properties of fresh and aged wood burning particles, Journal of Aerosol Science, http://dx.doi.org/10.1016/j.jaerosci.2012.08.006, 2012.

Matsuura, A., Sato, H., Sotoyama, W., Takahashi, A., and Sakurai, M.: AM1, PM3, and PM5 calculations of the absorption maxima of basic organic dyes, Journal of Molecular Structure: THEOCHEM, 860, 119-127, 10.1016/j.theochem.2008.03.028, 2008.

Mazzoleni, L. R., Zielinska, B., and Moosmüller, H.: Emissions of Levoglucosan, Methoxy Phenols, and Organic Acids from Prescribed Burns, Laboratory Combustion of Wildland Fuels, and Residential Wood Combustion, Environmental Science & Technology, 41, 2115-2122, 10.1021/es061702c, 2007.

McIntyre, C., and McRae, C.: Proposed guidelines for sample preparation and ESI-MS analysis of humic substances to avoid self-esterification, Organic Geochemistry, 36, 543-553, 2005.

Menon, S., Hansen, J., Nazarenko, L., and Luo, Y.: Climate effects of black carbon aerosols in China and India, Science, 297, 2250-2253, 10.1126/science.1075159, 2002.

Moosmuller, H., Arnott, W. P., Rogers, C. F., Chow, J., Frazier, C. A., Sherman, L. E., and Dietrich, D. L.: Photoacoustic and Filter Measurements Related to Aerosol Light Absorption During the Northern Front Range Air Quality Study (Colorado 1996/1997), Journal of Geophysical Research, 103:D21 28149-28157, 1998.

Moosmuller, H., Chakrabarty, R. K., Ehlers, K. M., and Arnott, W. P.: Absorption Angstrom coefficient, brown carbon, and aerosols: basic concepts, bulk matter, and spherical particles, Atmospheric Chemistry and Physics, 11, 1217-1225, DOI 10.5194/acp-11-1217-2011, 2011.

Myhre, C. E. L., and Nielsen, C. J.: Optical properties in the UV and visible spectral region of organic acids relevant to tropospheric aerosols, Atmospheric Chemistry and Physics, 4, 1759-1769, 2004.

Myhre, G., Berglen, T., Johnsrud, M., Hoyle, C., Berntsen, T., Christopher, S., Fahey, D., Isaksen, I., Jones, T., Kahn, R., Loeb, N., Quinn, P., Remer, L., Schwarz, J., and Yttri, K.: Modelled radiative forcing of the direct aerosol effect with multi-observation evaluation, Atmospheric Chemistry and Physics, 9, 1365-1392, 10.5194/acp-9-1365-2009, 2009.

Nakayama, T., Matsumi, Y., Sato, K., Imamura, T., Yamazaki, A., and Uchiyama, A.: Laboratory studies on optical properties of secondary organic aerosols generated during the photooxidation of toluene and the ozonolysis of alpha-pinene, J Geophys Res-Atmos, 115, Artn D24204

Doi 10.1029/2010jd014387, 2010a.

Nakayama, T., Matsumi, Y., Sato, K., Imamura, T., Yamazaki, A., and Uchiyama, A.: Laboratory studies on optical properties of secondary organic aerosols generated during the photooxidation of toluene and the ozonolysis of alpha-pinene, Journal of Geophysical Research-Atmospheres, 115, D24204, Artn D24204

Doi 10.1029/2010jd014387, 2010b.

Nakayama, T., Sato, K., Matsumi, Y., Imamura, T., Yamazaki, A., and Uchiyama, A.: Wavelength and NOx dependent complex refractive index of SOAs generated from the photooxidation of toluene, Atmospheric Chemistry and Physics, 13, 531-545, 10.5194/acp-13-531-2013, 2013.

Ng, N. L., Chhabra, P. S., Chan, A. W. H., Surratt, J. D., Kroll, J. H., Kwan, A. J., McCabe, D. C., Wennberg, P. O., Sorooshian, A., Murphy, S. M., Dalleska, N. F., Flagan, R. C., and Seinfeld, J. H.: Effect of NOx level on secondary organic aerosol (SOA) formation from the photooxidation of terpenes, Atmos Chem Phys, 7, 5159-5174, 2007a.

Ng, N. L., Kroll, J. H., Chan, A. W. H., Chhabra, P. S., Flagan, R. C., and Seinfeld, J. H.: Secondary organic aerosol formation from m-xylene, toluene, and benzene, Atmos. Chem. Phys. Discuss., 7, 3909-3922, 10.5194/acp-7-3909-2007, 2007b.

Nozie`re, B., and Esteve , W.: Light-absorbing aldol condensation products in acidic aerosols: Spectra, kinetics, and contribution to the absorption index Atmospheric Environment 41, 1150–1163, 2007.

Nozière, B., and Esteve, W.: Organic reactions increasing the absorption index of atmospheric sulfuric acid aerosols, Geophys. Res. Lett., 32, L03812, 10.1029/2004gl021942, 2005.

Ofner, J., Krüger, H. U., Grothe, H., Schmitt-Kopplin, P., Whitmore, K., and Zetzsch, C.: Physico-chemical characterization of SOA derived from catechol and guaiacol – a model substance for the aromatic fraction of atmospheric HULIS, Atmos. Chem. Phys., 11, 1-15, 10.5194/acp-11-1-2011, 2011.

Patterson, E. M., and Marshall, B. T.: Diffuse reflectance and diffuse transmission measurements of aerosol absorption at the First International Workshop on light absorption by aerosol particles, Applied Optics, 21, 387-393, 1982.

Presto, A. A., Huff Hartz, K. E., and Donahue, N. M.: Secondary Organic Aerosol Production from Terpene Ozonolysis. 2. Effect of NOx Concentration, Environmental Science & Technology, 39, 7046-7054, 10.1021/es050400s, 2005.

Putaud, J.-P., Raes, F., Van Dingenen, R., Brüggemann, E., Facchini, M. C., Decesari, S., Fuzzi, S., Gehrig, R., Hüglin, C., Laj, P., Lorbeer, G., Maenhaut, W., Mihalopoulos, N., Müller, K., Querol, X., Rodriguez, S., Schneider, J., Spindler, G., Brink, H. t., Tørseth, K., and Wiedensohler, A.: A European aerosol phenomenology—2: chemical characteristics of particulate matter at kerbside, urban, rural and background sites in Europe, Atmospheric Environment, 38, 2579-2595, http://dx.doi.org/10.1016/j.atmosenv.2004.01.041, 2004.

Pöschl, U.: Atmospheric Aerosols: Composition, Transformation, Climate and Health Effects, Angewandte Chemie International Edition, 44, 7520-7540, 10.1002/anie.200501122, 2005.

Randles, C., Russell, L., and Ramaswamy, V.: Hygroscopic and optical properties of organic sea salt aerosol and consequences for climate forcing, Geophysical Research Letters, 31, 10.1029/2004GL020628, 2004.

Rogge, W. F., Hildemann, L. M., Mazurek, M. A., and Cass, G. R.: Sources of Fine Organic Aerosol. 9. Pine, Oak, and Synthetic Log Combustion in Residential Fireplaces, Environmental Science & Technology, 32, 13-22, 10.1021/es960930b, 1998.

Rosenfeld, D., Lohmann, U., Raga, G. B., O'Dowd, C. D., Kulmala, M., Fuzzi, S., Reissell, A., and Andreae, M. O.: Flood or drought: How do aerosols affect precipitation?, Science, 321, 1309-1313, DOI 10.1126/science.1160606, 2008.

Runge, E., and Gross, E. K. U.: Density-Functional Theory for Time-Dependent Systems, Physical Review Letters, 52, 997-1000, 1984.

Saleh, R., Hennigan, C. J., McMeeking, G. R., Chuang, W. K., Robinson, E. S., Coe, H., Donahue, N. M., and Robinson, A. L.: Absorptivity of brown carbon in fresh and

photo-chemically aged biomass-burning emissions, Atmos. Chem. Phys. Discuss., 13, 11509–11536, 10.5194/acpd-13-11509-2013, 2013.

Sareen, N., Schwier, A. N., Shapiro, E. L., Mitroo, D., and McNeill, V. F.: Secondary organic material formed by methylglyoxal in aqueous aerosol mimics, Atmospheric Chemistry and Physics, 10, 997-1016, 2010.

Sato, K., Hatakeyama, S., and Imamura, T.: Secondary organic aerosol formation during the photooxidation of toluene: NOx dependence of chemical composition, J Phys Chem A, 111, 9796-9808, 10.1021/jp071419f, 2007.

Schauer, J. J., Kleeman, M. J., Cass, G. R., and Simoneit, B. R. T.: Measurement of Emissions from Air Pollution Sources. 3. C1−C29 Organic Compounds from Fireplace Combustion of Wood, Environmental Science & Technology, 35, 1716-1728, 10.1021/es001331e, 2001.

Schell, B., Ackermann, I. J., Hass, H., Binkowski, F. S., and Ebel, A.: Modeling the formation of secondary organic aerosol within a comprehensive air quality model system, Journal of Geophysical Research-Atmospheres, 106, 28275-28293, 2001.

Schnaiter, M., Schmid, O., Petzold, A., Fritzsche, L., Klein, K. F., Andreae, M. O., Helas, G., Thielmann, A., Gimmler, M., Möhler, O., Linke, C., and Schurath, U.: Measurement of Wavelength-Resolved Light Absorption by Aerosols Utilizing a UV-VIS Extinction Cell, Aerosol Science and Technology, 39, 249-260, 10.1080/027868290925958, 2005.

Schulz, M., Textor, C., Kinne, S., Balkanski, Y., Bauer, S., Berntsen, T., Berglen, T., Boucher, O., Dentener, F., Guibert, S., Isaksen, I., Iversen, T., Koch, D., Kirkevag, A., Liu, X., Montanaro, V., Myhre, G., Penner, J., Pitari, G., Reddy, S., Seland, O., Stier, P., and Takemura, T.: Radiative forcing by aerosols as derived from the AeroCom present-day and pre-industrial simulations, Atmospheric Chemistry and Physics, 6, 5225-5246, 2006.

Schwarzenbach, R. P., Gschwend, P. M., and Imboden, D. M.: Environmental Organic Chemistry, John Wiley&Sons Inc., New York, 1993.

Seinfeld, J. H., and Pandis, S. N.: Atmospheric Chemistry and Physics, Wiley, New York, 1998.

Shapiro, E. L., Szprengiel, J., Sareen, N., Jen, C. N., Giordano, M. R., and McNeill, V. F.: Light-absorbing secondary organic material formed by glyoxal in aqueous aerosol mimics, Atmos Chem Phys, 9, 2289-2300, 2009.

Song, C., Na, K., and Cocker, D. R.: Impact of the Hydrocarbon to NOx Ratio on Secondary Organic Aerosol Formation, Environmental Science & Technology, 39, 3143-3149, 10.1021/es0493244, 2005.

Stein, S. E., and Brown, R. L.: Estimation of normal boiling points from group contributions, Journal of Chemical Information and Computer Sciences, 34, 581-587, 10.1021/ci00019a016, 1994.

Sun, H., Biedermann, L., and Bond, T. C.: Color of brown carbon: A model for ultraviolet and visible light absorption by organic carbon aerosol, Geophys. Res. Lett., 34, L17813, 10.1029/2007gl029797, 2007.

Surratt, J. D., Gómez-González, Y., Chan, A. W. H., Vermeylen, R., Shahgholi, M., Kleindienst, T. E., Edney, E. O., Offenberg, J. H., Lewandowski, M., Jaoui, M., Maenhaut, W., Claeys, M., Flagan, R. C., and Seinfeld, J. H.: Organosulfate Formation in Biogenic Secondary Organic Aerosol, The Journal of Physical Chemistry A, 112, 8345-8378, 10.1021/jp802310p, 2008.

Tegen, I., Lacis, A., and Fung, I.: The influence on climate forcing of mineral aerosols from disturbed soils, Nature, 380, 419-422, 10.1038/380419a0, 1996.

Tolocka, M. P., Jang, M., Ginter, J. M., Cox, F. J., Kamens, R. M., and Johnston, M. V.: Formation of oligomers in secondary organic aerosol, Environ Sci Technol, 38, 1428-1434, 2004.

Zellner, R., Exner, M., and Herrmann, H.: Absolute OH quantum yields in the laser photolysis of nitrate, nitrite and dissolved H2O2 at 308 and 351 nm in the temperature range 278–353 K, Journal of Atmospheric Chemistry, 10, 411-425, 1990.

Zerner, M.: Reviews in Computational Chemistry, 2, 313, 1991.

Zhang, X., Lin, Y., Surratt, J., and Weber, R.: Sources, Composition and Absorption Angstrom Exponent of Light-absorbing Organic Components in Aerosol Extracts from the Los Angeles Basin, Environmental Science & Technology, 47, 3685-3693, 10.1021/es305047b, 2013.

Zhao, L., Ni, N., and Yalkowsky, S. H.: A Modification of Trouton's Rule by Simple Molecular Parameters for Hydrocarbon Compounds, Industrial & Engineering Chemistry Research, 38, 324-327, 10.1021/ie9803570, 1998.

Zhong, M., and Jang, M.: Light absorption coefficient measurement of SOA using a UV-Visible spectrometer connected with an integrating sphere, Atmospheric Environment, 45, 4263-4271, 10.1016/j.atmosenv.2011.04.082, 2011.

Zhong, M., Jang, M., Oliferenko, A., Pillai, G. G., and Katritzky, A. R.: The SOA formation model combined with semiempirical quantum chemistry for predicting UV-Vis absorption of secondary organic aerosols, Physical Chemistry Chemical Physics, 14, 9058-9066, 2012.

BIOGRAPHICAL SKETCH

Min Zhong was born in Sichuan, China in 1980. Min spent her first 22 years in China. Since high school, Min has decided to be dedicated to the environmental career. After earning the Bachelor of Science degree in environmental engineering, Min went to South Korea to obtain the Master of Science degree in environmental engineering at the Pohang University of Science and Technology. After working in an environmental engineering company, Min came to US for air pollution research in the Department of Environmental Engineering Sciences at the University of Florida. She received her Ph.D. degree from the University of Florida in the summer of 2013.